

UNIVERSITY OF SOUTHAMPTON
FACULTY OF PHYSICAL SCIENCES AND ENGINEERING
Electronics and Computer Science

**Surface Electrode Array Stimulation and Iterative Learning Control
for Hand Restoration after Stroke**

by

Anna Soska

A thesis submitted in partial fulfillment
for the degree of Doctor of Philosophy

Supervisors: Professor Eric Rogers and Doctor Christopher Freeman

April 30, 2014

Contents

Acknowledgements	5
1 Introduction	1
2 Background and Related Work	7
2.1 Human Hand	7
2.1.1 Bones of the hand	7
2.2 Hand Injuries and Therapy	11
2.2.1 Hand restoration after stroke	11
2.2.2 Hand assessment in therapy	12
2.2.3 Virtual Reality - based stroke rehabilitation	12
2.3 Functional Electrical Stimulation	13
2.3.1 FES Techniques	15
2.3.2 Electrode Array-based FES	16
2.3.3 FES Control Strategies	17
2.4 Iterative Learning Control	20
2.4.1 Optimal ILC Algorithms	21
2.5 ILC in Stroke Rehabilitation - Previous Research	23
3 The Hand Model and ILC	27
3.1 The 2D hand and wrist model	28
3.2 Musculotendon system	35
3.3 FES control of hand and wrist using Newton method-based ILC	39
3.4 Simulation Evaluation	42
4 Surface Electrode Array based Control of the Wrist and Hand	47
4.1 System and Problem Description	49
4.2 Identifying the System about an Operating Point	51
4.3 ILC Applied to Array Element Selection	53
4.4 Selection using Virtual Elements	56
4.4.1 Sparse optimisation for SEAS-based control of Hand and Wrist . .	58
4.4.2 Proximal Gradient Algorithm	60
4.4.3 Brute-force Searching Method	61
4.4.4 Two-step approach for ILC of SEAS	62
4.5 General ILC-based approach for SEAS	63
5 System Design and Experimental Procedure	67
5.1 Electrode Array and Multiplexer	67

5.2 Sensors	68
5.3 HaReS - software	70
5.3.1 Hares Game	71
5.4 Design Considerations and Settings	73
5.4.1 Choice of reference postures	74
5.4.2 Method of optimal pattern selection	74
5.4.3 Selection of Virtual Elements	77
5.5 Experimental Results	78
6 Conclusions and Future work	83
A Model and parameters	89
A.1 Model of the hand and wrist	89
A.2 Simulation parameters	90
References	93

Acknowledgements

First of all, I would like to thank my supervisors Prof. Eric Rogers and Dr. Christopher Freeman, for their help and professional support. A special gratitude I wish to express to my advisor Prof. Paul Lewin for his advice and positive feedback. I would like to also express my sincere appreciation to Dr. John Tudor, Dr. Kai Yang and Dr. Russel Torah for their help and inspiring work. I must also thank Prof. Neil White and Prof. David Shepherd for the encouraging discussions and support. Special thanks must go to Dr. Timothy Exell and to two brilliant electronics engineers: Simon Cole and Phuc le Dinh. And finally I would like to thank my family and friends: Daisy, Alexis, Kasia, Carol, Marek, Oli, Thanh, Mustafa, Engin and foremost Chris for his help and for motivating me to individual and creative thinking.

*"There are only two ways to live your life. One is as though nothing
is a miracle. The other is as though everything is a miracle."*

...

A. Einstein.

...

To my grandmother and to all stroke survivors.

Chapter 1

Introduction

Cerebrovascular accident, commonly known as a stroke, is a sudden death of brain cells in a localized area due to lack of oxygen. Stroke is one of the leading causes of serious long-term disabilities. Each year over 15 million people worldwide suffer a stroke for the first time and 5 million are left permanently disabled. Psychological and economic post-stroke consequences, such as an unemployment, functional dependency and impoverished participation, are therefore considerable.

Stroke is usually caused when a blood clot blocks a blood vessel in the brain, and acts like a dam stopping the blood reaching the regions downstream. As a result, some of the connecting nerve fibers die and the person suffers partial paralysis on one side of the body, termed hemiplegia. Loss of hand function is one of the most frequently persisting consequences of stroke and is often characterized by an inability to open the hand ([Kamper et al. \(2003\)](#)), due to finger extension deficit. This deficit is primarily due to a limited ability to activate the fingers extensor muscles ([Kamper and Rymer \(2001\)](#)), crucial to appropriately grasp and release objects when interacting with the environment and therefore essential for performing everyday activities ([Selzer et al. \(2006\)](#)).

Stroke sufferers demonstrate deficits both in accuracy and efficiency during hand manipulation such as grasping. Common stroke consequences affecting grasp function are: anticipatory hand shaping, premature hand closure, inadequate aperture and spasticity. Generally, hand motor impairments after a stroke can be divided into two major groups: 1) a deficit in motor execution, resulting from weakness, spasticity, and abnormal muscle synergies, 2) a deficit in higher-order processes, such as motor planning and motor learning, which lead to poorly formed sensorimotor associations and to impaired motor control ([Raghavan \(2007\)](#)). The goal of rehabilitation is to help stroke survivors regain the most independent level of functioning possible and to enable stroke patients to adjust and cope with their impairment.

The brain is continually and rapidly changing and through intensive and systematic task repetition, new connections can be formed and redundant ones disappear. The process by which neuronal circuits are modified by repeated experience and learning is called neuroplasticity ([Nudo \(2003\)](#)). Motor-learning research with subjects after stroke has shown that a high number of repetitions of task-specific activity can cause cortical changes and functional improvement ([Miltner et al. \(1998\)](#)).

During traditional rehabilitation, such as physical therapy which focuses on restoring general movement or occupational therapy concentrated on the patients re-learning everyday activities such as eating, drinking and self-care skills, stroke patients are assisted by physiotherapists in relearning their lost skills. Although these routine therapies are beneficial, they remain limited in their effectiveness in restoring full independent use of the impaired extremity, and no form has been found to be better than another ([Ernst \(1990\)](#)).

Successful rehabilitation interventions have laid stress on the importance of performing large numbers of high-intensity, repetitive motions. Unfortunately, sessions with therapists usually include only a relatively small number of motions and exercises. Additionally, traditional therapies are expensive and difficult to manage due to the limited amount of resources compared to the number of patients. Consequently many stroke survivors never regain the function of their affected limbs. Therefore, to experience significant recovery, stroke patients must perform a substantial number of daily exercises at home. Unfortunately, a study indicates only 31 % of patients actually perform home exercises as recommended by therapists ([Shaughnessy et al. \(2006\)](#)).

Evidence exists that intensive training by repetition appears to increase upper extremity function after stroke ([Teasell and Kalra \(2004\)](#)), especially when it is combined with appropriate feedback to patients about their progress ([Langhorne et al. \(2009\)](#)). Additionally, research has suggested that more interactive and intuitive rehabilitation systems, i.e. systems which enhance patients' thinking about moving in different directions, can potentially improve the learning experience and effectiveness of therapy ([Brewer et al. \(2007\)](#)). Enabling rehabilitation outside the hospital, supported by mobile technology, that motivates the patient, may reduce cost, increase intensity of therapy and shift the responsibility for good health from health professionals to patients ([Lang et al. \(2007\)](#)). Hence there is a pressing need to improve the effectiveness of treatments including development of novel home-based rehabilitation systems, which are adjustable to individual needs of patients. Significant advances in electronic technology has led to development of new techniques of upper-extremity rehabilitation such as Virtual Reality-based rehabilitation Functional Electrical Stimulation (FES). The general aim of these new techniques is to increase the effectiveness of rehabilitation, compared to traditional approaches.

Virtual Reality (VR) has been recognized as a highly motivating rehabilitation environment, which also naturally embeds the ability for flexible data bases, that can provide a customized real-time data collection and storage. Explicitly using feedback, VR can be treated as a form of advanced physical therapy and has a number of recognized advantages over conventional approaches ([Burdea \(2003\)](#)). These include the ability to graduate therapy and adapt automatically to a patient's (limited) functioning level, increasing patient motivation, transparent and computerized objective measures and visual presentation of progress. Appropriately designed games have the potential to motivate stroke patients to exercise by decreasing the monotony of hundreds of repeated motions and providing performance feedback. Therefore, game-based rehabilitation system could provide more interactive and intuitive training for rehabilitation, increasing both the quality and quantity of home therapy after stroke.

FES is a promising rehabilitation technique widely used to restore motor function of stroke patients with spasticity and hemiplegia. Re-learning skills after the stroke during repeated practice of a task requires sensory feedback. However, the problem is that most of stroke patients can hardly move and hence they do not receive the appropriate feedback from previous attempts needed to improve the next one. FES is able to induce functional movements in paralysed or weak limbs by delivering a series of electrical pulses to associated skeletal muscles. Most existing FES-based rehabilitation systems concentrate on regaining reaching function in the arm and only very few systems provide fine motion recovery for the wrist and hand. Consequently, the recovery of the hand and wrist has a delayed progression compared with the rest of the upper-limb. Patients with upper extremity paralysis typically regain motion starting from their shoulder over time gradually regaining motion in the elbow, wrist, and, at the end, the hand. The deficiency of FES-based stroke rehabilitation systems for restoration of hand and wrist function is partially due to a high complexity of hand anatomical structure and the technological limitations. The effectiveness of the FES is strongly related to the precision of stimulation in assisting functional movement ([Westerveld et al. \(2012\)](#)).

Commercially available large surface electrodes due to their weak selectivity and activation of several interfering muscles, are not suitable for precise control of hand and wrist. Such an activation of antagonist muscles generate movements interfering with desired ones. For example, the wrist interferes with finger flexors during grasping and finger extensors during prehension. Another problem is the variability in stimulation characteristics, which can appear due to the changes in the surface conditions of the skin and differences in positioning electrodes. Therefore, there is currently significant research into improving surface FES solutions, including the design of surface electrodes that consist of groups of array elements. The advantage of electrode arrays is that they provide the opportunity to activate an individual or a group of elements. Recent studies have shown that electrode arrays are a promising stimulation technology, that can be

used to overcome standard FES shortcomings such as finding the optimum electrode placement ([O'Dwyer et al. \(2006\)](#)) decreasing the muscle fatigue and increasing efficacy of use.

FES makes muscles work by causing electrical impulses to travel along nerves in a similar way as electrical impulses from the brain. If stimulation is controlled a desired movement can be made and its therapeutic effect can be enhanced when associated with the patient's voluntary movement ([Rushton \(2003\)](#)). Hence, to maximise effectiveness of FES-based stroke rehabilitation, precise control of stimulation is needed. Such a control should minimize the level of FES to promote the patient's maximum voluntary contribution to the movement.

One control approach that has been found to be highly effective when employed within stroke rehabilitation ([Freeman et al. \(2009b\)](#)) is, Iterative Learning Control (ILC). ILC is an example of feed-forward control that has its origins [Arimoto et al. \(1984a\)](#) in the industrial robotics area where many tasks involve repeating the same finite duration task over and over again. Rehabilitation strategies based on repetitive task performance are an example of such processes. In order to regain for example the ability to open the hand, the patient needs to repeat the exercises multiple times. In ILC the core idea is to use information gathered on previous executions to update the control signal used for the next one and thereby sequentially improve performance. Since the original work, ILC has become an established area of control systems research and applications ([Bristow et al. \(2006\)](#); [Ahn et al. \(2007\)](#); [Wang et al. \(2009\)](#)). In recent years ILC algorithms from the engineering domain have been applied to upper limb stroke rehabilitation for planar and 3D tasks. The ability of model-based ILC to modify the stimulation signal in response to physiological changes, in order to achieve highly accurate tracking by exploiting the repetitive nature of the task, has been confirmed in two clinical trials with stroke patients for the most recent results see, for example ([Freeman et al., 2012](#); [Hughes et al., 2009a](#); [Meadmore et al., 2012](#)). These studies do not include the hand and wrist, which has limited their effectiveness.

The main focus of this thesis is therefore, to develop model-based FES controllers for hand and wrist restoration after stroke. The main contributions of thesis are as follows:

- An overview of the background to the research is presented in Chapter 2. The anatomical complexity of the musculo-skeletal structure of the hand and wrist and the practical considerations and constraints are discussed relating to the application of the model-based control algorithms within stroke rehabilitation. The existing non-invasive technologies severely limit the application efficiency of such complex models in practice. Thus to overcome practical limitations, a novel method for control of the hand and wrist, which uses multi-channel surface electrode array-based stimulation has been developed.

- A clinically relevant model of the hand and wrist, incorporating stimulated muscles, is developed (Chapter 3). The model has been tested in simulations to investigate the ability of ILC in providing precise FES-based control of the hand and wrist motion. Performance when using only extrinsic muscles, that are compatible with using surface FES, are compared against using both extrinsic and intrinsic muscles. Simulation studies confirm feasibility and established efficacy of use of the dynamic hand model for the idealised case, in which the optimal selectivity of the muscles can be achieved.
- Several different control methods have been developed based on theoretical and experimental findings. These include gradient based algorithms for optimisation of electrode array stimulation and optimal ILC methods for control of the hand and wrist (Chapter 4). The experimental results, confirm the effectiveness of the approach (Chapter 5).
- A novel system for hand and wrist restoration has been designed for a stroke patients with spasticity and hemiplegia. It comprises the ILC-based control algorithms for electrode array stimulation with a game-based training environment that provides feedback to the patient (Chapter 5). Developing an effective rehabilitation system of hand and wrist for a wide group of stroke survivors is a challenging task and a source of multidisciplinary research aspects. The summary of the work and potential future research problems are discussed (Chapter 6).

Chapter 2

Background and Related Work

2.1 Human Hand

A normal functioning hand is one of the most important features for human independence. Research in anatomy and biomechanics has shown that the human hand has a very sophisticated and complex structure, consisting of many dedicated subsystems cooperated in a highly organised manner to form a powerful and precise device. The hand is composed of bones connected by joints which are actuated by muscles. These elements are described in turn next.

2.1.1 Bones of the hand

The skeletal structure of the human hand consists of 27 bones constituting the wrist, palm, four fingers (index, middle, fourth, little finger) and the thumb (Figure 2.1). The wrist, which connects the hand body to the forearm, is composed of eight cube-like bones arranged in two rows of four bones each. The palm (metacarpus) contains five long metacarpal bones. Fourteen phalangeal bones constitute the four fingers and thumb. Each of the four fingers consists of three phalanges (proximal, middle and distal phalanges), while the thumb has two (proximal and distal) phalanges (Tubiana et al., 1996).

The skeleton of the human hand can be treated as a complex manipulator consisting of a hierarchy of kinematic chains (the fingers). The skeleton thus defines the underlying kinematics of the hand and finger motion by constraining movement at the joints. There are four joints in each of the fingers: the Carpometacarpal (CMC) joint, placed between the carpal and metacarpal bones, the Metacarpophalangeal (MCP) joint between the metacarpals and the phalanges, the Proximal interphalangeal (PIP) and the Distal interphalangeal (DIP) joints which lie between the proximal and distal phalanges respectively. The thumb consists of three joints: CMC, MCP and interphalangeal (IP)

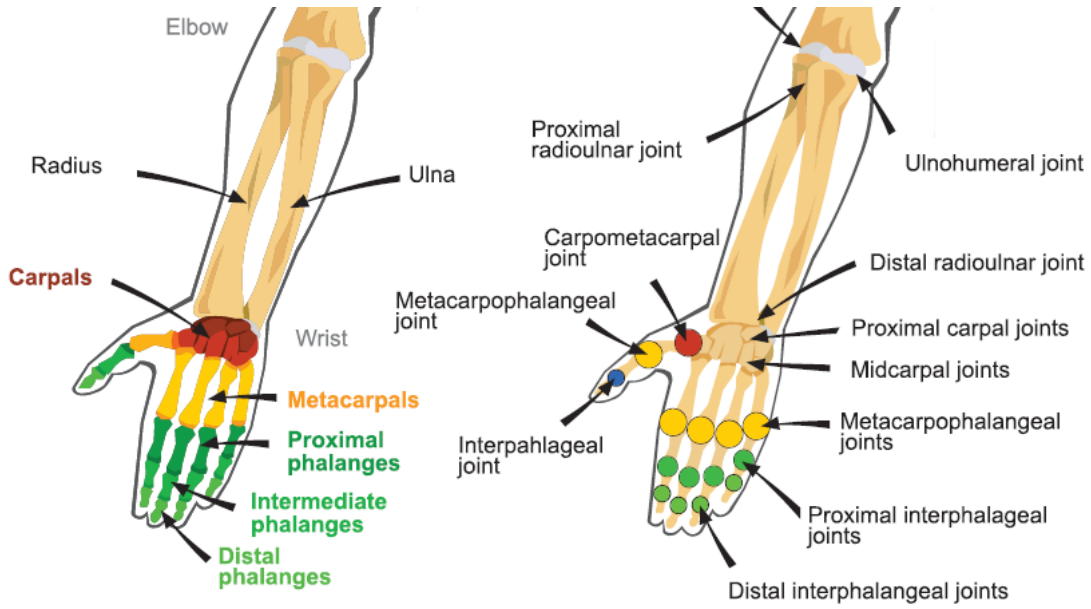


Figure 2.1: Hand bones and joints ([Kowalczewski \(2009\)](#))

joints (proximal, intermediate and distal). The CMC joint in the thumb is considered as a saddle joint with 2 degrees-of-freedom (DOF), the MCP joints in the fingers and thumb are considered condyloid and hinge-like joints (respectively) each with 2 DOF, and the IP joints of the fingers and thumb are hinge joints with 1 DOF.

In summary, the hand contains fifteen joints which afford approximately 27 degrees of freedom. There have been numerous attempts to model the kinematics of the hand by defining constraint sets on the angles of rotation of the joints [Cobos et al. \(2010b\)](#). The number of joints contained in the model together with the number of degrees of freedom of each joint defines the dimensionality of the control problem. Considerable attention has been given to constructing models with reduced dimensionality [Cobos et al. \(2010a, 2008, 2007\)](#). The results of several studies have demonstrated that the effective dimensionality of the human hand is much less than twenty and that the wrist can be considered as a single joint with two degrees of freedom. Moreover some studies have shown that 42 % of the movements of the hand involve the four fingers moving together, thus in many situations the four fingers can be considered as one virtual finger [Ingram et al. \(2008\)](#).

Lying on top of the skeleton the hand contains a complex network of muscles and tendons that are used to control its movements. The muscles of the hand are divided into two groups: intrinsic muscles (listed in Table 2.1) and extrinsic muscles, listed in Table 2.2. The extrinsic muscles are located proximally in the forearm, whereas the intrinsic muscles originate solely in the hand. In most FES systems only the extrinsic muscles

are stimulated. The extrinsic muscles can provide a good estimate of the location of the fingertip in the workspace for a fixed position of the wrist (Biggs et al., 1999).

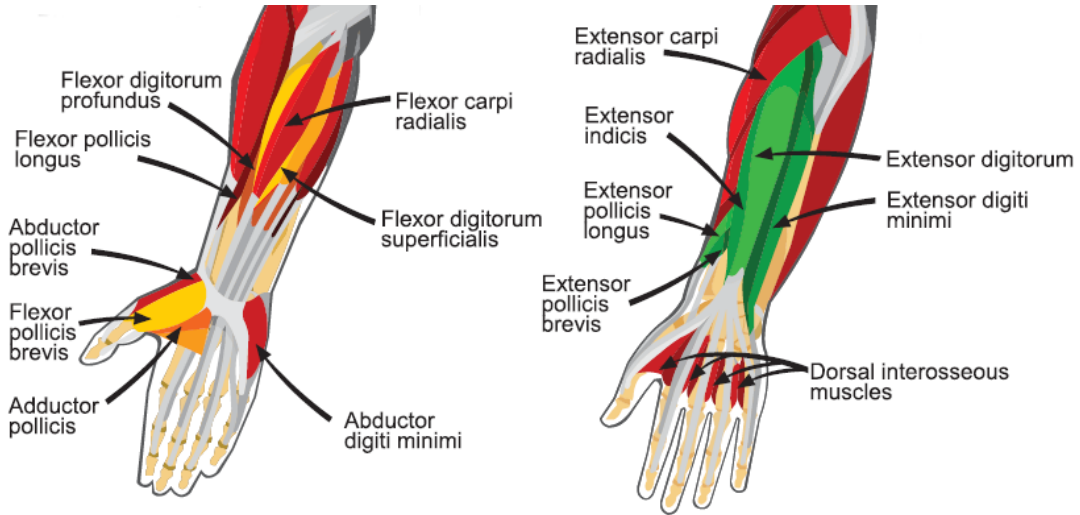


Figure 2.2: Hand muscles Kowalczewski (2009)

Muscle	Acts upon (Joint)	Movement
Flexor Digiti Minimi (FDM)	little finger	flexion
Flexor Pollicis Brevis (FPB)	Thumb (MCP)	
Lumbricals (LU)	all fingers (MCP)	
	all fingers (DIP/PIP)	extension
Dorsal Interossei (DI)	all fingers (MCP)	flexion & abduction
	all fingers (PIP/DIP)	extension
Palmer Interossei (PI)	all fingers (MCP)	flexion
	all fingers (PIP/DIP)	extension
Abductor Digitii Minimi (ADM)	Little finger (MCP)	
Abductor Pollicis Brevis (APB)	thumb (CMC/MCP)	abduction

Table 2.1: Intrinsic Muscles of the hand

Knowledge of the abilities and limitations of joints and muscles in a healthy hand is necessary to determine an optimal strategy to restore motor abilities in impaired patients. In order to perform simple grasps, the hand joints must be able to perform the basic movements shown in Figure 2.3. These are abduction/adduction and flexion/extension for the thumb and fingers.

Muscle	Acts upon (Joint)	Movement
Flexor Digitorium Superficialis (FS)	all fingers (PIP)/wrist	Flexion
Flexor Digitorium Profundus (FP)	all fingers (DIP)/wrist	
Flexor Pollicis Longus (FPL)	thumb (IP)	
Palmaris Longus (PL)	wrist	
Extensor Digitorium Communis (EC)	all fingers (all joints)/wrist	extension
Extensor Indicis (EI)	index (all joints)	
Extensor Pollicis Brevis (EPB)	thumb (MCP)	
Extensor Pollicis Longus (EPL)	thumb (IP)	
Extensor Digiti Minimi (EDM)	little finger	
Extensor Carpi Ulnaris (ECU)	wrist	extension & adduction
Extensor Carpi Radialis (ECR)	wrist	extension & abduction
Abductor Pollicis Longus	CMC/MCP	abduction

Table 2.2: Extrinsic Muscles of the hand

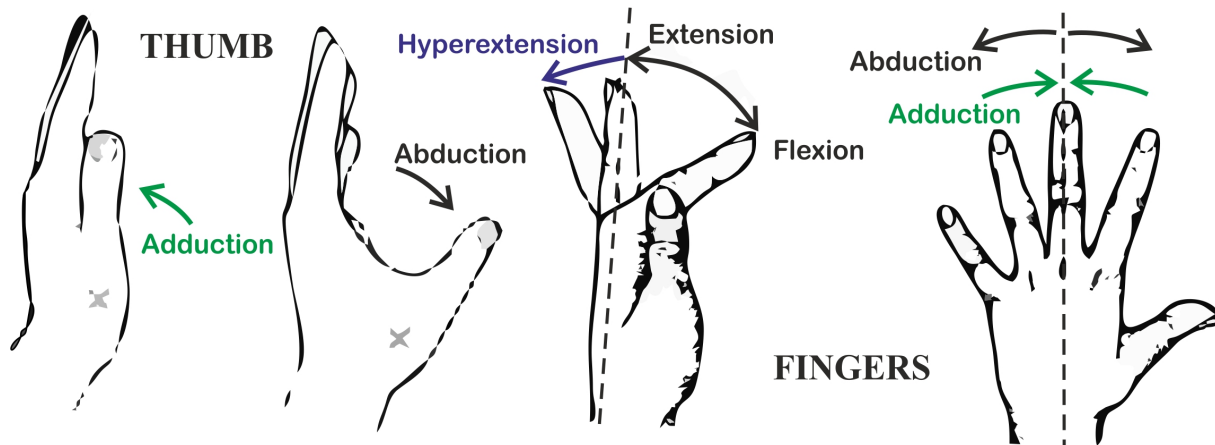


Figure 2.3: Movements of the thumb and fingers (for Surgery of The Hand, 1990)

1. Flexion/Extension

Flexion/extension is defined as the movement of a joint that results in a decrease/increase in the angle between two bones at the joint.

2. Adduction/Abduction

Adduction is a movement of the joint which brings the finger closer to the midline of the arm and hand (sagittal plane), and abduction is the opposite motion.

Two major types of hand motion can be distinguished: free and restricted. In free motion, the hand moves freely in space and the movements in free motion are opening and closing. Resisted motion is performed by the hand against an external resistance, for the purpose of exerting force on an external object. Many researchers have categorized the hand's functional position when manipulating objects. Although these classifications are not universally standardized the pinch grasp and the power grip are common in most of

these classifications.

Opening/Closing of the hand, using the terminology introduced above can be defined as extention/flexion of the fingers and abduction/adduction of the thumb from their initial to final positions. The position of the fingers can be defined by the angles of the finger joints.

2.2 Hand Injuries and Therapy

There are many injuries that can result in the loss of hand function. These include but are not limited to: Stroke, Multiple Sclerosis (MS), Spinal Cord Injury (SCI), Peripheral Nerve Injury and complications following hand surgery. Of all of these stroke is the leading cause of disability worldwide. The most common feature after stroke is the loss of muscle function for one or more muscles, termed paralysis. Hemiplegia, another common disability resulting from stroke, is unilateral paralysis in the upper extremity, that can severely limit a patients functional movement control. Research has shown that 80 % of acute stroke survivors lose arm and hand movement skills. Other impairments following stroke, that can affect functional motor recovery of hand, are abnormal synergies, contractures and spasticity. Abnormal synergies are patterned movements, that occur due to patients' inability to appropriately control individual muscles. Common synergies are flexion and extension synergies that appear when attempting to perform a separate flexion or extension of the fingers. Approximately, 25 % of stroke patients develop spasticity, the over-activity of monosynaptic muscle-stretch reflexes, that leads to increased resistance to a passive stretch.

2.2.1 Hand restoration after stroke

The main purpose of stroke therapy following loss of function in the hand is to reduce impairments and restore functional performance by improving joint range of motion. The function use of hand and forearm include: keeping full extension, hand grasping, hand holding, wrist flexion and extension, wrist rotation. Due to the fact that the disturbance of the the normal association between wrist and hand motion can additionally appear after stroke, wrist rehabilitation is also considered to be part of hand recovery. Treatment programs typically include the following goals:

- Achieve mass grasp and wrist fixation for grasp.
- Achieve active release of grasp.
- Achieve active extension for each finger with resistance.

- Alternate fist opening and closing and achieve voluntary hand extension and flexion.

Eye-hand coordination plays a key role in the effective restoration of hand function. This coordination is the ability to use the eyes and hands together to perform a particular task, such as handwriting. A number of techniques such as Geometric Forms or Pursuit Patterns have been employed for training of eye-hand coordination. During a rehabilitation session of this type a patient is encouraged to move one or both hands simultaneously along the specified patterns (usually geometric figures, lines). The error generated is the index that determines the level of control of the muscle to the hand and the patients' eye-hand coordination ability.

2.2.2 Hand assessment in therapy

Comprehensive and reproducible assessment of hand function is crucial for prescription of appropriate treatment program and further evaluation of its effectiveness. The therapy should be adjustable according to ongoing assessment over the course of the treatment program and thereby ensure optimal benefits to the patient. The traditional assessment of hand function includes evaluation of range of motion (ROM), testing of the strength of intrinsic and extrinsic muscles and evaluation of motor and sensory functions. ROM is a measurement of the distance or angle the joint can travel through over the course of its normal range of movement. It can be a useful index to measure the rehabilitation progress of stroke patients. The functional assessment is conducted through the use of activities of daily living (ADL) assessment boards that enables evaluation of different types of hand grip and object manipulation.

Subjective evaluations of hand function by a therapists form the basis of clinical assessments, but these evaluations tend to be performed in non-standardized ways, and therefore depend on the training and skills of the clinicians involved. Therefore, home-based rehabilitation systems, need to include reliable and objective self-assessment and testing methods to quantify effect of therapy and provide appropriate feedback to the patients.

2.2.3 Virtual Reality - based stroke rehabilitation

A number of research projects have investigated the problem of effective application of games for the purpose of stroke therapy. One area of research, has examined the potential of using commercial games with motion-based input devices such as the Sony Playstation 2 and Nintendo Wii ([Deutsch et al. \(2008\)](#)). However, the commercial console games are principally aimed at patients in the later stages of recovery, as they were

designed for users with a full range of motion. Consequently, they are not suitable for the majority of stroke patients, who are at the early stage of their recovery ([Flynn et al. \(2007\)](#)). Therefore, the majority of research has focused on development of dedicated games, that can be used by wider group of patients, some of which are listed in Table [\(2.3\)](#).

Research	Game description
Colombo et al. (2007)	simple game in which the patient tried to move a colored circle from an initial position to a goal position using a robotic device designed for arm rehabilitation
Huber et al. (2008)	haptic glove based games in which users scare away butterflies, play the piano, and squeeze virtual pistons to improve the player's finger flexion and extension.
Broeren et al. (2008)	several games for use with a pen-like haptic device that patients could position in 3D.
Burke et al. (2009)	a physics-based orange catching game and a whack-a-mouse game, both controlled with magnetic sensors and a vibraphone game which used a Wii remote as a pointing device

Table 2.3: Games in Stroke Rehabilitation

A review of the properties of virtual reality and gaming in the context of the needs of stroke patients suggests this to be a very promising and active research area. An appropriately designed game can be a fundamental element of a modern rehabilitation system, addressing the most important aspects of effective hand restoration. Game-based rehabilitation system can couple the advantages of modern and quantitative assessment methods and feedback, to make the rehabilitation process motivating and intensive for the patient. It can be also a modern dynamic training environment, that can be adjustable to the patients rate of recovery and performance.

2.3 Functional Electrical Stimulation

Functional Electrical Stimulation (FES) is a rehabilitation technique widely used to restore motor function of stroke patients. FES has theoretical support from neurophysiology and motor learning research. A body of clinical evidence exists to confirm its effectiveness in motor control recovery ([Pomeroy et al., 2006](#)). FES is able to induce functional movements in paralysed or weak limb, by delivering a series of electric pulses to associated skeletal muscles. **Skeletal muscles** are formed of a number of motor units, each motor unit consisting of a single motor neuron and all of the corresponding muscle fibers it innervates. Muscle fibres are cylindrical cells that can contract when

stimulated. A single impulse in a motor neuron results in a fast, transient contraction of a single motor unit (Lynch and Popovic, 2008). To maintain a constant tension in muscles, known as a tetanic contraction, motor neurons deliver impulses to their associated muscle fibers in a sequential asynchronous manner by recruiting adjacent motor units at different time intervals. This asynchronous recruitment ensures that the fatigue of physiologically activated muscle, a side effect of long muscle stimulation, increases slowly. The muscle fatigue reveals itself as the decreasing ability of the muscle to produce a maintained tetanic contraction of adequate power. The intensity of the resulting muscle contraction is determined by the frequency of the delivered pulses. The tetanic contraction of voluntary muscle is typically achieved at a frequency of 6 – 8 Hz.

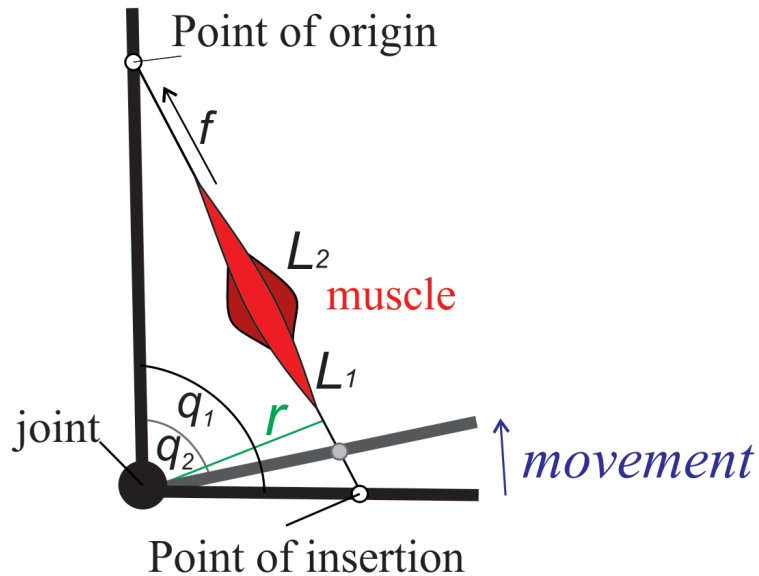


Figure 2.4: Schematic illustration of a muscle acting on a single joint, where q_1, q_2 are the joint angles, f is the pulling force applied by the muscle, L_1, L_2 are muscle lengths and r is the moment arm of the joint-muscle system.

In the simplest case one muscle acts at a single joint. The joint can represent for example, any of the finger joints. When the muscle contracts, it produces a force f (with magnitude f) that results in a torque τ on the joint crossed by the muscle, causing the joint angle to change by an amount $\Delta q = q_1 - q_2$ in a given time interval Δt , as illustrated in Figure 2.4. This can be observed as a finger movement.

The contraction is initiated by electrochemical signals from the brain and controlled by the nervous system. A paralyzed muscle does not exhibit voluntary contractions because it receives no signals from the brain. FES artificially induces a current in specific motor neurons, and therefore the paralysed muscle can be made to contract.

There exist different FES parameters that can be used to produce an effective motor response. These are: Pulse strength (amplitude) and duration (pulse width), pulse repetition rate (stimulation frequency), On-off time, Ramp time, Waveform. The tension produced in electrically stimulated muscle depends on the intensity and frequency of stimulation. The stimulation intensity is a function of the total charge transferred to the muscle, which depends on the pulse amplitude, duration, and frequency in addition to the shape of the pulse train [Lynch and Popovic \(2008\)](#). FES recruits motor units in a non-physiological synchronous manner, stimulating all of the motor units at the same time. Therefore, FES stimulation requires a much higher frequency (20 – 40 Hz) to achieve tetanic contraction. This can result in rapid muscle fatigue.

2.3.1 FES Techniques

A wide range of FES techniques have been proposed that use different electrodes to stimulate the motor units. Generally, these are two major types of stimulation:

- Invasive stimulation uses implanted electrodes such as: epimysial electrodes (placed on the surface of the muscle), intramuscular electrodes (placed within a muscle), and cuff electrodes (wrapped around the nerve that innervates the muscle)
- Non-invasive surface stimulation which uses self-adhesive electrodes or electrode arrays, that can be placed on the skin surface.

Surface FES can be an effective technique for stroke rehabilitation of the upper-limb, however, there exist many factors, that can affect the stimulation efficiency and its practical application ([Lyons et al. \(2004\)](#)). These factors include electrode type (size and electrode placement), a selection of the stimulation signal parameters and control of the stimulation. The sizes of the stimulation electrodes have direct effect on the current density. When the electrode size decreases the current density increases and vice versa (Lyons, 2004). The optimum size of electrode depends on the muscle stimulated and location of stimulation (Lyons, 2004).

Locating the optimal stimulation sites is critical to the effective application of surface stimulation. Usually the best stimulation site is the nearest to the muscle motor point, which provides the greatest amount of motor excitation with the minimal intensity of stimulation. Generally, the correct positions of the electrodes resulting in desired movements have to be found manually. This is time-consuming and relies heavily on the skill and experience of the therapist. Hence, there is currently significant research interest in improving surface FES solutions, including the design of surface electrodes that consist of groups of array elements.

2.3.2 Electrode Array-based FES

Recent studies have shown that electrode arrays are a promising stimulation technology, that can be used to overcome standard FES problems such as manually locating the optimum electrode placement ([O'Dwyer et al. \(2006\)](#)), decreasing resulting muscle fatigue and increasing overall function. The advantage of electrode arrays is that they provide the opportunity to activate an individual or a group of elements, which has been shown to improve muscle activation and sensitivity, compared with standard FES electrodes. Additionally they can eliminate the problem of repeated reattachment of electrodes, as the electrode once attached to the hand, can be automatically set via electrical circuitry to obtain its optimal configuration [Europa \(2009\)](#); [Popović-Bijelić et al. \(2005\)](#). Methods to assess and automatically select the optimal configuration of the multipad electrodes is currently an emerging and active area of research, where a range of these are discussed next.

[Schill et al. \(2009a\)](#) developed an adaptive multi-electrode array control approach, based on two criteria: the magnitude criterion and the dynamic criterion. In the first step, a reference movement of the wrist joint was generated manually and recorded using bending sensors. A set of evaluation movements was generated through application of different activation patterns to the multi-electrode array. These were then compared with the reference movement in order to find an electrode configuration which could produce movements that best fit the reference.

In ([O'Dwyer et al. \(2006\)](#)) a system consisting of an analogue de-multiplexer and an electrode matrix that used one channel of stimulation was developed. A key element of the system is an algorithm, which selected from a matrix of electrodes a single best electrode with which to provide the optimal orthotic performance for the subject. A clinical investigation on healthy subjects was conducted to test the proposed system. The results showed a high variation in hand response across different subjects. In addition, for all subjects tested an optimum response was found which showed some justification for the use of the proposed technique.

[Popović and Popović \(2009\)](#) developed an algorithm for automatic determination of shape and placement of the electrode stimulation pattern. The algorithm was based on the selection of 8 elements which minimized the aggregate error.

[Malešević and Popović \(2010\)](#) proposed a procedure for selecting pads within multi-pad electrode based on the muscle twitch response of stimulated muscles. The correlation of each pad and the muscle activated beneath was detected by an Artificial Neural Network (ANN). The ANN was trained using the characteristic acceleration wave shapes

acquired during wrist or finger flexion/extension movements, measured by MEMS sensors and goniometers.

2.3.3 FES Control Strategies

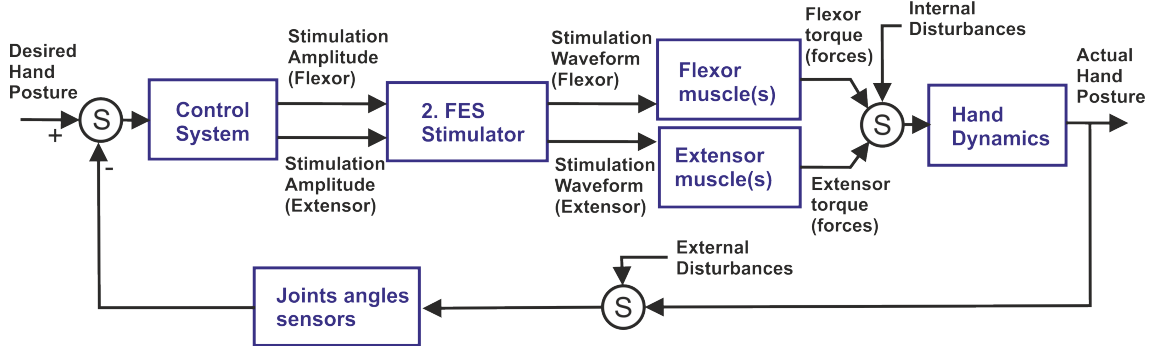


Figure 2.5: Example of FES schematic for hand and wrist rehabilitation.

In system engineering terms the musculoskeletal system can be considered as a plant to be controlled. In this analogy the muscles are actuators and the electrical pulses driving the actuators are control signals. The posture of the hand is typically defined by the angles of the hand joints. By calculating the appropriate electrical stimulation signal a desired output posture/trajectory can be followed.

There exist two main control strategies, that can be employed in FES-based control of the hand and wrist. These are: open-loop control and closed-loop control, that typically employs a model of the system. Open-loop control is the simplest method of control, which does not rely on the presence of sensors giving information on the plant. Open-loop controllers therefore do not adjust the input according to performance, and have no knowledge of the plant trajectory. In a closed-loop control system, the system output is monitored by a sensor and the data is fed to a controller which adjusts the control as necessary to maintain the desired system output. The control affects the system output, which in turn is measured and looped back to alter the control. A closed-loop control scheme for the hand and wrist is shown in Figure 5.9.

Determining the control signal is a challenging control problem, mainly due to the complexity of the musculotendon structure of the hand and wrist. Regulating angles/-torques of hand joints with FES involves controlling a highly coupled system since each joint is actuated by at least two muscle groups, these comprising either flexor muscles or extensor muscles. Furthermore most of the hand muscles are either bi-articular or multi-articular, which means they actuate simultaneously two or more joints respectively.

The controller provides the control signals needed to obtain a muscle force that produces a desired movement. Hence, the movement can be controlled indirectly by modulating

the stimulation parameters. Variations in these affect the stimulus applied to the tissues, determining the physiological response. Therefore, to achieve the precise control of the motion, the input-output response of the muscle must be known for use in model-based control approaches. There are several empirical models that reproduce the input-output response of a muscle. The most popular muscle model commonly used in FES control is the Hill model ([Hill \(1938\)](#)).

The Hill model describes the output force as the product of three independent experimentally measured factors: the force-length property, the force-velocity property, and the non-linear activation dynamics of the stimulation input. The actuation dynamics operate under the condition that the muscle has a constant length (isometric condition), and are almost always represented by a Hammerstein structure. Such a model comprises a static non-linearity in series with linear dynamics. The static non-linearity represents the static gain relation between stimulus activation level and the steady-state output torque, when the muscle is held at a fixed length and is termed the Isometric Recruitment Curve (IRC). The linear dynamics refers to the muscle contraction dynamics and in combination with IRC gives the overall torque generated by the muscle [Le et al. \(2010\)](#).

Open-Loop Controllers

The most widely used FES controllers, due to their simplicity, have an open-loop architecture. There exist a number of commercial FES systems for the hand and wrist, primarily based on this simple control technique.

The Bionic Glove is a fingerless glove that electronically senses wrist position and uses it to trigger a logical on-off signal to provide FES control of finger/thumb muscles. The degree of wrist angle allows the user to select their grasp or hand opening posture. The glove has three channels of electrical stimulation acting on the Flexor Pollicis Longus, Flexor Digitorum Superficialis, Flexor Pollicis Brevis and Adductor Pollicis. Practical tests involving nine impaired patients showed a significant increase in average grip force for palmer and lateral grasp ([Prochazka \(1997\)](#); [Popovic \(1999\)](#)).

The NESS H200 system contains inbuilt electrodes worn on the upper arm. This system provides a simple interface, that allows the user to select seven different stimulation patterns in order to assist hand grasp. The control unit applies suitable stimulation allowing the fingers and thumb to move while reaching, grasping and pinching. The effectiveness of the device was tested clinically with eighteen stroke patients, who exhibited upper body dysfunction ([Hendricks et al. \(2001\)](#)). Although the results showed increased motor function, especially in patients with moderate motor defects, the beneficial impact of the device was not clear.

Another type of FES system is triggered using position/force sensors in response to a command supplied by the user. The commercial system (**Freehand**), uses proportional control with a reference given by shoulder position sensing to regulate grip force for lateral and palmer grasp. It hence requires user feedback to achieve force control. The system uses implanted electrodes to ensure better selectivity over the muscle activation. The Freehand was tested with nine users and the results confirmed similar advantages in hand grasp function to the previously described commercial devices ([Taylor et al. \(2002\)](#)).

Another control technique is based on using Electromyographic (EMG) signals recorded from muscles. The EMG signals can be recorded from unimpaired users and replayed during FES grasp control of injured patients, thereby providing an open-loop reference. Alternatively, they are measured directly from the impaired user to provide a direct command input for FES control of impaired limb. In ([Hart et al. \(1998\)](#)) proportional control using wrist position together with EMG signals from the wrist have been used to provide grasp and release control. This study has shown wrist control is not affected by movements undertaken during reaching tasks and the function of the wrist is easy to re-learn by participants. The use of EMG control in practical applications is limited by the availability and range of usable muscles, in addition to distortion caused by the artefacts produced by the stimulated muscle. Additionally signals associated with paralysed muscle can be weak and unreliable to record.

Closed-Loop Controllers

Due to the anatomical complexity of the human hand relatively little research has considered closed-loop control of the hand. One of the few approaches in the literature is a multi-channel Proportional-Integral-Differential (PID) controller proposed by ([Watanabe \(2003\)](#)). This PID controller uses the error between the desired input and the actual measured output to generate a control signal for the plant. The controller acts on two degrees of freedom in the wrist joint, measured with a two-axis goniometer. To achieve wrist movement four muscles were stimulated using surface electrodes: Extensor Carpi Radialis (ECR), Extensor Carpi Ulnaris (ECU), Flexor Carpi Radialis (FCR) and the Flexor Carpi Ulnaris (FCU). The controller was tested on five neurologically intact patients and showed promising results.

Some advanced feedforward control architectures that use adaptive ANN have been applied to FES of the hand and/or wrist. In ([Fujita et al. \(1998\)](#)) work aiming to establish the feasibility of using an ANN learning controller for generating hand posture stimulus is presented. The training data for a three-layered neural network were obtained using a 3D magnetic position sensing system of FES hand motion. The controller

demonstrated the ability to cope with the non-linearity of the system. The disadvantage of using ANN controllers is the need of extensive training and the training procedure often not possible in real-time, which is required especially in case of clinical trials with stroke patients. Additionally there is no simple relationship between the learned weights of the neural network and the plant parameters, as the operation of the trained network has a hidden structure. This precludes stability and convergence analysis.

2.4 Iterative Learning Control

Iterative learning control (ILC) is an example of a feed-forward control approach, that can be an effective alternative for ANN controllers. ILC is a control methodology developed for uncertain dynamic systems that operate in a repetitive manner over a fixed time interval. ILC can improve the transient response and tracking performance of such systems by learning from past actions. The concept of ILC emerged extensively with publications of Arimoto et al. (1984a), that introduced firstly the Derivative-type ILC (D-type ILC) and Proportional-type ILC (P-type ILC) afterwards Arimoto et al. (1984b). Henceforward, ILC has remained a very active area of research and this has led to development of many new and advanced ILC schemes. These include: PID type algorithms, robust, adaptive, predictive and optimal ILC schemes, as well as approaches such as a fuzzy (F) - based ILC , Neural Network (NN) - based ILC and Fuzzy Neural Network (FNN)-based ILC for both linear and nonlinear systems. ILC algorithms has been widely implemented on industrial robot manipulators, certain types of medical equipment and within manufacturing. Originating from the field of robotics, ILC still attracts significant research interest in both theoretical and experimental domains Bristow et al. (2006).

The main concept of ILC is to iteratively find an input sequence such that the output of the system is as close as possible to a desired output, using information gathered from past trial(s). Hence, the ILC is an iterative approach, it can be formulated in the discrete-time domain. The state space representation of a general nonlinear discrete-time time-invariant control system has following form:

$$\begin{aligned} \mathbf{x}_k(t+1) &= \mathbf{f}[\mathbf{x}_k(t), \mathbf{u}_k(t)] \\ \mathbf{y}_k(t) &= \mathbf{h}[\mathbf{x}_k(t)] \end{aligned} \quad (2.1)$$

where $k = 1, 2, \dots$ is the trial index, $t \in [0, 1, 2, \dots, N - 1]$ is the sample number and $\mathbf{x}_k(t)$, $\mathbf{u}_k(t)$ and $\mathbf{y}_k(t)$ are the state, input and output vectors respectively on the k^{th} trial.

Let $\mathbf{y}_d(t)$ denotes the desired (reference) trajectory and $\mathbf{e}_k(t) = \mathbf{y}_d(t) - \mathbf{y}_k(t)$ is the error on k^{th} trial. The principal design idea behind ILC is to make the tracking error

signal converge to zero as the number of trials goes to infinity.

P-type

In the simples P-type ILC, controller learns from the error of the current trial (k) and produces the input for the next trial ($k+1$) in the form:

$$\mathbf{u}_{k+1}(t) = \mathbf{u}_k + L\mathbf{e}_k(t) \quad (2.2)$$

where L denotes the learning gain.

Phase-Lead ILC

Instead of using the instant error, Phase-Lead ILC can anticipate the error at advance time step λ , that can be varied to accommodate changes in the system. The phase lead control update law is following:

$$\mathbf{u}_{k+1}(t) = \mathbf{u}_k(t) + L\mathbf{e}_k(t + \lambda) \quad (2.3)$$

where \mathbf{u}_k and \mathbf{u}_{k+1} are the control inputs of the current and next trial respectively, t is the sample number, L is proportional learning gain and λ is the phase-lead in samples. The term $L\mathbf{e}_k(t + \lambda)$ is the core novel feature of ILC as it uses data that is not causal in the standard systems sense. In particular, ILC at sample instant p allows the use of information at future values of p , where this is possible because this term uses information generated on the previous trial. If such a term is not possible then it can be shown that the ILC can be expressed as a standard feedback control scheme.

2.4.1 Optimal ILC Algorithms

Optimisation is a process of determining the best solution for varieties of problems. Optimal ILC attempts to find solution to a control problem using certain optimisation criterion, termed cost function. Usually the cost function provides some description of the tracking error, which supposed to be minimized by the controller. Standard ILC cost function can be expressed as:

$$\min_{\mathbf{u}} \|\mathbf{y}_d - \mathbf{g}(\mathbf{u})\|^2 \quad (2.4)$$

Gradient-based ILC

The gradient-based ILC algorithm ILC update law is following

$$\mathbf{u}_{k+1} = \mathbf{u}_k + \alpha \mathbf{g}'(\mathbf{u}_k)^T \mathbf{e}_k \quad (2.5)$$

where the derivative $\mathbf{g}'(\mathbf{u}_k)$ is equivalent to the system linearisation around \mathbf{u}_k and is represented by the $pN \times mN$ matrix

$$\mathbf{g}'(\mathbf{u}_k) = \begin{bmatrix} \frac{\partial \mathbf{g}_1}{\partial \mathbf{u}_k(0)} & \frac{\partial \mathbf{g}_1}{\partial \mathbf{u}_k(1)} & \cdots & \frac{\partial \mathbf{g}_1}{\partial \mathbf{u}_k(N-1)} \\ \frac{\partial \mathbf{g}_2}{\partial \mathbf{u}_k(0)} & \frac{\partial \mathbf{g}_2}{\partial \mathbf{u}_k(1)} & \cdots & \frac{\partial \mathbf{g}_2}{\partial \mathbf{u}_k(N-1)} \\ \vdots & \vdots & \ddots & \vdots \\ \frac{\partial \mathbf{g}_N}{\partial \mathbf{u}_k(0)} & \frac{\partial \mathbf{g}_N}{\partial \mathbf{u}_k(1)} & \cdots & \frac{\partial \mathbf{g}_N}{\partial \mathbf{u}_k(N-1)} \end{bmatrix} \quad (2.6)$$

Note, that local tracking of an arbitrary reference is only possible if $\mathbf{g}'()$ has full row rank which also implies $m \leq p$ since the convergence within is $P(\mathbf{I} - \alpha \mathbf{g}'(\mathbf{u}_{\text{inf}}) \mathbf{g}'(\mathbf{u}_k)^T) < 1$.

Newton method-based ILC

As the name suggests, Newton method-based ILC is based on the Newton algorithm used in non-linear optimization. Translating the Newton algorithm to the considered ILC problem leads to the following ILC update in the case where $\mathbf{g}'()$ is square and full rank

$$\mathbf{u}_{k+1} = \mathbf{u}_k + \mathbf{g}'(\mathbf{u}_k)^{-1} \mathbf{e}_k \quad (2.7)$$

Calculating the inverse and derivative is computationally expensive, so writing equation (2.7) as

$$\mathbf{u}_{k+1} = \mathbf{u}_k + \mathbf{z}_{k+1} \quad (2.8)$$

converts the problem to that of solving the equation $\mathbf{z}_{k+1} = \mathbf{g}'(\mathbf{u}_k)^{-1} \mathbf{e}_k$, or

$$\mathbf{e}_k = \mathbf{g}'(\mathbf{u}_k) \mathbf{z}_{k+1} \quad (2.9)$$

In this way calculation of the inverse is avoided. Further details appear in [Lin et al. \(2006a\)](#).

Point to point ILC

The application of ILC in the area of point-to-point motion control offers the potential to benefit from the ability to learn from experience gained over previous trials of the task. Point-to-point ILC is a technique applied to tracking tasks which require the plant output to reach given points at selected time instants, without the specification of intervening reference points [Freeman and Tan \(2011\)](#) and [Freeman et al. \(2011\)](#). The method of [Freeman et al. \(2011\)](#) is applied for plant output specified at a fixed number, M , of sample instants given by N_1, N_2, \dots, N_M , where $M \leq N$. Let the prescribed values of the output at these instants be $\mathbf{u}_1, \mathbf{u}_2, \dots, \mathbf{u}_M$, where $\mathbf{u}_i \in \mathbb{R}^p$. The gradient

method may be applied to such point-to-point constraints simply by exchanging (2.4) for

$$\min_u \|\bar{\mathbf{y}}_d - \Phi \mathbf{g}(\mathbf{u})\|_2^2 \quad (2.10)$$

where the $pM \times pN$ matrix Φ has block-wise components

$$\Phi_{i,j} = \begin{cases} \mathbf{I}_p & j = N_i, \quad i = 1, 2 \dots M \\ \mathbf{0}_p & \text{otherwise} \end{cases} \quad (2.11)$$

where \mathbf{I}_p and $\mathbf{0}_p$ are the $p \times p$ identity and zero matrices respectively, and the hand configurations at the M points of interest are contained in the vector

$$\bar{\mathbf{y}}_d = \left[\mathbf{y}_1^T \quad \mathbf{y}_2^T \quad \cdots \quad \mathbf{y}_M^T \right]^T \in \mathbb{R}^{pM} \quad (2.12)$$

The gradient descent iterative solution to (3.53) is

$$\mathbf{u}_{k+1} = \mathbf{u}_k + \beta (\Phi \mathbf{g}'(\mathbf{u}_k))^T (\bar{\mathbf{y}}_d - \Phi \mathbf{g}(\mathbf{u}_k)) \quad (2.13)$$

which in the ILC framework, using experimentally recorded data \mathbf{q}_k , is

$$\mathbf{u}_{k+1} = \mathbf{u}_k + \beta (\Phi \mathbf{g}'(\mathbf{u}_k))^T (\bar{\mathbf{y}}_d - \Phi \mathbf{y}_k) \quad (2.14)$$

It is possible to show that the feasibility space is enlarged compared with the standard tracking framework. In particular Φ can be selected to ensure $\Phi \mathbf{g}'()$ has full row rank and hence guarantee feasibility. Given an underactuated setup, conditions can be derived for the existence of a feasible tracking task by reducing the point-to-point times [Freeman et al. \(2011\)](#).

2.5 ILC in Stroke Rehabilitation - Previous Research

ILC can be applied to processes that are required to repeat the same finite duration task over and over again. One form of stroke rehabilitation is to ask the patient to make an attempt to complete a task, such as reaching out over a table top to a cup, with FES assistance. During each attempt, the error between a prescribed path and that actually generated by the patient can be measured and then used in the rest time to update the FES signal to be applied on the next attempt. A critical objective is that if the patient is improving with each attempt then the level of voluntary effort should increase and the applied stimulation decrease. In ILC the core idea is to use information gathered on previous executions to update the control signal used for the next one and thereby sequentially improve performance. [Dou et al. \(1999\)](#) has confirmed that ILC schemes can effectively react to time-varying effects of the muscle fatigue which comprises a major component of the non-linearity in the system and reject repeatable uncertainties and



Figure 2.6: Planar arm movements rehabilitation system

disturbances. Currently, there is no research involving the application of ILC in FES of hand function. Existing ILC systems for the upper-limb are focused only on restoration of arm movements.

ILC mediated by Functional Electrical Stimulation has been used in robotic-assisted rehabilitation of the upper-limb after a stroke, to produce two different systems, each with successful clinical trials. [Freeman et al. \(2009b\)](#) presented results of the application of two forms of ILC to control the stimulation level used to assist hemiplegic patients in completion of planar reaching tasks. The planar rehabilitation system used in the clinical trials is shown in Figure 2.6.

The training procedure was based on tracking elliptical trajectories in a repetitive mode. During the clinical trials, patients were asked to track a spot of light by moving a vertical rod over a flat board. If they tracked the target well, then on the next attempt the stimulation support was reduced, and if not it was increased. Treatment consisted of performing a selection of 27 treatment tasks, comprising three different trajectories, each with three levels of reach extension in one of three oriented directions. The clinical trials have shown promising results of arm function improvement after only 18 treatment sessions ([Hughes et al. \(2009b\)](#)). To increase the accuracy of performance, dynamic models of the arm were developed ([Freeman et al. \(2009a\)](#)). This was the first use of advanced model-based electrical stimulation controllers in clinical trials, that was precise enough to support the Rushton hypothesis ([Freeman et al. \(2008\)](#)). [Cai et al. \(2011\)](#) presented results of the subsequent research programme in which ILC algorithms were used to assisted 3D movements of the patient's arm to deliver effective treatment. Research confirmed the efficacy of the 3D arm rehabilitation system ([Meadmore et al. \(2011\)](#)). The system is shown in Figure 2.7.

The work so far conducted using ILC focuses on the restoration of arm movements. The next step in recovering the use of the upper extremity is the relearning of hand

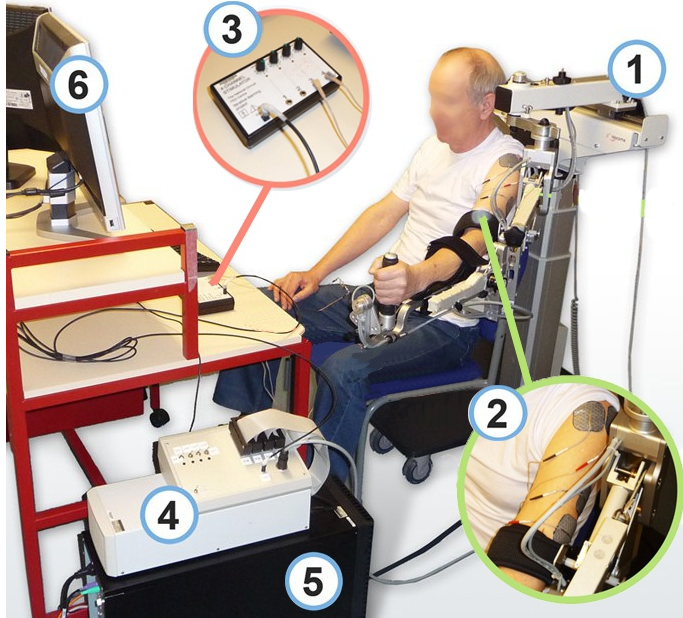


Figure 2.7: 3D Arm rehabilitation system for stroke patients. The system includes a mechanical robotic unweighting system used to support patient's arm - ARMEO (1), FES hardware (2,3), control system and user software including custom-made virtual reality module (4,5,6).

functions. Design of appropriate control algorithms is a key element of any FES-based rehabilitation system. ILC algorithms were chosen for this purpose, as they were recognized to be an effective FES control method for the arm. However, the use of ILC controllers for the hand and wrist to adjust stimulation parameters during task performance, in order to assist the patient's intention as accurately as possible remains an challenging open research question. The next step is therefore to investigate the possibility of using ILC for FES control of hand and wrist and ultimately incorporate the control procedures into the FES-based rehabilitation system.

Chapter 3

The Hand Model and ILC

The hand can be considered as a mechanical system and it is possible to apply mechanical principles to study it. In this context, it involves two elements: muscles serve as the motor to provide driving force, and tendons, bones, and joints transmit the motor's driving force ([Valero-Cuevas et al., 2003](#)). The overall structure is arranged around skeletal joints and links. The complexity of the human hand makes the construction of accurate models a very challenging task. However the usefulness and necessity of using such models in many different science disciplines and problems, makes hand modelling an extremely active research area. Hand models arise in areas such as surgery ([Esteki and Mansour, 1997](#)), biomechanics, robotics [Miller et al. \(2005\)](#); [Deshpande et al. \(2009\)](#), and computer graphics [Sueda et al. \(2008\)](#).

The diversity of existing hand models results from consideration of many different factors such as: model application, level of complexity, and anatomical accuracy. Generally, hand models can be modelled in terms of three main aspects: kinematics, dynamics, and shape. In control analysis, only the two first aspects, kinematics and dynamics, are of principal importance. Kinematic models describe the motion position, velocity and acceleration of bodies and systems without consideration of the forces that cause the motion. Conversely, dynamics focuses on the causes of the motion ([Spong and Vidyasagar, 1989](#)). Biomechanical models are characterized by their great complexity and anatomical accuracy, building on kinematic hand model based on the underlying skeleton structure of the hand. This consists of a hierarchical arrangement of bones which combine to form a complete musculoskeletal model ([Albrecht et al., 2003](#); [Tsang et al., 2005](#)). Musculoskeletal modeling has been a mainstream topic of biomechanics research worldwide over the last three decades. This class of model requires the intensive use of multibody system dynamics analysis tools integrated with an understanding of which aspects of the underlying biological model are most important. The control problem under consideration in this thesis requires use of an anatomically accurate model, containing muscles and tendons.

This chapter provides an overview of the development of hand model. A variety of models with different level of kinematic and dynamic complexity (2D and 3D case) was analysed over the course of the study. Since this model will be used in clinical tests with patients, rather than purely for the purposes of simulation, care was taken to develop simplest possible model that integrates realistic anatomical and physiological aspects alongside a standard kinematic and dynamic representation of a multi-body system.

3.1 The 2D hand and wrist model

The 2D hand and wrist model suitable for clinical use includes a single composite finger, representing the combined action of four fingers, wrist and neglects the thumb orientation. The finger and wrist are modeled as 3-link rigid body system, consisting of 3 active revolute joints, as shown in Figure 3.1. This still provides an accurate representation of the hand since 42% of the functional movements of the hand involve the four fingers moving together (Ingram et al., 2008). Link 1 represents the II-V Metacarpal bones connected by the wrist joint, Links 2 and 3 represent proximal and middle phalangeals of the finger connected by the Metacarpal-Phalangeal joint (MCP) and Proximal-Interphalangeal joint (PIP) respectively.

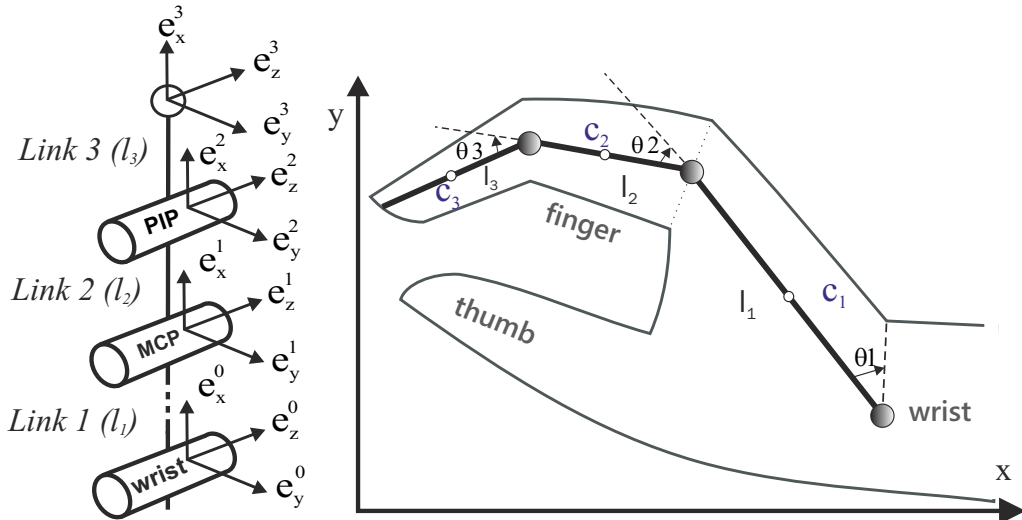


Figure 3.1: Planar hand model

The kinematic model of the finger together with the coordinate frames is shown in Figure 3.1. The x -, y - and z -directions of the i^{th} frame in a right-handed Cartesian coordinate system are denoted by \mathbf{e}_x^i , \mathbf{e}_y^i and \mathbf{e}_z^i respectively. The coordinate frame \mathbf{e}^0 , \mathbf{e}^1 , \mathbf{e}^2 are located in each joint of the finger (wrist, MCP and PIP joints respectively). The joint \mathbf{e}^3 has origin at the tip of the finger. The angles θ_1 , θ_2 and θ_3 represents the

three rotations of the metacarpal bones about wrist and proximal and middle phalanges about MCP and PIP joints respectively.

In general, frame i can be expressed in frame $i + 1$ coordinates by means of the rotation matrix ${}^i\mathbf{T}_{i+1}$

$$\mathbf{e}^i = {}^i\mathbf{T}_{i+1}\mathbf{e}^{i+1} \quad (3.1)$$

and the rotation matrices for $i = 0, 1, 2, 3$ assume the form

$${}^i\mathbf{T}_{i+1} = \begin{bmatrix} \cos(\theta_{i+1}) & -\sin(\theta_{i+1}) & 0 \\ \sin(\theta_{i+1}) & \cos(\theta_{i+1}) & 0 \\ 0 & 0 & 1 \end{bmatrix} \quad (3.2)$$

By extension, to go from frame i to frame $i + 2$ a multiplication of the rotation matrices can be used

$$\mathbf{e}^i = {}^i\mathbf{T}_{i+1} {}^{i+1}\mathbf{T}_{i+2} \mathbf{e}^{i+2} \quad (3.3)$$

and to go from frame $i + 1$ to frame i the inverse of the rotation matrices is applied

$$\begin{aligned} \mathbf{e}^{i+1} &= {}^{i+1}\mathbf{T}_i \mathbf{e}^i \\ \mathbf{e}^{i+1} &= ({}^i\mathbf{T}_{i+1})^{-1} \mathbf{e}^i \end{aligned} \quad (3.4)$$

These transformations are now used to obtain a dynamic model of the system.

Equations of motion

The dynamic model is formulated using the Lagrange method. The Lagrange's equation of motion for a non-conservative system is given by:

$$\frac{d}{dt} \left(\frac{\partial L}{\partial \dot{\mathbf{q}}} \right) - \frac{\partial L}{\partial \mathbf{q}} = \mathbf{Q}^{\text{NC}} \quad (3.5)$$

where \mathbf{q} denotes the generalized coordinates of the system:

$$\mathbf{q} = [\theta_1, \theta_2, \theta_3] \quad (3.6)$$

and L is the Lagrangian defined as the difference between kinetic energy (K) and potential energy (V):

$$L = K - V \quad (3.7)$$

The term \mathbf{Q}^{NC} represents the component due to non-conservative forces such as damping and externally applied torque. Substituting (3.7) into (3.5) gives:

$$\frac{d}{dt} \left(\frac{\partial K}{\partial \dot{\mathbf{q}}} \right) - \frac{\partial K}{\partial \mathbf{q}} + \frac{\partial V}{\partial \mathbf{q}} = \mathbf{Q}^{NC} \quad (3.8)$$

The kinetic energy can be expressed in terms of the mass matrix $\mathbf{M}(\mathbf{q})$:

$$K = \frac{1}{2} \dot{\mathbf{q}}^T \mathbf{M}(\mathbf{q}) \dot{\mathbf{q}} \quad (3.9)$$

The first derivative of kinetic energy K with respect to \mathbf{q} can be rewritten as

$$\frac{\partial K}{\partial \mathbf{q}} = \frac{1}{2} \begin{bmatrix} \dot{\mathbf{q}}^T \frac{\partial \mathbf{M}}{\partial q_1} \dot{\mathbf{q}} \\ \vdots \\ \dot{\mathbf{q}}^T \frac{\partial \mathbf{M}}{\partial q_n} \dot{\mathbf{q}} \end{bmatrix} \quad (3.10)$$

The first derivative of kinetic energy K with respect to $\dot{\mathbf{q}}$ can be expressed as

$$\frac{\partial K}{\partial \dot{\mathbf{q}}} = \frac{\partial}{\partial \dot{\mathbf{q}}} \left[\frac{1}{2} \dot{\mathbf{q}}^T \mathbf{M}(\mathbf{q}) \dot{\mathbf{q}} \right] = \mathbf{M}(\mathbf{q}) \dot{\mathbf{q}} \quad (3.11)$$

Substituting (3.9),(3.10) and (3.11) into (3.8) yields

$$\mathbf{M}(\mathbf{q}) \ddot{\mathbf{q}} + \underbrace{\dot{\mathbf{M}}(\mathbf{q}) \dot{\mathbf{q}} - \frac{1}{2} \frac{\partial}{\partial \mathbf{q}} [\dot{\mathbf{q}}^T \mathbf{M}(\mathbf{q}) \dot{\mathbf{q}}]}_{\mathbf{C}(\mathbf{q}, \dot{\mathbf{q}})} + \underbrace{\frac{\partial V(\mathbf{q})}{\partial \mathbf{q}}}_{\mathbf{G}(\mathbf{q}, \dot{\mathbf{q}})} = \mathbf{Q}^{NC} \quad (3.12)$$

Equation (3.12) can be expressed in more compact form

$$\mathbf{M}(\mathbf{q}) \ddot{\mathbf{q}} + \mathbf{C}(\mathbf{q}, \dot{\mathbf{q}}) + \mathbf{G}(\mathbf{q}, \dot{\mathbf{q}}) = \mathbf{Q}^{NC} \quad (3.13)$$

where $\mathbf{M}(\mathbf{q})$ is the inertia matrix, $\mathbf{C}(\mathbf{q}, \dot{\mathbf{q}})$ denotes the centrifugal and Coriolis forces, $\mathbf{G}(\mathbf{q}, \dot{\mathbf{q}})$ is the vector of the gravitational forces and \mathbf{Q}^{NC} vector of non-conservative forces.

Kinetic energy

The kinetic energy of a single rigid body can be described by

$$T = \frac{1}{2} m \dot{\mathbf{r}}^T \dot{\mathbf{r}} + \frac{1}{2} \boldsymbol{\omega}^T \mathbf{I}_O \cdot \boldsymbol{\omega} \quad (3.14)$$

The first term of the right hand side relates to the translational kinetic energy of the rigid body, where m is its mass and $\dot{\mathbf{r}}$ is the velocity of the center of mass (\mathbf{r} is the position of the center of mass). The second term represents the rotational kinetic energy of the

rigid body, where rotation is about a fixed point O . The angular velocity vector $\boldsymbol{\omega}$ represents all the rotations from the base frame to the body-fixed frame. The tensor \mathbf{I}_O is the mass moment of the inertia tensor of the rigid body with respect to the point of rotation.

The kinetic energy of a system composed of multiple bodies is the sum of the kinetic energy of each body. Thus kinetic energy of the three-link finger equals

$$T = \frac{1}{2} \sum_{i=1}^3 m_i \dot{\mathbf{r}}_i^T \dot{\mathbf{r}}_i + \frac{1}{2} \sum_{i=1}^3 \boldsymbol{\omega}_i^T \mathbf{I}_{O_i} \boldsymbol{\omega}_i \quad (3.15)$$

where m_i is a mass of i -th phalangeal, $i = 1, 2, 3$, \mathbf{I}_{O1} is the mass moment of inertia tensor of the proximal phalangeal with respect to the MCP joint and \mathbf{I}_{O2} , \mathbf{I}_{O3} are the mass moment of inertia tensor of the middle and distal phalangeals with respect to the PIP and DIP joints respectively. Each limb is considered as a cylinder about the local x-axis, hence the mass moment of inertia can be expressed using the following formulae:

$$I_x = mr_c^2 \quad (3.16)$$

$$I_y = I_z = \frac{mr_c^2}{4} + \frac{ml_c^2}{12} \quad (3.17)$$

where m is the mass, r_c the radius and l_c the length of the cylinder. Firstly, the mass moment of inertia tensor with respect to the centre of mass is determined. The mass moment of inertia tensors with respect to the center of mass are expressed as

$$\begin{aligned} \mathbf{I}_{CM1} &= \mathbf{e}^{1^T} \begin{bmatrix} I_1 & 0 & 0 \\ 0 & I_2 & 0 \\ 0 & 0 & I_2 \end{bmatrix} \mathbf{e}^1 \quad , \quad \mathbf{I}_{CM2} = \mathbf{e}^{2^T} \begin{bmatrix} I_3 & 0 & 0 \\ 0 & I_4 & 0 \\ 0 & 0 & I_4 \end{bmatrix} \mathbf{e}^3 \\ \mathbf{I}_{CM1} &= \mathbf{e}^{3^T} \begin{bmatrix} I_5 & 0 & 0 \\ 0 & I_6 & 0 \\ 0 & 0 & I_6 \end{bmatrix} \mathbf{e}^3 \end{aligned} \quad (3.18)$$

Secondly, the Parallel Axes Theorem (3.19) is used to calculate the mass moment of inertia tensors with respect to the point of rotation.

$$\mathbf{I}_O = \mathbf{I}_{CM} + m (\mathbf{r}^T \mathbf{r} \mathbf{I} - \mathbf{r} \mathbf{r}^T) \quad (3.19)$$

with \mathbf{I} the identity tensor. The resulting mass moment of inertia about each of the joints (MCP, PIP and DIP) for the three phalanges respectively are

$$\begin{aligned}\mathbf{I}_{\mathbf{O}1} &= \mathbf{e}^{1^T} \begin{bmatrix} J_1 & 0 & 0 \\ 0 & J_2 & 0 \\ 0 & 0 & J_2 \end{bmatrix} \mathbf{e}^1 \quad , \quad \mathbf{I}_{\mathbf{O}2} = \mathbf{e}^{2^T} \begin{bmatrix} J_3 & 0 & 0 \\ 0 & J_4 & 0 \\ 0 & 0 & J_4 \end{bmatrix} \mathbf{e}^3 \\ \mathbf{I}_{\mathbf{O}3} &= \mathbf{e}^{3^T} \begin{bmatrix} J_5 & 0 & 0 \\ 0 & J_6 & 0 \\ 0 & 0 & J_6 \end{bmatrix} \mathbf{e}^3\end{aligned}\tag{3.20}$$

with $J_1 = I_1$, $J_2 = I_2 + m_1 c_1^2$, $J_3 = I_3$, $J_4 = I_4 + m_2 c_2^2$, $J_5 = I_5$, and $J_6 = I_6 + m_3 c_3^2$.

The position vectors are:

$$\begin{aligned}\mathbf{r}_1 &= [c_1 \ 0 \ 0] \mathbf{e}^1 \\ \mathbf{r}_2 &= [l_1 \ 0 \ 0] \mathbf{e}^1 + [c_2 \ 0 \ 0] \mathbf{e}^2 \\ \mathbf{r}_3 &= [l_1 \ 0 \ 0] \mathbf{e}^1 + [l_2 \ 0 \ 0] \mathbf{e}^2 + [c_3 \ 0 \ 0] \mathbf{e}^3\end{aligned}\tag{3.21}$$

The velocity vectors can be determined by calculating the derivatives of the position vectors

$$\dot{\mathbf{r}}_i = \frac{d\mathbf{r}_i}{dt}\tag{3.22}$$

The vectors of angular velocity equal

$$\boldsymbol{\omega}_1 = \dot{\theta}_1 \mathbf{e}_z^1\tag{3.23}$$

$$\boldsymbol{\omega}_2 = \boldsymbol{\omega}_1 + \dot{\theta}_2 \mathbf{e}_z^2\tag{3.24}$$

$$\boldsymbol{\omega}_3 = \boldsymbol{\omega}_2 + \dot{\theta}_3 \mathbf{e}_z^3\tag{3.25}$$

Potential energy

The potential energy of a system is the sum of the internal energy (for example elastic energy) and the potential energy of the conservative external forces V

$$V = \sum_{i=1}^M \int_0^{x^i} K_i(y) y dy - \sum_{j=1}^N m_j \mathbf{g}^T \mathbf{r}_j\tag{3.26}$$

where M is the number of springs, $K_i(y)$ the nonlinear stiffness function of spring i and x^i the elongation of the spring. The gravitational acceleration vector is denoted by \mathbf{g} . In the case considered we can assume that the only conservative external force is the gravity force and that the muscle groups which actuate each joint produce a stiffness that can be represented by a spring with zero elongation at the initial position $\theta_{0,i}$ and

with a stiffness k_i , $i = 1, 2, 3$. In the simplest case, the potential energy of the finger equals

$$V = \sum_{i=1}^3 \left[\frac{1}{2} k_i (\theta_{0,i} - \theta_i)^2 - m_i \mathbf{g}^T \mathbf{r}_i \right] \quad (3.27)$$

with the gravitational acceleration vector \mathbf{g} aligned with the axis $-\mathbf{e}_z^1$. However during purely horizontal movement of the finger the gravity can be neglected.

Generalized non-conservative forces

The generalized non-conservative forces consist of all externally applied non-conservative forces and moments, together with, all forces and moments due to damping and friction.

$$\mathbf{Q}^{NC} = \sum_{i=1}^{n_F} \left(\frac{d\mathbf{a}_i}{d\mathbf{q}} \right) \mathbf{F}_i^{NC} + \sum_{j=1}^{n_M} \left(\frac{d\theta_j}{d\mathbf{q}} \right) \boldsymbol{\omega}^T(\theta_j) \mathbf{M}_j^{NC} \quad (3.28)$$

where n_F , n_M represent the number of applied non-conservative forces and moments respectively. In addition, \mathbf{a}_i is the absolute position vector of the point at which \mathbf{F}_i^{NC} is exerted, θ_j the rotational parameters and $\boldsymbol{\omega}(\theta_j)$ a column vector containing the directions of rotation.

The finger model consists of revolute joints, thus only generalized non-conservative moments appear. In each direction of rotation viscous friction and a driving torque are considered ($n_M = 3$). In the simplest case, the vector of non-conservative moments can be written in the form

$$\mathbf{M}^{NC} = \underbrace{\begin{bmatrix} \tau_1 \\ \tau_2 \\ \tau_3 \end{bmatrix}}_{\boldsymbol{\tau}} - \underbrace{\begin{bmatrix} b_1 \dot{\theta}_1 \\ b_2 \dot{\theta}_2 \\ b_3 \dot{\theta}_3 \end{bmatrix}}_{\mathbf{F}} \quad (3.29)$$

where \mathbf{F} is the vector of friction with b_i the viscous friction coefficient and $\boldsymbol{\tau}$ represents the vector of applied torque.

Combining (3.13), (3.28) and (3.29), the dynamic model of the human finger can be rewritten into the form

$$\mathbf{M}(\mathbf{q}) \ddot{\mathbf{q}} + \mathbf{C}(\mathbf{q}, \dot{\mathbf{q}}) + \mathbf{F}(\mathbf{q}, \dot{\mathbf{q}}) + \mathbf{G}(\mathbf{q}, \dot{\mathbf{q}}) = \boldsymbol{\tau} \quad (3.30)$$

where $\boldsymbol{\tau}$ is the vector of moments produced through application of FES to muscles of the fingers, and $\mathbf{F}(\mathbf{q}, \dot{\mathbf{q}})$ is the vector of frictional components acting about each joint. (Freeman et al., 2009b).

Electrically stimulated muscles of the hand generate pulling forces causing the finger/thumb movement. Kinetic functions of the musculotendon units in the fingers,

however, are especially difficult to evaluate due to their anatomical complexity and multiarticular character. However, moment arms at the different joints will differ, determining the relative effect of stimulation at each joint.

Each human finger has at least 6 muscles and 7 in the case of the index finger. The strength of the finger depends on the anatomical structure and the maximum effort of each individual muscle involved ([Brook et al., 1995](#)). Moreover, muscles of fingers act through a complex tendon network, (the extensor mechanism). The network, firstly approximated by Winslow as a longitudinally symmetric tendon rhombus, was modified in subsequent research ([Sancho-Bru et al., 2001](#); [Valero-Cuevas et al., 2007](#)).

The anatomical structure of fingers takes as inputs muscular actions and produces as outputs motions and forces. Many of the muscles/tendons within the finger span more than one joint, which means the muscle forces to joint torque relationship becomes more complicated. The tension along the muscle or tendon remains the same, even as it changes direction when crossing different joints. However, its moment arms at the different joints will differ, determining its relative effect at each joint in terms of actuating torque. The transformation from positive muscle forces \mathbf{f} to the lower - dimensional net joint torques $\boldsymbol{\tau}$ at the finger joints can be defined as in ([Valero-Cuevas, 2009](#))

$$\boldsymbol{\tau} = \mathbf{R}(\mathbf{q})\mathbf{f} = \begin{bmatrix} r_{11} & \dots & r_{1j} \\ \vdots & \ddots & \vdots \\ r_{i1} & \dots & r_{ij} \end{bmatrix} \begin{bmatrix} f_1 \\ \vdots \\ f_j \end{bmatrix} \quad (3.31)$$

where $\mathbf{R}(\mathbf{q})$ is matrix of moment arms where each entry is the signed scalar moment arm value that transforms a positive muscle force into torques at the various joints it crosses. Most techniques for estimating moment arm values rely on kinematic measurements, such as correlation between the tendon excursion and the resultant joint rotation ([Brook et al., 1995](#)), or the geometric distance between the tendon action line and the joint estimated using medical imaging techniques ([Wilson et al., 1999](#)).

Calculation of moment arms values

The r_{ij} element of the moment arm matrix can be evaluated by differentiating the excursion (displacement) E of the j^{th} tendon with respect to the i^{th} joint angle

$$r_{ij} = \frac{\partial E_j(q_i)}{\partial q_i} \quad (3.32)$$

Several dynamic muscle models of the finger have been developed to describe the kinetic functions of finger-muscle tendons. Landsmeer ([Landsmeer, 1955](#)) laid the foundation

of later studies on spatial relationships between tendons and muscles and their associated joints in the hand. This paper proposed three different models of tendon-joint displacement relationships for flexion/extension of the finger. Although there is a lack of quantitative information in his studies, Landsmeer's models provided a basis for much future research. Determining exact muscle or tendon forces for dynamic modelling is extremely difficult. There exists the difficulty of measuring the exact forces in the different tendons and muscles as various forces come into action at different points to produce a particular movement. Most of models use inverse dynamics to examine the muscle force coordination patterns that generate the observed movements (Brook et al., 1995) or fingertip force patterns (Sancho-Bru et al., 2001). Additionally, existing models are only valid for certain hand configurations (Chao et al., 1976; Roloff et al., 2006; Sghaier et al., 2007).

3.2 Musculotendon system

The musculoskeletal structure of the finger and wrist included in the model is shown in Figure 3.2. The wrist joint is assumed to be actuated by three extensor muscles: Extensor Communis (EC), Extensor Carpi Radialis Longus (ECR) and Extensor Carpi Ulnaris (ECU). The muscles of the finger act through a complex tendon network, termed the extensor mechanism. The network is approximated by a longitudinally symmetric tendon rhombus, consisting of active and the passive tendons, as shown in Figure 3.2. The proposed finger model is based on the biomechanical model given in (Theodorou et al., 2011). The extensor mechanism of the finger includes 5 active tendons, driven by independently controlled muscles: the Flexor Digitorum Profundus (FDP), the Extensor Digitorum Communis (EC), the Ulnar and Radial Interosseous (UI and RI), the Lumbrical muscle (LU), and 3 passive tendons: the Radial Band (RB) the Ulnar Band (UB) and the Extensor Slip (ES).

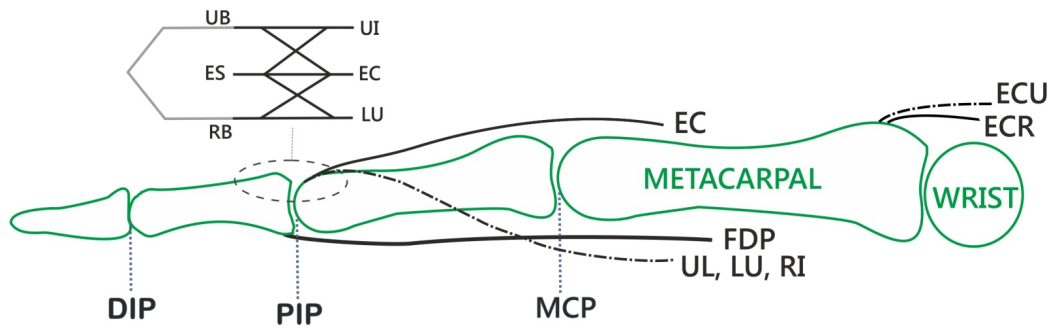


Figure 3.2: The network of the finger tendons (Vigouroux et al., 2006)

For the flexor muscle FDP, III. Landsmeer's model shown in Figure 3.3 is used ([Landsmeer, 1955](#)), where excursion is given by

$$E^{tendon} = \theta d^{tendon} + 2y^{tendon} \left(1 - \frac{\theta/2}{\tan(\theta/2)} \right) \quad (3.33)$$

where d^{tendon} is the distance from the straight part of the tendon towards the long axis and θ is the corresponding angle rotation. The term y^{tendon} corresponds to the distance from the end of the straight part towards the joint centre. This distance is measured along the axis of the bone.

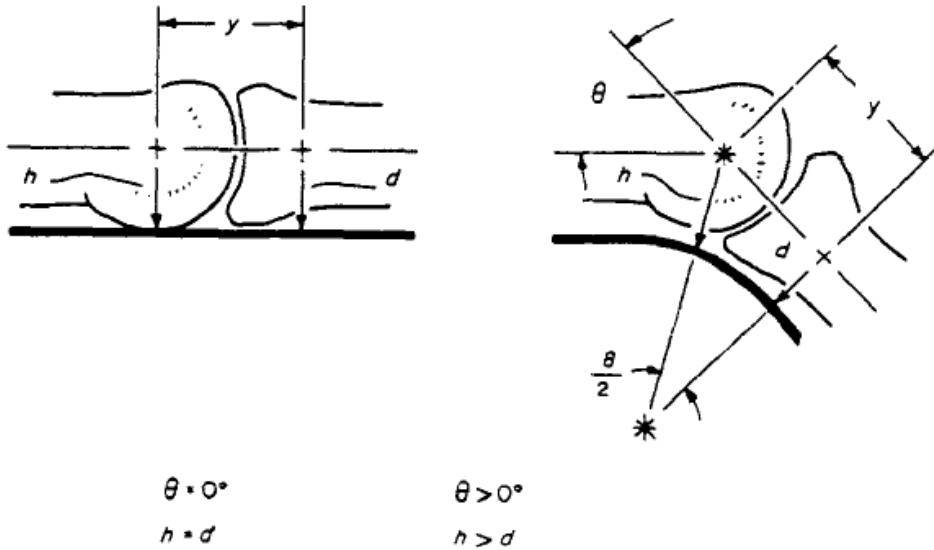


Figure 3.3: The III Landsmeer model of the finger ([Armstrong and Chaffin, 1978](#))

The remaining tendons are modelled as second order polynomial approximation of (3.33)

$$(b^{tendon} + h^{tendon}\theta)\theta \quad (3.34)$$

where b^{tendon} and h^{tendon} are constants.

The tendon excursion of the EC is a function of the wrist and MCP with the addition of the displacement, transformed to the PIP joint through the extensor mechanism

$$E^{EC} = -r_1^{EC}\theta_1 - r_2^{EC}\theta_2 + L(E_1, E_2, E_3) \quad (3.35)$$

where

$$E_1 = E^{ES}, \quad E_2 = E^{UB}, \quad E_3 = E^{RB} \quad (3.36)$$

and $L(E_1, E_2, E_3)$ is the excursion function defined as

$$L(E_1, E_2, E_3) = \sum_{i=1}^3 w_i E_i = 0, \quad w_i > 0 \quad \forall j = 1, 2, 3 \quad (3.37)$$

The excursions of remaining tendons in the considered case are expressed as functions of finger extension/flexion angles θ_2 and θ_3 . They are as follows

$$\begin{aligned} E^{FDP} &= \sum_{i=2}^3 \theta_i^{FDP} + 2y_i^{FDP} \left(1 - \frac{\theta_i/2}{\tan(\theta_i/2)} \right) \\ E^{ES} &= -r^{ES}\theta_3 \\ E_{RB} &= -(b^{RB} + h^{RB}\theta_3)\theta_3 \\ E_{UB} &= -(b^{UB} + h^{UB}\theta_3)\theta_3 \\ E^{RI} &= (b^{RI} + h^{RI}\theta_2)\theta_2 + E^{UB} \\ E^{UI} &= (b^{UI} + h^{UI}\theta_2)\theta_2 + E^{UB} \\ E^{LU} &= (b^{LU} + h^{LU}\theta_2)\theta_2 + E^{RB} - E^{FDP} \\ E^{ECU} &= (b^{ECU} + h^{ECU}\theta_1)\theta_1 \\ E^{ECR} &= (b^{ECR} + h^{ECR}\theta_1)\theta_1 \end{aligned} \quad (3.38)$$

Hence, applying (3.32), each column of moment arm matrix $\mathbf{R}(\mathbf{q})$ represents the moment arm vector corresponding to each muscle, yielding

$$\mathbf{R}(\mathbf{q}) = [\mathbf{R}^{FDP}, \mathbf{R}^{LU}, \mathbf{R}^{UI}, \mathbf{R}^{RI}, \mathbf{R}^{EC}, \mathbf{R}^{ECR}, \mathbf{R}^{ECU}] \quad (3.39)$$

Here the moment arm vectors for FDP is

$$\mathbf{R}^{FDP} = \begin{bmatrix} 0 \\ d_1^{FDP} + y_1^{FDP} \left(\frac{\sin(\theta_2) - \theta_2}{2 \sin^2(\theta_2)} \right) \\ d_2^{FDP} + y_2^{FDP} \left(\frac{\sin(\theta_3) - \theta_3}{2 \sin^2(\theta_3)} \right) \end{bmatrix} \quad (3.40)$$

and the moment arm vector for LU is given by

$$\mathbf{R}^{LU} = \begin{bmatrix} 0 \\ b^{LU} + 2h^{LU}\theta_2 - R_{\theta_2}^{FDP} \\ -b^{RB} - 2h^{RB}\theta_3 - R_{\theta_3}^{FDP} \end{bmatrix} \quad (3.41)$$

The moment arm vector for UI is

$$\mathbf{R}^{UI} = \begin{bmatrix} 0 \\ b^{UI} + 2h^{UI}\theta_2 \\ -b^{UB} - 2h^{UB}\theta_3 \end{bmatrix} \quad (3.42)$$

and the moment arm vector for EC has the form

$$\mathbf{R}^{EC} = \begin{bmatrix} -r_1^{EC} \\ -r_2^{EC} \\ -w_1 r^{ES} + w_2 R_{\theta_3}^{UB} + w_3 R_{\theta_3}^{RB} \end{bmatrix} \quad (3.43)$$

where

$$R_{\theta_3}^{UB} = -(b^{UB} + 2h^{UB}\theta_3) \quad (3.44)$$

$$R_{\theta_3}^{RB} = -(b^{RB} + 2h^{RB}\theta_3) \quad (3.45)$$

The moment arm vector for ECR equals

$$\mathbf{R}^{ECR} = [b^{ECR} + 2h^{ECR}, \quad 0, \quad 0]^T \quad (3.46)$$

and the moment arm vectors for ECU is

$$\mathbf{R}^{ECU} = [b^{ECU} + 2h^{ECU}, \quad 0, \quad 0]^T \quad (3.47)$$

Using relation (3.31), the torque at each joint can now be calculated as a function of the force in each muscle and the current joint angle vector. Each element of the muscle force vector $\mathbf{y}(\mathbf{u}, \mathbf{q}, \dot{\mathbf{q}})$ comprises the moment produced through the application of FES signal $u_j(t)$ to the j^{th} stimulated muscle, with

$$\mathbf{u} = [u_1 \quad \cdots \quad u_m]^T \quad (3.48)$$

As discussed in (Le et al., 2010), the most prevalent form of muscle representation is a Hill-type model of the form

$$y_i(u_i(t), q_i, \dot{q}_i) = h_i(u_i, t) \times F_{m,i}(l_{m,i}, \dot{l}_{m,i}), \quad i = 1, \dots, m \quad (3.49)$$

Here the term, $h_i(u_i, t)$ is a Hammerstein structure incorporating a static non-linearity, $h_{IRC,i}(u_i)$, representing the isometric recruitment curve, cascaded with linear activation dynamics, $h_{LAD,i}(t)$. These typically are second order, and in the considered case are modeled as a second order critically damped system with a natural frequency ω_n , and will be represented by the state-space model matrices $\mathbf{M}_{A,i}$, $\mathbf{M}_{B,i}$, $\mathbf{M}_{C,i}$. The term $F_{m,i}(l_{m,i}, \dot{l}_{m,i})$ models the multiplicative effect of the muscle length $l_{m,i}$ and muscle velocity on the active torque developed by the muscle.

3.3 FES control of hand and wrist using Newton method-based ILC

Often physical systems must be considered in the presence of constraints. The considered FES scheme shown in Figure 5.9, is an example of system with input constraints as it is required to generate only suitable electrical pulse signals to activate appropriate muscles in the hand and wrist. The activated muscles contract developing muscle forces, that combine to produce a desired movement/torque of the musculoskeletal system. Different stimulation parameters can be used as controlled variables, i.e. the current/voltage amplitude or the duration of the stimulus pulses (pulse width). In the considered case, the pulse width parameter was chosen to be the input of the system, since it provides a more consistent response across subjects, requires a smaller charge per stimulus pulse, and allows for greater selectivity of recruitment. The practical values of pulse width, that can be safely apply during the trials on human subjects, are within a range $[0, 350\mu\text{s}]$.

To take the design constraints as discussed into account, the point-to-point Newton method-based ILC with input constraint is used. The algorithm is applied to the hand and wrist system in simulation to investigate feasibility and performance capabilities prior to its future experimental use.

System description

From (A.1) the relationship between stimulation and joint angles can be expressed in state-space form as

$$\begin{aligned} \dot{\mathbf{x}}(t) &= \begin{bmatrix} \dot{\mathbf{q}} \\ \mathbf{M}(\Phi)^{-1}\mathbf{X}(\mathbf{q}, \dot{\mathbf{q}}) \\ \mathbf{M}_{A,1}x_1 \\ \vdots \\ \mathbf{M}_{A,p}x_p \end{bmatrix} + \begin{bmatrix} \mathbf{0} \\ \mathbf{0} \\ \mathbf{M}_{B,1}h_{IRC,1}(u_1) \\ \vdots \\ \mathbf{M}_{B,p}h_{IRC,p}(u_p) \end{bmatrix} \\ &:= \mathbf{f}(\mathbf{x}(t), \mathbf{u}(t)) \\ \mathbf{q}(t) &= [\mathbf{I} \quad \mathbf{0} \quad \cdots \quad \mathbf{0}] \mathbf{x}(t) := \mathbf{h}(\mathbf{x}(t)) \end{aligned} \tag{3.50}$$

where $\mathbf{x} = [\mathbf{q}^T, \dot{\mathbf{q}}^T, x_1^T \cdots x_j^T]^T$ and $\mathbf{X}(\mathbf{q}, \dot{\mathbf{q}})$ has i^{th} row



$$\mathbf{R}_i(\mathbf{q})\mathbf{M}_{C,i}x_i F_{m,i}(\mathbf{q}, \dot{\mathbf{q}}) - \mathbf{C}_i(\mathbf{q}, \dot{\mathbf{q}}) + \mathbf{F}_i(\mathbf{q}, \dot{\mathbf{q}}) \tag{3.51}$$

Hence, the ILC is an iterative approach, it can be formulated in the discrete-time domain. The discretised nonlinear stimulated hand and wrist system (3.50) has form

$$\begin{aligned}\mathbf{x}_k(t+1) &= \mathbf{f}[\mathbf{x}_k(t), \mathbf{u}_k(t)] \\ \mathbf{q}_k(t) &= \mathbf{h}[\mathbf{x}_k(t)]\end{aligned}\quad (3.52)$$

where $k = 1, 2, \dots$ is the trial number, $t \in [0, 1, 2, \dots, N - 1]$ is the sample number and $\mathbf{x}_k(t)$, $\mathbf{u}_k(t)$ and $\mathbf{q}_k(t)$ are the state, input and output vectors respectively on the k^{th} trial. To replace (3.52) with a set of algebraic equations in \mathbb{R}^N , define the shifted input and output vectors as

$$\begin{aligned}\mathbf{u}_k &= [\mathbf{u}_k(0)^T, \mathbf{u}_k(1)^T, \dots, \mathbf{u}_k(N-1)^T]^T \in \mathbb{R}^{mN} \\ \mathbf{q}_k &= [\mathbf{q}_k(1)^T, \mathbf{q}_k(2)^T, \dots, \mathbf{q}_k(N)^T]^T \in \mathbb{R}^{pN}\end{aligned}$$

and the relationship between the input and output time-series can be expressed by the following algebraic functions

$$\begin{aligned}\mathbf{q}_k(1) &= \mathbf{h}(\mathbf{x}_k(1)) = \mathbf{h}(\mathbf{f}(\mathbf{x}_k(0), \mathbf{u}_k(0))) \\ &= \mathbf{g}_1(\mathbf{x}_k(0), \mathbf{u}_k(0)) \\ &\vdots \\ \mathbf{q}_k(N) &= \mathbf{h}(\mathbf{x}_k(N)) = \mathbf{h}(\mathbf{f}(\mathbf{x}_k(N-1), \mathbf{u}_k(N-1))) \\ &= \mathbf{g}_N(\mathbf{x}_k(0), \mathbf{u}_k(0), \mathbf{u}_k(1), \dots, \mathbf{u}_k(N-1))\end{aligned}$$

Hence the system (3.50) can be represented as

$$\mathbf{q}_k = \mathbf{g}(\mathbf{u}_k), \quad \mathbf{g}(\cdot) = [\mathbf{g}_1(\cdot)^T, \mathbf{g}_2(\cdot)^T, \dots, \mathbf{g}_N(\cdot)^T]^T$$

To control hand posture it is necessary to specify the joint positions at a fixed number, $M \leq N$, of sample instants given by $1 \leq n_1 < n_2 < \dots < n_M \leq N$. Let the prescribed joint positions at these instants be

$$\mathbf{q}^* = [\mathbf{q}^*(0)^T, \mathbf{q}^*(1)^T, \dots, \mathbf{q}^*(M-1)^T]^T \in \mathbb{R}^{pM}$$

ILC can be considered an iterative numerical solution to the problem of finding a control input which solves

$$\min_{\mathbf{u}} J(\mathbf{u}) \quad \text{subject to} \quad \Lambda \mathbf{u} \preceq \mathbf{b}, \quad J(\mathbf{u}) = \|\mathbf{q}^* - \Phi \mathbf{g}(\mathbf{u})\|_2^2 \quad (3.53)$$

Here $J(\mathbf{u})$ is the point-to-point error norm, and the $pM \times pN$ matrix Φ has block-wise entries

$$\Phi_{i,j} = \begin{cases} I_p & j = n_i, \quad i = 1, 2, \dots, M \\ 0_p & \text{otherwise} \end{cases} \quad (3.54)$$

where I_p and 0_p are the $p \times p$ identity and zero matrices respectively. Due to the requirement that each FES input is bounded, $u_m \leq u_i \leq u_M$, it is necessary to apply vector inequality constraints on the system input of the form $\Lambda \mathbf{u} \preceq \mathbf{b}$, where $\Lambda = [-I, I]^T$ and $\mathbf{b} = [u_m \dots u_m, u_M \dots u_M]^T$.

Temporarily neglecting the constraint, the iterative solution of the ILC optimisation problem via the Newton method is

$$\begin{aligned}\mathbf{u}_{k+1} &= \mathbf{u}_k - \nabla^2 J(\mathbf{u}_k)^{-1} \nabla J(\mathbf{u}_k) \\ &= \mathbf{u}_k + (\Phi \mathbf{g}'(\mathbf{u}_k))^\dagger (\mathbf{q}^* - \Phi \mathbf{g}(\mathbf{u}_k))\end{aligned}\quad (3.55)$$

where $\mathbf{g}'(\mathbf{u}_k) = \frac{\delta \mathbf{g}(\mathbf{u}_k)}{\delta \mathbf{u}}$, and in the ILC framework $\mathbf{q}^* - \Phi \mathbf{g}(\mathbf{u}_k)$ is replaced with the experimental point-to-point error $\mathbf{e}_k = \mathbf{q}^* - \Phi \mathbf{q}_k$. The descent direction term in (3.55) is the solution $\bar{\mathbf{u}}$ to

$$\min_{\bar{\mathbf{u}}} \|\bar{\mathbf{u}}\|_2^2 \quad \text{subject to} \quad \Phi \mathbf{g}'(\mathbf{u}_k) \bar{\mathbf{u}} = \mathbf{e}_k \quad (3.56)$$

and hence applying the constraint $\Lambda \mathbf{u}_{k+1} \preceq \mathbf{b}$, which translates to $\Lambda \bar{\mathbf{u}} \preceq \mathbf{b} - \Lambda \mathbf{u}_k$, (3.53) is solved using

$$\mathbf{u}_{k+1} = \mathbf{u}_k + \Delta \mathbf{u}_k \quad (3.57)$$

with $\Delta \mathbf{u}_k$ the solution to

$$\min_{\bar{\mathbf{u}}} \|\bar{\mathbf{u}}\|_2^2 \quad \text{subject to} \quad \left\{ \begin{array}{l} \Phi \mathbf{g}'(\mathbf{u}_k) \bar{\mathbf{u}} = \mathbf{e}_k \\ \Lambda \bar{\mathbf{u}} \preceq \mathbf{b} - \Lambda \mathbf{u}_k \end{array} \right.$$

From (Freeman and Tan, 2011) this is solved by applying the gradient method to

$$\min_{\mathbf{u}} \|\mathbf{y}_r - \Phi \mathbf{y}_k - \Phi \mathbf{g}'(\mathbf{u}_k) \mathbf{u}\|_2^2 \quad \text{subject to} \quad \Lambda \mathbf{u} \preceq \mathbf{b} - \Lambda \mathbf{u}_k$$

using the barrier method, with corresponding update

$$\mathbf{u}_{j+1} = \mathbf{u}_j + \alpha (\Phi \mathbf{g}'(\mathbf{u}_k))^T (\mathbf{e}_k - \Phi \mathbf{g}'(\mathbf{u}_k) \mathbf{u}_j) - \frac{1}{\tau_j} \Lambda^T \mathbf{d} \quad (3.58)$$

applied to the plant $\Phi \mathbf{g}'(\mathbf{u}_k)$, where the elements of \mathbf{d} are given by $d_i = 1/(b_i - \Lambda_i^T(\mathbf{u}_j + \mathbf{u}_k))$. This is performed multiple times between trial k and $k+1$ in order to generate the decent term $\Delta \mathbf{u}_k$ in (3.57). The parameter τ_j is increased at each inter-trial update j in order to reach the hard constraint, as described in (Freeman and Tan, 2011). Note that no large matrix calculations are required within (3.58) since $\mathbf{w} = \mathbf{g}'(\mathbf{u}_k) \mathbf{v}$ corresponds to the linear time-varying system

$$\begin{aligned}\tilde{\mathbf{x}}(t+1) &= \mathbf{A}(t) \tilde{\mathbf{x}}(t) + \mathbf{B}(t) \mathbf{v}(t) \\ \mathbf{w}(t) &= \mathbf{C}(t) \tilde{\mathbf{x}}(t) + \mathbf{D}(t) \mathbf{v}(t) \quad t = 0, \dots, N-1\end{aligned}$$

where

$$\begin{aligned}\mathbf{A}(t) &= \left(\frac{\partial \mathbf{f}}{\partial \mathbf{x}} \right)_{\mathbf{u}_k(t), \mathbf{x}_k(t)}, & \mathbf{B}(t) &= \left(\frac{\partial \mathbf{f}}{\partial \mathbf{u}} \right)_{\mathbf{u}_k(t), \mathbf{x}_k(t)} \\ \mathbf{C}(t) &= \left(\frac{\partial \mathbf{h}}{\partial \mathbf{x}} \right)_{\mathbf{u}_k(t), \mathbf{x}_k(t)}, & \mathbf{D}(t) &= \left(\frac{\partial \mathbf{h}}{\partial \mathbf{u}} \right)_{\mathbf{u}_k(t), \mathbf{x}_k(t)}\end{aligned}$$

Similarly the term $\mathbf{w} = (\mathbf{g}'(\mathbf{u}_k))^T \mathbf{v}$ equates to the system

$$\begin{aligned}\tilde{\mathbf{x}}(t+1) &= \mathbf{A}^T(t)\tilde{\mathbf{x}}(t) + \mathbf{C}^T(t)\mathbf{v}(N-1-t) \\ \mathbf{w}(N-1-t) &= \mathbf{B}^T(t)\tilde{\mathbf{x}}(t) + \mathbf{D}^T(t)\mathbf{v}(N-1-t)\end{aligned}$$

Convergence and robustness properties are given in (Freeman and Tan, 2011), and in particular, convergence to zero error requires that $\Phi \mathbf{g}'(\mathbf{u}_k)$ has full row rank. This thereby allows point-to-point locations to be chosen to recover feasibility in the presence of a high coupled interaction matrix $\mathbf{R}(\mathbf{q})$.

3.4 Simulation Evaluation

a b
| 27

Simulation results are given using a sampling frequency of 100Hz. The clinically relevant task is to move the hand from initial flexed position to position $\theta_1 = 1.57$, $\theta_2 = 0.47$ and $\theta_3 = 0.21$, representing opening the hand to grasp an object. To investigate feasibility of surface FES two separate cases are considered 1) stimulation is applied to all muscles, 2) only extrinsic muscles are stimulated. Practical stimulation limits of $u_m = 0$, $u_M = 350\mu s$ are applied. Initial simulation results show that a wide variety of point-to-point movements can be achieved via extrinsic muscle stimulation, however the stimulation requires higher levels of stimulation signal. As representative output from an extensive set of simulations Figures 3.4 and 3.5 show joint trajectories over 10 trials, together with FES inputs on the final trial. As seen in Figures 3.6 and 3.7, error convergence in both cases shows high accuracy achieved in a small number of trials. The results hence confirm the potential of assisting movement using extrinsic muscles, that are compatible with surface FES but indicate increased input norms, and hence likelihood of fatigue, especially for the EC muscle.

Although simulation studies have established the feasibility of model-based ILC of the hand and wrist using FES of extrinsic muscles, the practical use of the considered model of the hand and wrist is strongly related to the selectivity of stimulation, which in case of surface stimulation depends of the size and appropriate placement of the electrodes. Although research has provided evidences, that it is possible to selectively stimulate different fingers (Westerveld et al., 2012). This is most likely the result of stimulation of individual muscle parts through individual nerve branches, i.e. contraction of different branches of EDC can induce extention of separate fingers. Thus to be able to apply

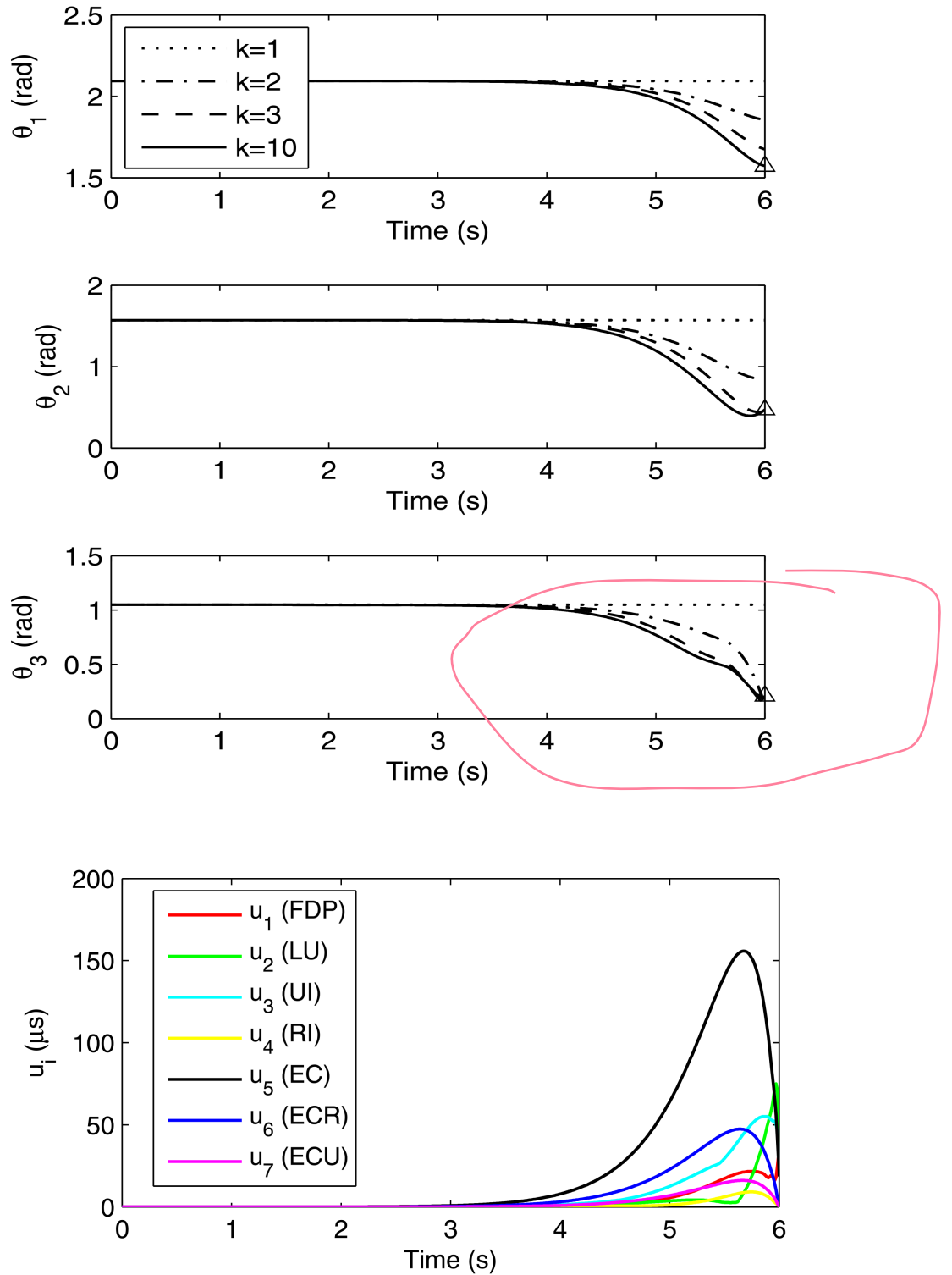


Figure 3.4: Stimulation of extrinsic and intrinsic muscles using Newton method-based point-to-point ILC with inequality constraint.

the proposed model-based control of such a selective stimulation additional knowledge of the subject's model and its properties is required.

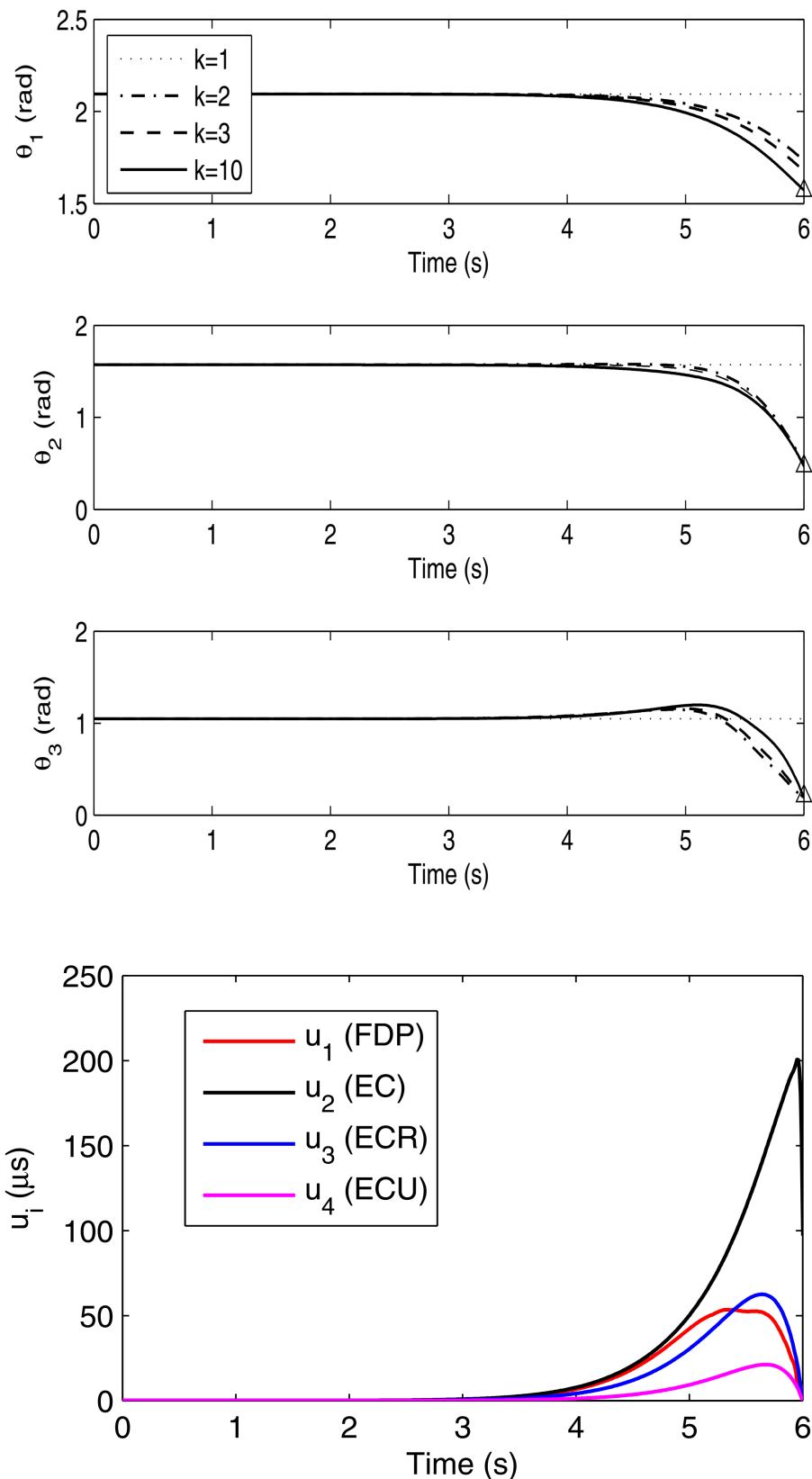


Figure 3.5: Stimulation of extrinsic muscles using Newton method-based point-to-point ILC with inequality constraint.

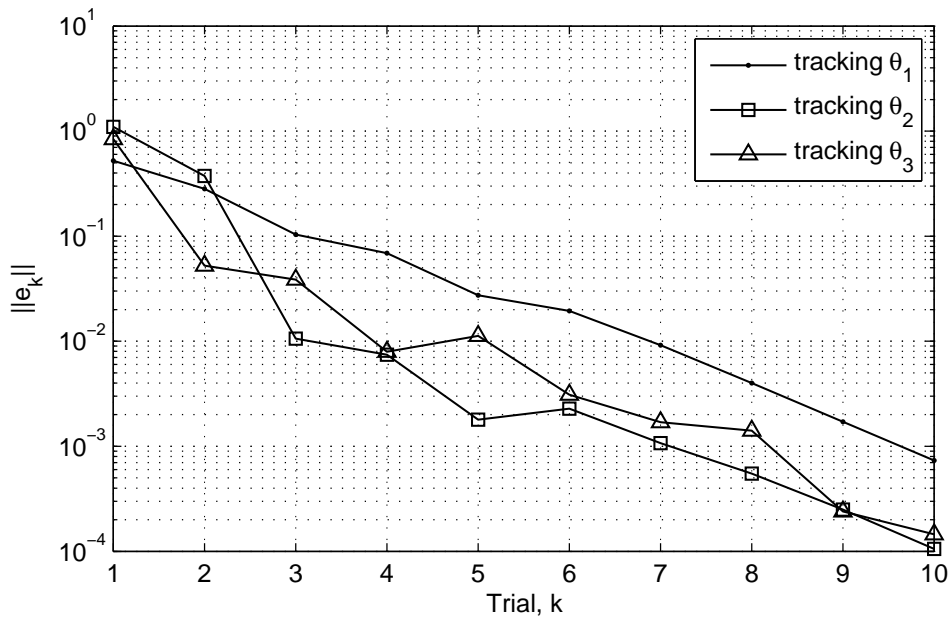


Figure 3.6: Stimulation of extrinsic and intrinsic muscles using Newton method-based point-to-point ILC: error norm.

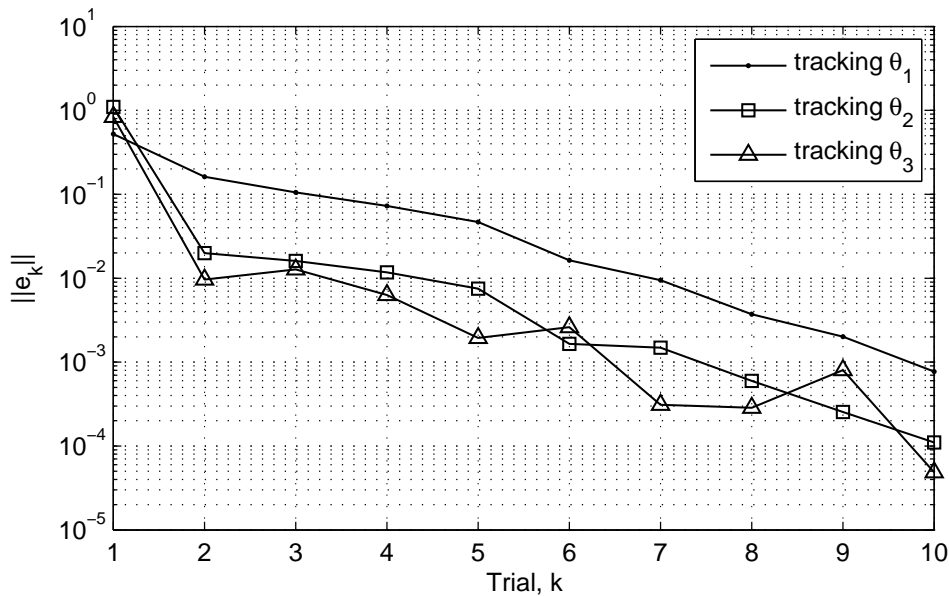


Figure 3.7: Stimulation of extrinsic muscles using Newton method-based point-to-point ILC with inequality constraint: error norm.

Clearly the complexity and number of muscles in the model must align with those muscles likely to be actuated through the proposed surface stimulation. The model extends beyond what is likely to be achievable, which allows scope for future application using implanted electrodes or more precise electrode arrays. However, proposed model can be easily modified (i.e. by removing/adding muscles) once the selectivity of stimulation is established experimentally. The choice of the model depends on the selectivity of the task, i.e. cylindrical release requires less selectiveness than assisting the pinch grip or other more complex manual tasks. These are the factors, that require further research and examination in order to efficiently use the model-based control of hand and wrist in practice. Some of these aspects of the overall problem are discussed in the next chapter.

Chapter 4

Surface Electrode Array based Control of the Wrist and Hand

Surface Electrode Array Stimulation (SEAS) is a non-invasive method of muscle activation, that uses adhesive electrodes placed on the surface of the patient skin above the location of the desired muscles. SEAS induces movement in a paralysed or weak limb by sending a series of electrical pulses to associated skeletal muscles through activation of chosen elements of electrode array. Activated elements constitute a stimulation pattern. The optimal activation pattern is a map that determines which electrode or combination of electrodes must be activated to achieve a desired movement [Schill et al. \(2009b\)](#). The movement is controlled by modulation of the control input \mathbf{u} . In the multi-channel case, separate stimulation signals can be passed through selected elements of electrode array, see Figure 4.1.

SEAS has the potential to be an effective technique for stroke rehabilitation of the upper-limb. However, the effectiveness of the method is strongly related to the precision and accuracy of the stimulation. The precision of stimulation is associated with the accurate selection of the optimal stimulation pattern and with the selectivity of stimulation ([Westerveld et al., 2012](#)). These are essential for functionality and ease of application. The specific character of SEAS-based control of the human hand and wrist, makes the design process a difficult task compared with the control of mechanical systems, where the main difficulties arise from the biomechanical nature of the system. This requires that the additional patient-oriented factors such as patient response and safety issues are taken into account during the process of controller design and implementation.

Small electrodes are able to more precisely target muscles for selective activation than larger electrodes ([Westerveld et al., 2012](#)), potentially inducing more precise movements of the fingers and wrist if the stimulation signal is appropriately controlled. The higher selectivity of stimulation allows the development of more effective and advanced training

systems by enabling the practice of more complex and precise movements of hand and wrist.

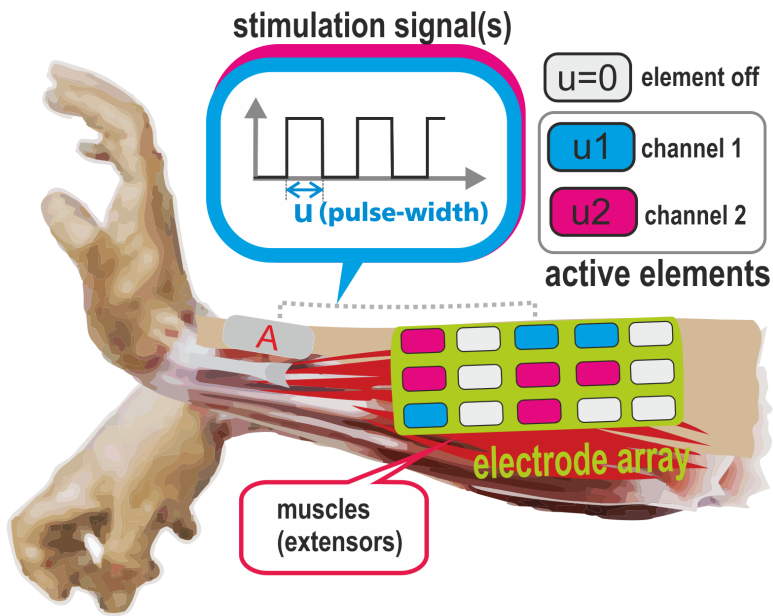


Figure 4.1: Surface Electrode Array Stimulation - schematic of technique

For smaller electrodes there is a higher possibility of deviation in electrode location during the movement occurring. Additionally, a larger number of smaller electrodes is required to span all the area of the target muscles, compared with larger electrodes used for the same purpose. This increases the search space for optimisation algorithms, making the problem of selecting optimal stimulation patterns more difficult task.

Another recognised problem, that can limit practical use of SEAS is the activation of sensory receptors on the skin surface during the stimulation process. The sensation of stimulation and level that can trigger the pain vary from one subject to another. Single element stimulation can cause irritation and discomfort or even pain sensation, if the stimulation intensity increased above a certain limit [Lyons et al. \(2004\)](#). Generally the smaller single element the lower the level of the stimulation that triggers the pain sensation.

To overcome this problem a group of single array elements was selected to emulate the single elements of the electrode array and were used in the optimization procedure. This emulated single array element is termed a “virtual element” of the electrode array. Each type of “virtual element” can be defined by its size (the number of single electrode array elements) and the spatial configuration of the single elements used.

4.1 System and Problem Description

In the most general case the problem of how to select the stimulation level applied to each virtual element is based on representing the hand and wrist as a non-linear dynamic system. Consider m elements and p joint angles and at time t define the input and output vectors

$$\mathbf{u}(t) = \begin{bmatrix} \mathbf{u}_1(t) \\ \vdots \\ \mathbf{u}_m(t) \end{bmatrix} \in \mathbb{R}^m, \quad \mathbf{y}(t) = \begin{bmatrix} \mathbf{y}_1(t) \\ \vdots \\ \mathbf{y}_p(t) \end{bmatrix} \in \mathbb{R}^p \quad (4.1)$$

To model the relationship between stimulation inputs and joint angle outputs, the non-linear discrete-time system

$$\begin{aligned} \mathbf{x}(t+1) &= \mathbf{f}(\mathbf{x}(t), \mathbf{u}(t)) \\ \mathbf{y}(t) &= \mathbf{h}(\mathbf{x}(t)), \quad \mathbf{x}(0) = x_0 \end{aligned} \quad (4.2)$$

model is assumed over the sample times $t = 0, 1, \dots, N - 1$ with state vector $x \in \mathbb{R}^r$. Here $f(\cdot)$ and $h(\cdot)$ are assumed to be continuously differentiable with respect to t and the total time duration is $T = (N - 1)T_s$.

An equivalent analysis description uses the supervectors

$$\mathbf{u} = \begin{bmatrix} \mathbf{u}(0) \\ \vdots \\ \mathbf{u}(N-1) \end{bmatrix} \in \mathbb{R}^{mN}, \quad \mathbf{y} = \begin{bmatrix} \mathbf{y}(1) \\ \vdots \\ \mathbf{y}(N) \end{bmatrix} \in \mathbb{R}^{pN} \quad (4.3)$$

to give $\mathbf{y} = \mathbf{g}(\mathbf{u})$ where

$$\mathbf{g}(\cdot) = \left[\mathbf{g}_1(\cdot)^T \quad \cdots \quad \mathbf{g}_N(\cdot)^T \right]^T \quad (4.4)$$

with elements

$$\begin{aligned} \mathbf{g}_i(\mathbf{x}(0), \mathbf{u}(0), \mathbf{u}(1), \dots, \mathbf{u}(i-1)) &= \mathbf{h}(\mathbf{x}(i)) \\ &= \mathbf{h}(\mathbf{f}(\mathbf{x}(i-1), \mathbf{u}(i-1))), \\ &= \mathbf{h}(\mathbf{f}(\mathbf{f}(\mathbf{x}(i-2), \mathbf{u}(i-2)), \mathbf{u}(i-1))), \\ &\vdots \\ &= \mathbf{h}(\mathbf{f}(\mathbf{f}(\cdots \mathbf{f}(\mathbf{x}(0), \mathbf{u}(0)), \cdots, \mathbf{u}(i-2)), \mathbf{u}(i-1))), \end{aligned} \quad (4.5)$$

over $i = 1, \dots, N$. In this formulation $\mathbf{g}(\cdot)$ represents the hand and wrist response to applied stimulation.

The general problem of tracking a desired reference $y_d(t)$, alternatively expressed by the supervector

$$\mathbf{y}_d = \begin{bmatrix} \mathbf{y}_d(0) \\ \vdots \\ \mathbf{y}_d(N-1) \end{bmatrix} \in \mathbb{R}^{pN} \quad (4.6)$$

requires the construction of a sequence of stimulation inputs, $\{\mathbf{u}_k\}_{k=0,1,\dots,\infty}$ such that

$$\lim_{k \rightarrow \infty} \|\mathbf{y}_d - \mathbf{g}(\mathbf{u}_k)\| = 0, \quad \lim_{k \rightarrow \infty} \|\mathbf{u}_d - \mathbf{u}_k\| = 0 \quad (4.7)$$

where \mathbf{u}_d is a fixed input signal given by

$$\mathbf{u}_d = \begin{bmatrix} \mathbf{u}_d(0) \\ \vdots \\ \mathbf{u}_d(N-1) \end{bmatrix} \in \mathbb{R}^{mN}. \quad (4.8)$$

and $\|\cdot\|$ denotes an appropriate norm.

Selecting the sampling time that exceeds the steady-state response time of the system and setting $N = 1$ ($T = T_s$), giving

$$\mathbf{u} = \mathbf{u}(0), \quad \mathbf{y} = \mathbf{y}(1), \quad \mathbf{g}(\cdot) = \mathbf{g}_1(\cdot) \quad (4.9)$$

This equates to the ‘steady-state’ tracking problem is a special case of the full dynamic problem. Although the algorithms described in this chapter can address both cases, the former requires far shorter identification tests to produce a models needed in the algorithms which follow. Consider an operating point, \mathbf{u}_a , given by

$$\mathbf{u}_a = \begin{bmatrix} u_{a,1} & \cdots & u_{a,m} \end{bmatrix}^T \in \mathbb{R}^m \quad (4.10)$$

Then it is possible to represent the linearized system about $\mathbf{u} = \mathbf{u}_a$ as

$$\begin{aligned} \mathbf{g}'(\mathbf{u}_a) &= \left. \frac{\partial \mathbf{g}}{\partial \mathbf{u}} \right|_{\mathbf{u}=\mathbf{u}_a} = \begin{bmatrix} \left. \frac{\partial g_{1,1}}{\partial u_1} \right|_{u=u_a} & \cdots & \left. \frac{\partial g_{1,1}}{\partial u_m} \right|_{u=u_a} \\ \vdots & \ddots & \vdots \\ \left. \frac{\partial g_{1,p}}{\partial u_1} \right|_{u=u_a} & \cdots & \left. \frac{\partial g_{1,p}}{\partial u_m} \right|_{u=u_a} \end{bmatrix} \\ &= \begin{bmatrix} \left. \frac{\partial y_1}{\partial u_1} \right|_{u=u_a} & \cdots & \left. \frac{\partial y_1}{\partial u_m} \right|_{u=u_a} \\ \vdots & \ddots & \vdots \\ \left. \frac{\partial y_p}{\partial u_1} \right|_{u=u_a} & \cdots & \left. \frac{\partial y_p}{\partial u_m} \right|_{u=u_a} \end{bmatrix} \in \mathbb{R}^{p \times m} \end{aligned} \quad (4.11)$$

4.2 Identifying the System about an Operating Point

Suppose it is desired to identify the linearized system about $\mathbf{u} = \mathbf{u}_a = \mathbf{0}$ using experimental data. Then the procedure is to set the stimulation to zero on all channels except u_i , and slowly increase u_i whilst measuring y . Strictly the derivative at $u_i = 0$ should be estimated, as shown in Figure 4.2 and this produces a whole set of linearization points

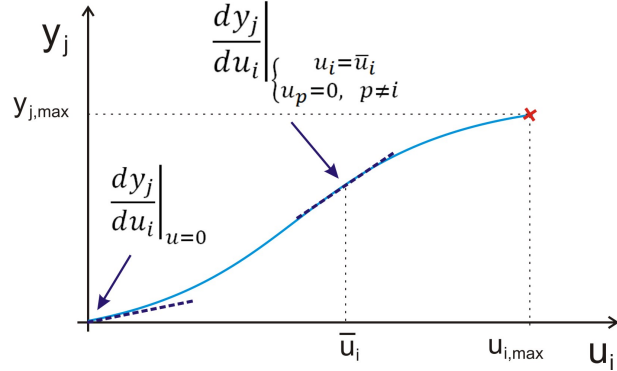


Figure 4.2: Linearization points for u_i with $u_p = 0, p \neq i$.

for u_i . They can hence be averaged to produce a representative model that is more valid within a region about $u_i = 0$. If the maximum stimulation is $u_{i,max}$, giving rise to a monotonic increase in y_j , with maximum value $y_{j,max}$, then the average value of $\frac{\partial y_j}{\partial u_i}$ is

$$\frac{1}{u_{i,max}} \int_0^{y_{j,max}} \frac{\partial y_j}{\partial u_i} du_i = \frac{y_{j,max}}{u_{i,max}} \quad (4.12)$$

i.e. the average value equates to the simple ratio of output to applied input. If $u_{i,max}$ is small, (4.12) provides an approximate value of $\left. \frac{\partial y_j}{\partial u_i} \right|_{u=0}$.

The alternative is to not average, but to produce a set of linearized models at different operating points, \bar{u}_i , where each \bar{u}_i produces a column vector

$$\left. \frac{\partial y}{\partial u_i} \right|_{\begin{cases} u_i = \bar{u}_i \\ u_p = 0, p \neq i \end{cases}} \quad (4.13)$$

To produce a consistent linearized system $g'(\cdot)$, the above can only be combined with other columns that are linearized about zero. Hence if there are M linearization points for each input (including zero), then this procedure produces M^m models.

Identifying the System about an Arbitrary Operating Point by Averaging

To reliably calculate the linearized system about $\mathbf{u} = \mathbf{u}_a$ using experimental data, a slow ramp is applied to each input u_i over the set of inputs

$$S_i = \left\{ u_{a,i} - \frac{u_{i,width}}{2}, \quad u_{a,i} - \frac{u_{i,width}}{2} + \Delta u_i, \right. \\ \left. u_{a,i} - \frac{u_{i,width}}{2} + 2\Delta u_i, \quad \dots, \quad u_{a,i} + \frac{u_{i,width}}{2} \right\}$$

whilst the other inputs are fixed at $u_j = u_{a,j}$. The response of the j^{th} output, y_j^i , is shown in Figure 4.3. The required estimate of $\left. \frac{\partial y_j}{\partial u_i} \right|_{u=u_a}$ is then calculated by averaging

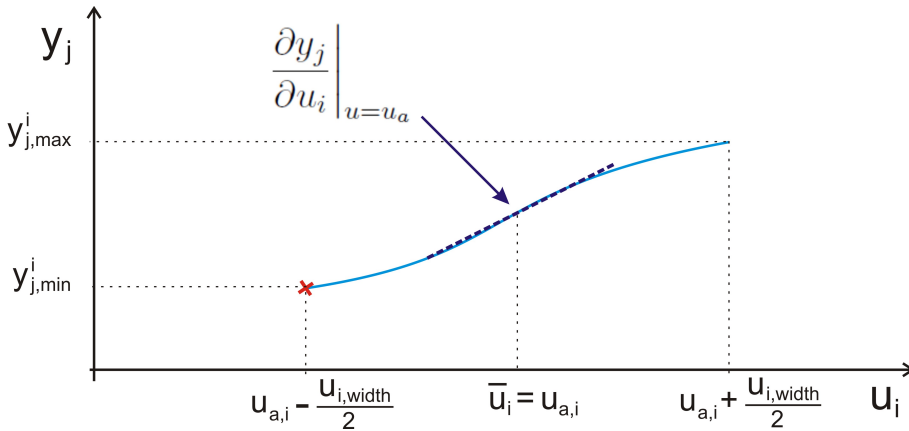


Figure 4.3: Linearization points about u_a .

provided $u_{i,width}$ is sufficiently small. The result is given by

$$\left. \frac{\partial y_j}{\partial u_i} \right|_{u=u_a} \approx \frac{1}{u_{i,width}} \sum_{u_i \in S_i} \left. \frac{\partial y_j}{\partial u_i} \right|_{u=u_a} \Delta u_i = \frac{y_{j,max}^i - y_{j,min}^i}{u_{i,width}} \quad (4.14)$$

Applying the above to all outputs, yields

$$\begin{bmatrix} \left. \frac{\partial y_1}{\partial u_i} \right|_{u=u_a} \\ \vdots \\ \left. \frac{\partial y_p}{\partial u_i} \right|_{u=u_a} \end{bmatrix} = \left. \frac{\partial \mathbf{y}}{\partial \mathbf{u}_i} \right|_{u=u_a} \approx \frac{\mathbf{y}_{max}^i - \mathbf{y}_{min}^i}{u_{i,width}} \quad (4.15)$$

where

$$\mathbf{y}_{max}^i = \begin{bmatrix} y_{1,max}^i \\ \vdots \\ y_{p,max}^i \end{bmatrix} \in \mathbb{R}^p, \quad \mathbf{y}_{min}^i = \begin{bmatrix} y_{1,min}^i \\ \vdots \\ y_{p,min}^i \end{bmatrix} \in \mathbb{R}^p \quad (4.16)$$

Each test hence populates the i^{th} column of (4.11).

4.3 ILC Applied to Array Element Selection

The problem of finding a stimulation profile, \mathbf{u} , which produces the required posture, \mathbf{y}_d , can be expressed as

$$\text{minimize } f(\mathbf{u}), \quad f(\mathbf{u}) = \|\mathbf{y}_d - \mathbf{g}(\mathbf{u})\|_2^2 \quad (4.17)$$

subject to constraints on \mathbf{u} . A general algorithm to solve this problem is given next :

Step 1. Set $k = 0$ and set the initial input to $\mathbf{u}_0 = \mathbf{0}$.

Step 2. Apply \mathbf{u}_k to the system experimentally and record \mathbf{y}_k . Calculate the error $\mathbf{e}_k = \mathbf{y}_d - \mathbf{y}_k$.

Step 3. Linearize the system about the operating point input \mathbf{u}_k to obtain the linear model $\mathbf{g}'(\mathbf{u}_k)$.

Step 4. Using the model of the previous step, update the control input using any linear gradient based ILC approach, i. e. Gradient ILC, Newton-based ILC.

Step 5. Increment k and go to step 2.

The process of linearization followed by input updating is used by a broad class of nonlinear minimization algorithms, which use experimental data collected during the trials of the underlying repetitive process to minimize an objective function. Here, to solve the problem of minimising the tracking error norm, the implementation of the process within ILC framework is developed.

As an example, inverse ILC in the update step 4 of above procedure is now considered. This corresponds to ‘Newton method-based ILC’ [Lin et al. \(2006b\)](#), one technique in the wide class of gradient-based algorithms, which has well defined convergence criteria (see, for example, [Ortega and Rheinboldt \(1970\)](#)). It has also been used in unconstrained and constrained ILC [Freeman \(2012\)](#) approaches. The new input can be calculated applying Newton method based ILC in step 4 as follows:

$$\mathbf{u}_{k+1} = \mathbf{u}_k + \mathbf{v}_k^* \quad (4.18)$$

where \mathbf{v}_k^* is the solution to the following problem:

$$\text{minimize } f_k(\mathbf{v}), \quad f_k(\mathbf{v}) = \|\mathbf{e}_k - \mathbf{g}'(\mathbf{u}_k)\mathbf{v}\|_2^2 \quad (4.19)$$

Without constraints, the solution to (4.19) will be non-unique if $\mathbf{g}'(\mathbf{u}_k)$ does not have full row rank (which will be the case if, for example, $m > p$). To avoid this problem, (4.19) can be augmented as

$$\begin{aligned} & \text{minimize} && \|\mathbf{v}\|_2^2 \\ & \text{subject to} && \mathbf{e}_k = \mathbf{g}'(\mathbf{u}_k)\mathbf{v} \end{aligned} \quad (4.20)$$

which has the solution

$$\mathbf{v}_k^* = \left((\mathbf{g}'(\mathbf{u}_k))^T \mathbf{g}'(\mathbf{u}_k) \right)^{-1} (\mathbf{g}'(\mathbf{u}_k))^T \mathbf{e}_k = (\mathbf{g}'(\mathbf{u}_k))^\dagger \mathbf{e}_k \quad (4.21)$$

Constraints are required to ensure that the experimentally applied stimulation signal \mathbf{u}_k is practically achievable. When the FES stimulator supports multi-channel stimulation and the number of channels is not less than the number of elements of the electrode array, the only constraint is due to the control input limits and the control problem can be solved using the ILC-Newton based method with boundary input constraints as described in previous chapter.

A challenging problem occurs, when the number of channels available is less than the number of elements in the electrode array. In such a case, finding an optimal stimulation pattern can be considered as an integer programming problem, or a sparse optimisation problem due to the presence of additional constraints. The different approaches to solve this optimisation problem are described next.

Limited number of stimulation levels - penalty function approach

In the case when n-number of stimulation levels is available the stimulation signal must satisfy

$$u_{k,i} \in \mathcal{U}_n, \quad \forall k \quad (4.22)$$

$$0 \leq \mathcal{U}_{n,j} \leq 300, \quad j = 1, 2, \dots, n \quad (4.23)$$

where \mathcal{U}_n is a set with n non-zero distinct elements (which can change at each trial k , but here are assumed to be predetermined) with $\mathcal{U}_{n,j}$ denoting the j^{th} element. Here n is the number of channels supported by the hardware. The problem (4.19) is hence

replaced by

$$\begin{aligned} & \text{minimize} \quad \|v\|_2^2 \\ \text{subject to} \quad & \begin{cases} e_k = g'(\mathbf{u}_k)v, \\ v_i \in \{\tilde{u}_1 - u_{k,i}, \tilde{u}_2 - u_{k,i}, \dots, \tilde{u}_n - u_{k,i}\}, \\ -u_{k,i} \leq v_i \leq 300 - u_{k,i} \end{cases} \end{aligned} \quad (4.24)$$

This last problem can be solved in simulation between experimental trials. Hence the inequality constraint can be removed since the applied solution will always satisfy it through appropriate selection of \mathcal{U}_n . It is shown in (Freeman, 2012) that repeated application of gradient ILC (an implementation of the gradient descent algorithm) to the problem (4.19), converges to a solution which solves (4.20). It is hence necessary to apply the gradient descent algorithm to the problem

$$\begin{aligned} & \text{minimize} \quad f_k(v), \quad f_k(v) = \|e_k - g'(\mathbf{u}_k)v\|_2^2 \\ \text{subject to} \quad & v_i \in \{\tilde{u}_1 - u_{k,i}, \tilde{u}_2 - u_{k,i}, \dots, \tilde{u}_n - u_{k,i}\} \end{aligned} \quad (4.25)$$

whilst also ensuring the solution, v_k^* , satisfies the constraint. This then is used in step 4 to produce the next input, via $\mathbf{u}_{k+1} = \mathbf{u}_k + v_k^*$.

To solve (4.25) first substitute for the optimized variable to give

$$\begin{aligned} & \text{minimize} \quad \tilde{f}_k(\tilde{v}), \quad \tilde{f}_k(\tilde{v}) = \|e_k - g'(\mathbf{u}_k)(\tilde{v} - \mathbf{u}_k)\|_2^2 \\ \text{subject to} \quad & \tilde{v}_i \in \{\tilde{u}_1, \tilde{u}_2, \dots, \tilde{u}_n\} \end{aligned} \quad (4.26)$$

This problem can be solved using gradient descent optimization by introducing a suitable penalty function. Accordingly, the problem (4.26) becomes

$$\begin{aligned} & \text{minimize} \quad \tilde{f}_k(\tilde{v}), \quad \tilde{f}_k(\tilde{v}) = \|e_k - g'(\mathbf{u}_k)(\tilde{v} - \mathbf{u}_k)\|_2^2 \\ & \quad + \tau \sum_i^m \varphi(\tilde{v}_i), \end{aligned} \quad (4.27)$$

where τ is a penalty multiplier for values not in the set \mathcal{U}_n , and $\varphi(\tilde{v}_i)$ is the penalty term for the i^{th} variable. Different forms of the discrete penalty function are possible, and here the sine-function form (Shin et al., 1990) is employed and a suitable form is

$$\varphi(\tilde{v}_i) = \sin \left(\frac{2\pi (\tilde{v}_i - \frac{1}{4}(\tilde{u}_{j+1} + 3\tilde{u}_j))}{\tilde{u}_{j+1} - \tilde{u}_j} \right) + 1, \quad \tilde{u}_j \leq \tilde{v}_i \leq \tilde{u}_{j+1} \quad (4.28)$$

The scalar multiplier τ is initially zero and is increased gradually to ensure that the converged solution satisfies the constraint in (4.26) that $\tilde{v}_i \in \{\tilde{u}_1, \dots, \tilde{u}_n\}$. Application

of the gradient algorithm to (4.27) gives

$$\tilde{v}_{l+1} = \tilde{v}_l + (\mathbf{g}'(\mathbf{u}_k))^T (\mathbf{e}_k - \mathbf{g}'(\mathbf{u}_k)(\tilde{v}_l - \mathbf{u}_k)) + \tau_l \chi_l \quad (4.29)$$

where $\tilde{v}_0 = u_k$. Now the vector χ_l has elements

$$\begin{aligned} \chi_{l,i} &= \frac{\partial \varphi(\tilde{v}_i)}{\tilde{v}_i}, & \tilde{u}_j \leq \tilde{v}_i \leq \tilde{u}_{j+1} \\ &= \frac{2\pi}{(\tilde{u}_{j+1} - \tilde{u}_j)} \cos \left(\frac{2\pi (\tilde{v}_{l,i} - \frac{1}{4}(\tilde{u}_{j+1} + 3\tilde{u}_j))}{\tilde{u}_{j+1} - \tilde{u}_j} \right) \end{aligned} \quad (4.30)$$

The solution obtained after sufficient inter-trial iterations of (4.29), \tilde{v}_k^* , is used to obtain the new input $u_{k+1} = \tilde{v}_k^*$.

4.4 Selection using Virtual Elements

Virtual elements (VEs) potentially provide more effective and practical base units of stimulation. These can simply be incorporated into the previous approach by redefining the underlying stimulation elements to be constructed of multiple array elements. The inherent non-linearity of the system means that more accurate results will be produced by extending the number of possible input elements, so that the same element appears in multiple independent input units. This does not violate the assumption of local linearity since linearization is based on a single operating point, and the subsequent input increase treats the input elements as independent. Each input is termed a ‘virtual element’ since it no longer encompasses a single array element, but a set of elements that can be overlapped. This approach embeds richer model information, and can be analysed using the approaches of Section 4.3.

Suppose the electrode array is rectangular with m_v vertical elements and m_h horizontal elements, and hence $m = m_v \times m_h$. The requirement that the elements comprising each virtual element be adjacent to each other reduces the number of placements and hence size of the input vector. The following virtual element dimensions are considered

$$\begin{aligned} \mathbf{u}^{1hv} &\in \mathbb{R}^{(m_v \times m_h)} && \text{virtual = real elements} \\ \mathbf{u}^{2v} &\in \mathbb{R}^{(m_h \times (m_v - 1))} && 2 \text{ vertical VEs} \\ \mathbf{u}^{2h} &\in \mathbb{R}^{((m_h - 1) \times m_v)} && 2 \text{ horizontal VEs} \\ \mathbf{u}^{2hv} &\in \mathbb{R}^{((m_h - 1) \times (m_v - 1))} && 2 \text{ horizontal + 2 vertical VEs} \end{aligned} \quad (4.31)$$

These inputs are assumed to be independent and can be combined under the assumption of local linearity. Hence the augmented input vector is given by

$$\mathbf{u} = \begin{bmatrix} \mathbf{u}^{1hv} \\ \mathbf{u}^{2v} \\ \mathbf{u}^{2h} \\ \mathbf{u}^{2hv} \end{bmatrix} \in \mathbb{R}^{(2(m_h(m_v-1)+(m_h-1)m_v)+1)} \quad (4.32)$$

and (4.11) in this case can be written as

$$\begin{aligned} \mathbf{g}'(\mathbf{u}_a) &= \frac{\partial \mathbf{g}}{\partial \mathbf{u}} \Big|_{\mathbf{u}=\mathbf{u}_a} \in \mathbb{R}^{p \times (2(m_h(m_v-1)+(m_h-1)m_v)+1)} \\ &= \left[\frac{\partial \mathbf{g}}{\partial \mathbf{u}^{1hv}} \Big|_{\mathbf{u}=\mathbf{u}_a} \frac{\partial \mathbf{g}}{\partial \mathbf{u}^{2v}} \Big|_{\mathbf{u}=\mathbf{u}_a} \frac{\partial \mathbf{g}}{\partial \mathbf{u}^{2h}} \Big|_{\mathbf{u}=\mathbf{u}_a} \frac{\partial \mathbf{g}}{\partial \mathbf{u}^{2hv}} \Big|_{\mathbf{u}=\mathbf{u}_a} \right] \\ &= \begin{bmatrix} \frac{\partial y_1}{\partial u^{1hv}} \Big|_{u=u_a} & \frac{\partial y_1}{\partial u^{2v}} \Big|_{u=u_a} & \frac{\partial y_1}{\partial u^{2h}} \Big|_{u=u_a} & \frac{\partial y_1}{\partial u^{2hv}} \Big|_{u=u_a} \\ \vdots & \vdots & \vdots & \vdots \\ \frac{\partial y_p}{\partial u^{1hv}} \Big|_{u=u_a} & \frac{\partial y_p}{\partial u^{2v}} \Big|_{u=u_a} & \frac{\partial y_p}{\partial u^{2h}} \Big|_{u=u_a} & \frac{\partial y_p}{\partial u^{2hv}} \Big|_{u=u_a} \end{bmatrix} \end{aligned} \quad (4.33)$$

where, for example,

$$\begin{bmatrix} \frac{\partial y_1}{\partial u^{1hv}} \Big|_{u=u_a} \\ \vdots \\ \frac{\partial y_p}{\partial u^{1hv}} \Big|_{u=u_a} \end{bmatrix} = \begin{bmatrix} \frac{\partial y_1}{\partial u_1^{1hv}} \Big|_{u=u_a} & \cdots & \frac{\partial y_1}{\partial u_{m_v \times m_h}^{1hv}} \Big|_{u=u_a} \\ \vdots & \ddots & \vdots \\ \frac{\partial y_p}{\partial u_1^{1hv}} \Big|_{u=u_a} & \cdots & \frac{\partial y_p}{\partial u_{m_v \times m_h}^{1hv}} \Big|_{u=u_a} \end{bmatrix} \quad (4.34)$$

Each column of (4.34) is identified by the ramp identification approach of Section 4.2. Hence, for example

$$\begin{bmatrix} \frac{\partial y_1}{\partial u_i^{1hv}} \Big|_{u=u_a} \\ \vdots \\ \frac{\partial y_p}{\partial u_i^{1hv}} \Big|_{u=u_a} \end{bmatrix} = \frac{\partial y}{\partial u_i^{1hv}} \Big|_{u=u_a} \approx \frac{y_{max}^{1hv,i} - y_{min}^{1hv,i}}{u_{i,width}^{1hv}} \quad (4.35)$$

where $y_{max}^{1hv,i}$, $y_{min}^{1hv,i}$ are the joint outputs corresponding to the ramp test applied to the i^{th} element of virtual element $1hv$.

The approach of Section 4.3 is applied unchanged except that

1. the constraints on the input applied experimentally must be referred back to the vector, $\hat{\mathbf{u}}$ which is being updated, and

2. having updated $\hat{\mathbf{u}}$ the input applied experimentally must be constructed by combining the virtual element solutions.

This requires each virtual element input to be written in terms of the resulting, combined element output. Hence we map the virtual input vectors to the applied stimulation vector component \hat{u} through matrices containing ones and zeros:

$$\begin{aligned}\hat{\mathbf{u}} &= \Phi_{1hv} u^{1hv}, \quad \Phi_{1hv} \in \mathbb{R}^{m \times (m_h \times m_v)} \\ \hat{\mathbf{u}} &= \Phi_{2v} u^{2v}, \quad \Phi_{2v} \in \mathbb{R}^{m \times (m_h \times (m_v - 1))} \\ \hat{\mathbf{u}} &= \Phi_{2h} u^{2h}, \quad \Phi_{2h} \in \mathbb{R}^{m \times ((m_h - 1) \times m_v)} \\ \hat{\mathbf{u}} &= \Phi_{2hv} u^{2hv}, \quad \Phi_{2hv} \in \mathbb{R}^{m \times ((m_h - 1) \times (m_v - 1))}\end{aligned}\tag{4.36}$$

Hence

$$\hat{\mathbf{u}} = \left[\begin{array}{cccc} \Phi_{1hv} & \Phi_{2v} & \Phi_{2h} & \Phi_{2hv} \end{array} \right] \begin{bmatrix} \mathbf{u}^{1hv} \\ \mathbf{u}^{2v} \\ \mathbf{u}^{2h} \\ \mathbf{u}^{2hv} \end{bmatrix} = \Phi \mathbf{u}\tag{4.37}$$

where

$$\Phi = \left[\begin{array}{cccc} \Phi_{1hv} & \Phi_{2v} & \Phi_{2h} & \Phi_{2hv} \end{array} \right]\tag{4.38}$$

and the constraint (4.22) becomes

$$\hat{\mathbf{u}}_{k,i} = \Phi_i \mathbf{u}_k \in \mathcal{U}_n\tag{4.39}$$

where Φ_i is the i^{th} row of Φ , so that the constraints on problem (4.19) become

$$v_i \in \{\tilde{u}_1 - \Phi_i u_k, \tilde{u}_2 - \Phi_i u_k, \dots, \tilde{u}_n - \Phi_i u_k\}\tag{4.40}$$

and the problem and solution given by (4.26), (4.27), (4.28), (4.29), (4.30) are identical except for the substitution

$$\tilde{u}_i \iff \tilde{u}_i - \Phi_i u_k + u_{k,i}.\tag{4.41}$$

Remark 4.1. The form of (4.33) means that the optimization problem (4.26) may be performed sequentially for each virtual element form in turn, before moving onto the next step of minimizing the remaining joint error, whilst transferring the constraints so that the final solution satisfies (4.22). This procedure enables a simple set of uncoupled constraints to be imposed on each sub-problem.

4.4.1 Sparse optimisation for SEAS-based control of Hand and Wrist

The multi-channel SEAS-based control of fingers and wrist in the case when the number of channels available is less than the number of elements in the electrode array can be considered as a sparse optimisation problem with cardinality and minimum threshold

constraints. These can be expressed as:

$$\begin{aligned} & \text{minimize } f(\mathbf{u}) := \|\mathbf{g}(\mathbf{u}) - \mathbf{y}_d\|_2^2 \\ & \text{s.t. } \|\mathbf{u}\|_0 \leq n \\ & u_{\min} = 0 \leq u_i \leq u_{\max} = 300, \quad i = 1, \dots, m \end{aligned} \tag{4.42}$$

where $f : R^m \rightarrow R$ is assumed to be a continuously differentiable function, $n > 0$ is an integer that denotes the number of channels and $\|\mathbf{u}\|_0$ is the l_0 norm of \mathbf{u} , which is equal to the number of non-zero components in \mathbf{u} . Note, that in general case the f is not assumed to be a convex function, which together with the non-convex constraint function, refers to a general non-linear optimisation problem, which is complex NP-hard. However, assuming linearity of the static model allows the problem to be relaxed to a standard convex optimisation problem as described next.

Static linear model with sparsity

Assume that system is linearized around \mathbf{u}_0 and $\mathbf{g}'(\mathbf{u}_0) = \mathbf{G}$ and this assumption of linearity then gives rise to the simpler procedure:

$$\begin{aligned} & \text{minimize } \|\mathbf{y}_d - \mathbf{Gu}\|_2^2 \\ & \text{s.t. } \|\mathbf{u}\|_0 \leq n \\ & 0 \leq u_i \leq u_{\max}, \quad i = 1, \dots, m \end{aligned} \tag{4.43}$$

where $\mathbf{G} \in R^{p \times m}$, $\mathbf{y}_d \in R^p$, s is an integer satisfying $1 \leq n \leq m$ and n denotes the number of channels of the stimulation that are available. The problem (4.43) can be replaced by the following l_1 -regularized least squares problem

$$\begin{aligned} & \text{minimize } \|\mathbf{y}_d - \mathbf{Gu}\|_2^2 + \tau \|\mathbf{u}\|_1 \\ & 0 \leq u_i \leq u_{\max}, \quad i = 1, \dots, m \end{aligned} \tag{4.44}$$

where $\|\cdot\|_1$ denotes the l_1 -norm, which equals the sum of the absolute values of the components of \mathbf{u} . The presence of the l_1 term is used to induce the sparsity in the optimal solution of (4.43). Equivalently, the problem (4.45) can be replaced with the following minimization problem

$$\begin{aligned} & \text{minimize } \|\mathbf{y}_d - \mathbf{Gu}\|_2^2 + \tau \mathbf{1}^T \mathbf{u} \\ & 0 \leq u_i \leq u_{\max}, \quad i = 1, \dots, m \end{aligned} \tag{4.45}$$

where $\mathbf{1} \in \mathbb{R}^m$ denotes the vector with all entries equal to 1 and $\tau \leq n$.

4.4.2 Proximal Gradient Algorithm

Recently, there has been growing interest in convex optimization techniques for system identification, which is motivated by the success of convex methods for sparse optimization and by the development of new classes of algorithms for large-scale non-differentiable convex optimization, such as proximal gradient methods ([Vandenberghe, 2012](#)).

The proximal gradient method is an extension of the gradient algorithm to problems with simple constraints or with simple non-differentiable terms in the cost function, such as $\|\mathbf{u}\|_1$. It is typically a fast method and handles many types of non-differentiable problems that occur in the practice. The proximal gradient algorithm applies to a convex problem in which the cost function J can be split into two components: differentiable function $g(\cdot)$ and non-differentiable term $h(\cdot)$

$$\text{minimize } J(\mathbf{u}) = g(\mathbf{u}) + h(\mathbf{u}) \quad (4.46)$$

In the previously considered sparse problem for SEAS, these terms were given by $g(\mathbf{u}) = \|\mathbf{y}_d - \mathbf{Gu}\|_2^2$ and $h(u) = \tau\|\mathbf{u}\|_1$ respectively. To solve the composite optimisation problem (4.46), a proximal optimisation problem needs to be solved. The problem can be formulated as follows:

$$\mathbf{u}_{k+1} = \arg \min_{\mathbf{u}} \|\mathbf{u} - (\mathbf{u}_k - \alpha_k \mathbf{g}'(\mathbf{u}_k))\|_2^2 + \alpha_k h(\mathbf{u}) \quad (4.47)$$

where the solution of (4.47) is the proximal gradient algorithm of the form:

$$\mathbf{u}_{k+1} = \text{prox}_{\alpha_k h} [\mathbf{u}_k - \alpha_k \mathbf{g}'(\mathbf{u}_k)] \quad (4.48)$$

Each iteration of above proximal-gradient method (4.48) requires the calculation of the proximity operator $\text{prox}_{\alpha_k h}$, as described next.

Box-constrained Proximity Operator with l_1 -norm

The solution for the box-constrained version of the proximity operation for the considered problem (4.45) can be expressed as:

$$u_i^* = \min(\max(\hat{u}_i, u_{\min}), u_{\max}) \quad (4.49)$$

where

$$\hat{u}_i = \text{sgn}(u_i) \max(|u_i| - \tau \alpha_k, 0) \quad (4.50)$$

is the well known shrinkage or soft-tresholding operator.

This problem can be solved using the Accelerated Proximal Gradient (APG) method, which is one of the fastest methods from the wider group of Proximal Gradient-based approaches (Nesterov, 2004, 2013). The APG method for the considered case of hand and wrist control can be expressed as the following procedure

The Accelerated Proximal Gradient for SEAS with cardinality constrained inputs

1. Apply $\mathbf{u}_k = \mathbf{u}_0$ to the system experimentally and record \mathbf{y}_k . Calculate the postural joint error $\mathbf{e}_k = \mathbf{y}_d - \mathbf{y}_k$
2. Linearize the system about the operating point input u using the approach described in section (4.2)
3. Set $\mathbf{v}_0 = \mathbf{v}_{-1} = \mathbf{0}$, set $t_0 = t_{-1} = 1$ and $L \geq \lambda_{max}(\mathbf{G}^T \mathbf{G})$, where L denotes the smallest Lipschitz constant and λ_{max} is the maximum eigenvalue.
4. Calculate the new input using APG method with sparse non-negative upper bound constraints and adaptive step size t_k .

$$\begin{aligned}
 \mathbf{u}_k &:= \mathbf{v}_k + \frac{t_{k-1} - 1}{t_k} (\mathbf{v}_k - \mathbf{v}_{k-1}) \\
 \mathbf{u}_{k+1} &:= \mathbf{u}_k - \frac{1}{K} [\mathbf{G}^T (\mathbf{G}\mathbf{u}_k - \mathbf{y}_d) - \tau \mathbf{1}] \\
 &:= \mathbf{u}_k - \frac{1}{L} (\mathbf{G}\mathbf{e}_k^T - \tau \mathbf{1}) \\
 v_{k+1} &:= \min[\max(0, u_{k+1}), u_{max}] \\
 t_{k+1} &:= \frac{1}{2}(1 + \sqrt{1 + 4t_k^2})
 \end{aligned} \tag{4.51}$$

5. Increment k and go to step 4.
-

4.4.3 Brute-force Searching Method

The brute-force algorithm selects a combination of electrodes with up to n separate pulse width levels of stimulation to provide the best performance. The main parameters of the algorithm are the input rate u_{rate} and maximal number of elements that can be selected

(activated elements) n_{active} and p the number of array elements. Hence the number of possible solutions is equal to

$$s = \frac{p!}{n_{active}!(p - n_{active})!} n_{active}^n \frac{(u_{max} - u_{min})}{u_{rate}} \quad (4.52)$$

Let \mathcal{U}_s denotes the set of all possible solutions for chosen parameters. This can be expressed as:

$$\mathcal{U}_s = \{\mathbf{u}_1, \dots, \mathbf{u}_s\} \quad (4.53)$$

The algorithm finds the best solution, which can be expressed as:

$$\begin{aligned} \min_k & \quad \|\mathbf{G}\mathbf{u}_k - \mathbf{y}_d\|_2^2 \\ k &= 1, \dots, s \end{aligned} \quad (4.54)$$

and the parameters dictate the speed and accuracy of the searching procedure. Small u_{rate} , can improve the performance of the algorithm, but increases the search space.

Applying any of the methods introduced in this chapter results in finding the sparse input vector \mathbf{u} , which defines the optimal stimulation pattern.

4.4.4 Two-step approach for ILC of SEAS

A two-step approach has been developed in which the problem of the tracking of a reference, when having only n stimulation channels is addressed as follows:

- Step 1. Select an optimal stimulation pattern that consists of upto n array elements, i.e using previously described penalty function method or sparse optimisation method.
- Step 2. Apply ILC-based approach with boundary input constraints for the electrode elements selected in Step 1 to calculate new stimulation profile.

Optimal Stimulation Pattern, sparse input vector and Virtual Electrode Array

An optimal stimulation pattern, can be defined by sparse input vector \mathbf{u} , which consists of upto n non-zero electrode elements, i.e. $\mathbf{u} = [u_1 = v_1, 0, u_2 = v_2, u_3 = v_2, 0 \dots 0, u_n = v_1]$. Each of the elements or group of elements having the same value of input can be treated as a single element of new virtual electrode array, so that $v_1(t)$ is applied to 1 group of elements of the original electrode array , ..., $v_i(t)$ to $i - th$ group of elements and finally the last $n - th$ group is assigned to $v_n(t)$. This results in new vector of $m = n$ inputs \mathbf{v} , which constitutes the new virtual electrode array that consists of only n pads.

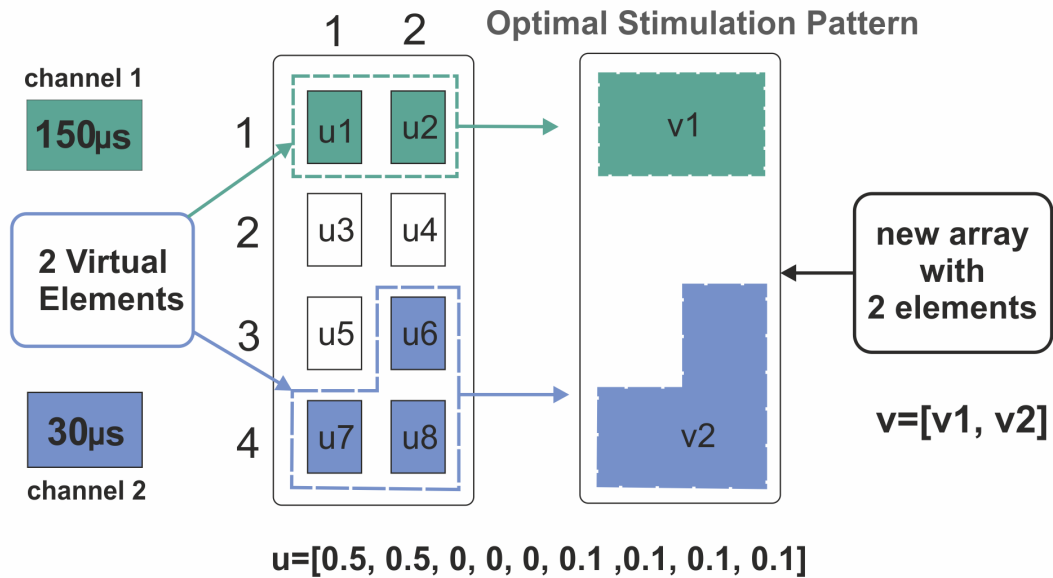


Figure 4.4: Optimal Stimulation Pattern - schematic of mapping array elements → input vector u

Example: Let the optimal stimulation pattern for the exemplar array (2×4) be represented by the sparse input vector u , then the non-negative elements in the sparse vector u constitute a new virtual electrode array that consists of only 2 elements as shown in Figure 4.4

4.5 General ILC-based approach for SEAS

A general approach has been developed, that combines all previously described methods as shown in Figure 4.5. The different parameters and design setting covered by the approach are following.

- k - number of trials: single-step approach ($k = 1$), multiple-trials approach ($k > 1$)
- m - number of single elements in electrode array
- Electrode Array Elements: single electrode array elements, VEs - a group of single elements is treated as single array elements
- n - number of channels, number of separate stimulation signals supported by stimulator, multi-channels SEAS $n > 1$
- Optimal Pattern Selection Methods: Penalty function method, Sparse optimisation method, Brute-force method
- ILC-based methods: Gradient ILC, Newton method ILC.

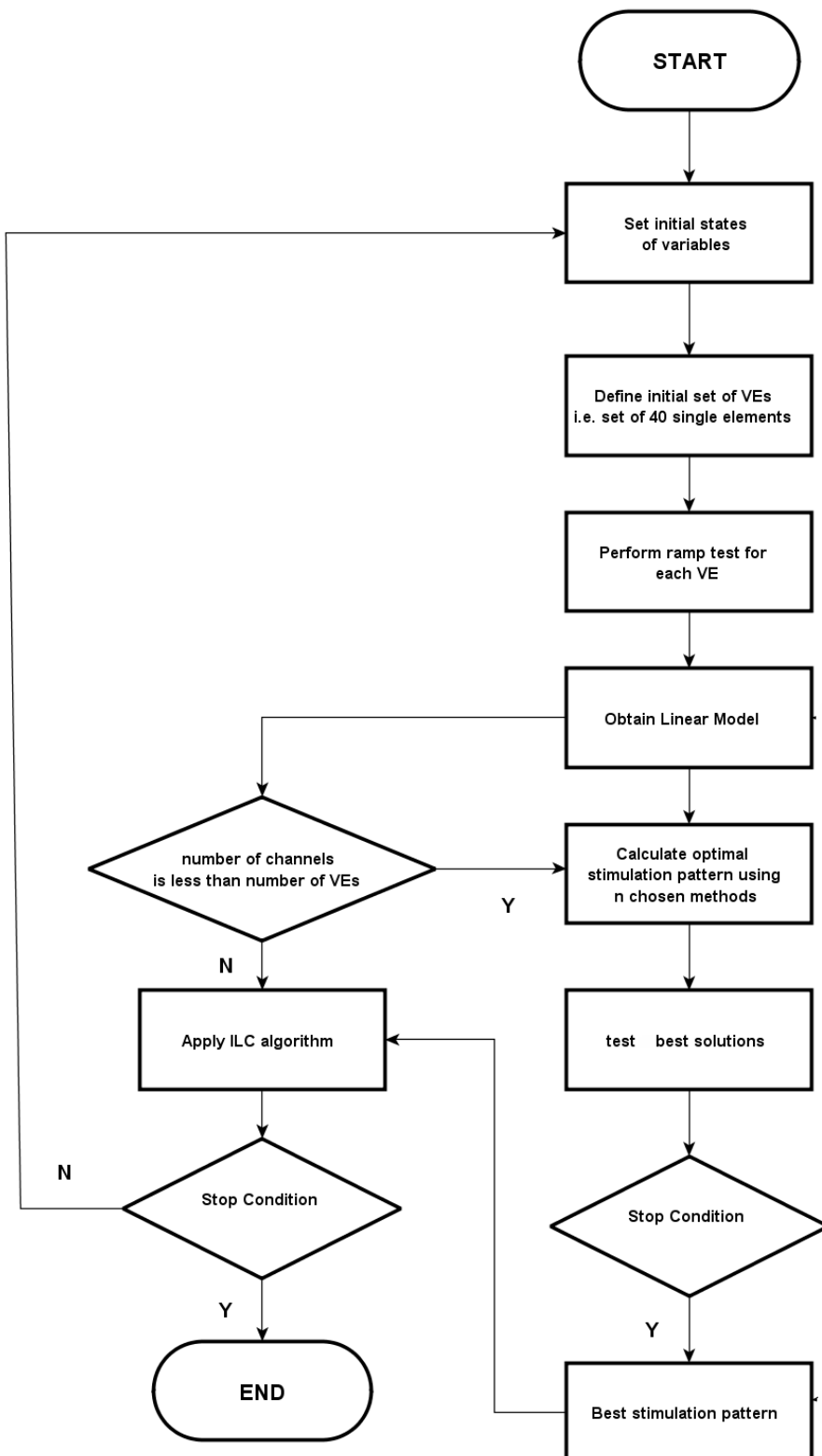


Figure 4.5: General Iterative Approach for SEAS-based control of the hand and wrist

Method	channels	trials
ILC with input boundary constraints	$n \geq m$	multiple-trials ($k \geq 1$)
ILC with optimisation	$n < m$	$k \geq 1$
Optimal Pattern Selection Methods	$n < m$	$k = 1$

Table 4.1: Exemplar methods for selected configuration of different parameters of the general procedure

SEAS-based technologies can differ in respect to parameters such as: the number of single elements in the electrode array , number of separate stimulation signals supported by the hardware. The general approach developed can be applied to a variety of possible design specification of existing and future SEAS-based technologies. The exemplar methods used in the general approach for different configuration settings are presented in Table 4.1. The system design and the practical results for the system specification and selected settings of the procedure applied in experimental trials are discussed next.

Chapter 5

System Design and Experimental Procedure

The Hand Restoration System (HaReS) uses SEAS mediated by specifically designed optimisation algorithms, including ILC-based methods. The sensors used in the system are two 5DT gloves (model for left and right hand) and goniometers. The hardware is combined with graphical user interface, which allows the patients to interact with a specially designed game-based training environment. The main components of the system are shown in Figure 5.1.

5.1 Electrode Array and Multiplexer

The electrode arrays used in the system, consists of 40 (5x8) elements. The electrode array is controlled by custom made multiplexor, that can access and route two separate stimulation signals to desired array elements. The multiplexor is controlled by Matlab via a dSpace card which outputs a pulse-width modulated signal which is amplified by a commercial Odstock stimulator unit. The Arduino board then uses the information from dSpace to output appropriate signals to control shift registers array Dinh (2012). To enable control of the stimulation, a commercial stimulator was specially modified.

The stimulation parameters, pulse-width, amplitude and frequency have been selected to ensure a smooth muscle contraction. The controller hardware produces a 5V 40Hz square pulse train with variable pulse-width for each channel. This is then fed into the amplification stage of the stimulator, resulting in bi-phasic voltage-amplified stimulation pulses. The amplitude of the pulses for each channel have to be determined manually, whereas the pulselwidth was chosen to be the input parameter, that can be controlled automatically by the Matlab controller. The pulse-width has been safety-limited to be between 0 and $300\mu s$.

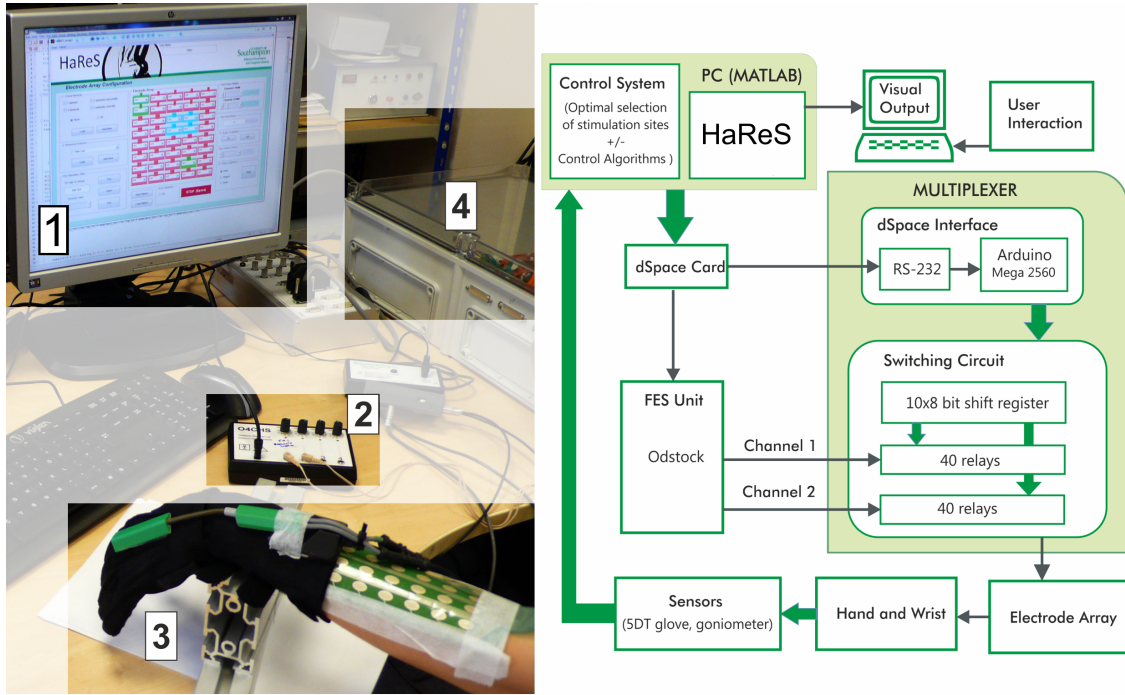


Figure 5.1: **Hardware components:**

- (1) Control Module , (2) FES Stimulator (3) Sensors and Electrode Array, (4) Multiplexor

5.2 Sensors

The Biometrics twin axis goniometer SG75 was used to record the movement data of the wrist. The goniometer permits the simultaneous measurement of angles in two planes, e.g. wrist flexion/extension and radial/ulnar deviation. The raw angles of flexion and adduction (or abduction) are calculated using the linear calibration functions:

$$\Theta_{flexion} = 90.9091(\Theta_{raw} - 2.5292) \quad (5.1)$$

$$\Theta_{abduction} = 89.2857(\Theta_{raw} - 2.5246) \quad (5.2)$$

To measure finger joint position the 5DT 5 Ultra glove was used due to its lower cost compared to other commercially available sensing gloves and high accuracy of measurements. The high data quality and data rate make it ideal for realistic real-time applications such as game control and interaction. The glove has two fiber-optic flexion/extension sensors per finger and one abduction sensor between fingers. Each sensor reading represents an integer from 0 to 4095 due to the analog-to-digital conversion electronics embedded in the glove circuitry. The glove has high resolution and is able to detect changes in fingertip position as small as 0.12 mm. However, the range of integers corresponding

to a full flexion of the glove changes from finger to finger, due to the position of the sensing element within the glove fabric. Therefore, it was necessary to determine the relationship between these integers and the finger angles for each finger and each glove. The relationship between raw integer data values and flexing angle values are found to be close to linear. This linear relationship was confirmed by bending the sensors across the acceptable range of angles in small intervals and obtaining the correlating raw data values.

The sensors used in the 5dt glove do not measure exact anatomical joint angles (MC,PIP). Mapping from the raw data into the degrees with the assumption that the values represent the real anatomical joint angles leads to a complex non-linear calibration function and using, for example a complex piece-wise polynomial fitting method. However, the data can be normalised or represent the approximate values of anatomical flexion/extension angles for each joint. Thus the sensor outputs were obtained using linear calibration method, which simplify the procedure and enables individual calibration to be performed for each subject before a trial session.

Finger	MCP (F/E)	PIP (F/E)	MCP (Ab/Ad)
Index	80/0	100/0	13/42
Middle	80/0	100/0	8/35
Ring	80/0	100/0	14/20
Little	80/0	100/0	19/33

Table 5.1: Range of movements for the joints MCP and PIP of the fingers used in calibration

Data Normalisation:

$$out_{norm} = \frac{(raw_{val} - raw_{min})}{(raw_{max} - raw_{min})} \quad (5.3)$$

Data Calibration:

$$out_{calib} = \frac{(raw_{val} - raw_{min})}{(raw_{max} - raw_{min})} max \quad (5.4)$$

where *max* can be e.g. the maximal joint flexion in degrees shown in Table 5.2

Finger	MCP RAW (max/min)	PIP RAW (max/min)	MCP (Ab/Ad)
Index	3219 / 2762	2483 / 1259	3665 / 3273
Middle	1468/875	3029/2376	3112/3037
Ring	2256/1846	3038/2457	3384/3038
Little	2682/2476	3257/2231	

Table 5.2: Range of movements for the joints MCP and PIP of the fingers used in calibration

5.3 HaReS - software

The graphical user interface (GUI) allows patients to interact with a software, which is used in conjunction with the rehabilitation hardware and SEAS-based control methods. A specially designed game provides clear feedback and interactive and motivating training environment, based on measuring selected quantitative features of hand function such as ROM and tracking error. Additionally GUI provides manual and automatic configuration methods for the electrode array and control methods described in previous chapter (Chapter 4).

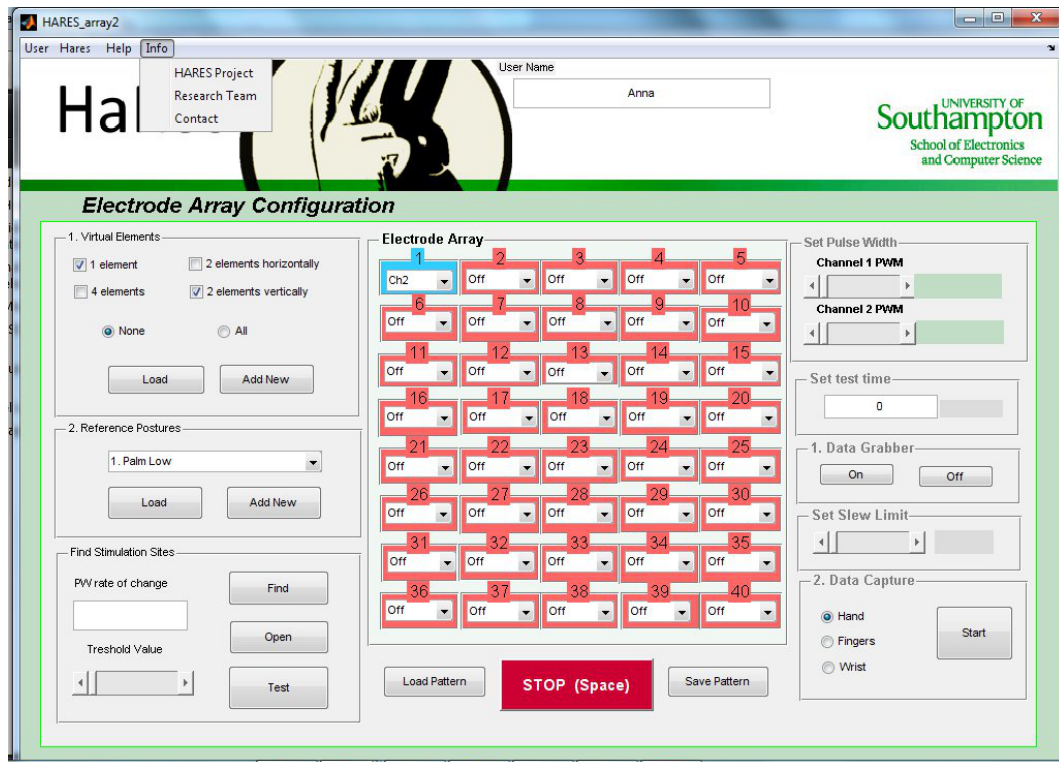


Figure 5.2: Graphical User Interface

5.3.1 Hares Game

Hares is an arcade game designed specifically for the purpose of stroke rehabilitation of patients with hemiplegia and spasticity of hand and wrist. The cognitive and motor task of the game is to control position of the pad (hat) in such a way that the number of caught objects (hares) is maximized. In the simplest case, the different scenarios of the game and levels of difficulties are defined by three aspects: the number of objects falling, the position of the objects on the screen (including spatial configuration of the objects), the speed of falling. The exercise motion can either be focused on a single muscle motion such as wrist flexion, or can train a movement, that requires combined and coordinated using of multiple muscles such as hand opening, index pointing. The beta version of the game is shown in Figure 5.3. In the game-based training environment



Figure 5.3: Hares game

the feedback is provided in form of the scoring. Generally, the better tracking patients achieve during the training session the higher scores they get. The formula proposed in considered case is following:

$$score = [(1 - normalized_error) * 100] \quad (5.5)$$

The scoring formula in the simplest case can be determined based on the tracking error. However other parameters such as speed of movement, number of the repetition, difficulty level in the game (including cognitive and motoric difficulty level) may be also take into account.

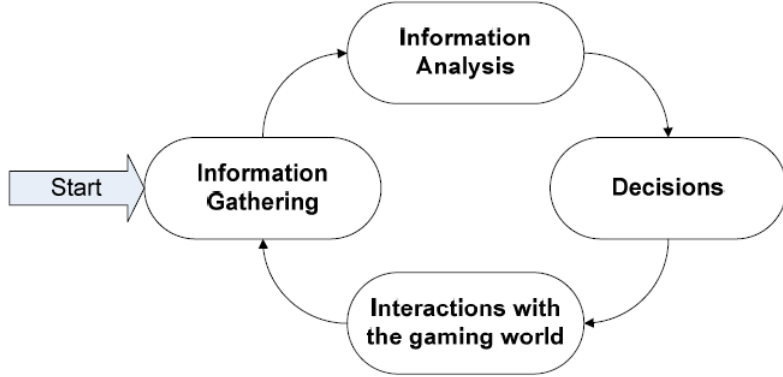


Figure 5.4: Interactive cycle in the playing game experience

While playing a game, the patient interacts with a virtual universe, which receives player's responds and control inputs (hand movements) by changing its status. Information regarding the outcome of the interaction is then conveyed to player (i.e. scoring), and eventually gathered and used by the user to decide what to do next, as shown in Figure 5.4. This cycle is repeated iteratively, until the player wins or loses the game, or simply decides to suspend temporarily his/her training session.

Before running the game, a set of trajectories (i.e. hand opening) for the specified in the game task (movement of the pad to the right) have to be defined. A set of trajectories are stored as the assessment tasks used in Hares Game. Taking into the considerations the level of patient's disability, the path of trajectories are defined with respect to the range of motion capabilities of the participant's hand.

The trajectories are restricted by the game workspace which in the simplest horizontal plane is specified as the (maximal-ROM-of-healthy-person/x-screen-resolution). The trajectories are parametrized and classified according to the difficulty level, which for the simplest case is defined as the normalized value [0, 1]. Here, 1 denotes the trajectory with the highest level of difficulty represented by the maximal horizontal displacement of the hat on the screen.

Trajectories (tasks) can be switched during the training process, or in other words during playing the game by the user. The three modes of switching of the trajectories with respect to the task defined in the game architecture are proposed. These are: Switching Mode off (repeating all the time the same task, tracking the same trajectory), Random Mode (simple random selection from the set of predefined trajectories), Intelligent Mode: choice of task/trajectory is indicated by the metric (patient performance). This is presented in the Figure 5.5.

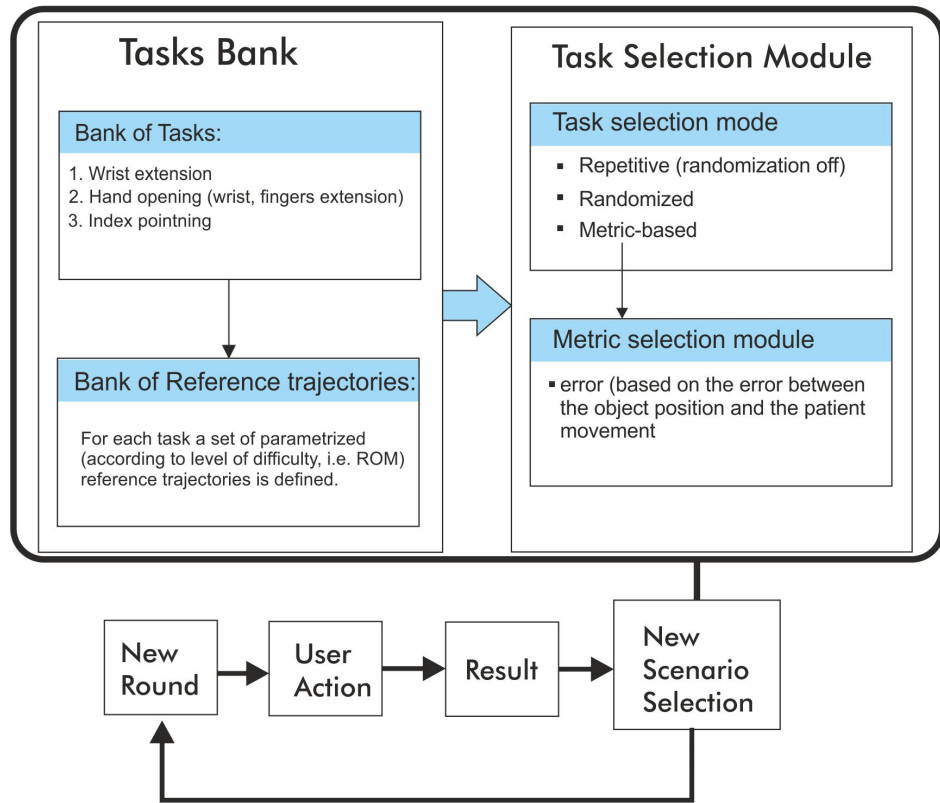


Figure 5.5: Selection of a task

Electrode Array Configuration Module provides interface to manual and/or auto selection of appropriate stimulation patterns for a pre-defined group of reference postures/trajectories, which constitute the set of patients control movements, that can be exercised during the game-based training session. Data collected during configuration of electrode array and during the game-based training session can be stored providing feedback to the patient or to the therapist about the training duration, frequency of training sessions and their effectiveness.

5.4 Design Considerations and Settings

The specific character of FES-based control of the human hand and wrist, makes the design process a difficult task compared with the control of mechanical systems. The main difficulties emerge from the biomechanical nature of the system. This necessitates the consideration of additional patient-oriented factors such as patient response, voluntary effort and safety issues need to be also taken into account during the process of controller design and implementation. Some of the problems mentioned above are considered next.

5.4.1 Choice of reference postures

A set of different reference postures has been chosen, practical limitations of the technique, clinical needs and special Virtual-Reality based character of the Hand Rehabilitation System.

Reference Posture	Movement
Spastic Hand (initial posture)	Fingers and wrist flexed
Natural Posture	All fingers relaxed, natural posture of unimpaired hand
Opened Hand	Fingers and wrist extended and wrist without abduction/adduction
Pointing	Index finger extended, other fingers flexed and wrist without abduction/adduction

Table 5.3: Reference postures

The initial posture and appropriate reference postures are listed in Table 5.3. These postures are used in the optimisation procedures to minimize the norm error between the desired reference posture and that recorded during the trial.

5.4.2 Method of optimal pattern selection

The main difficulty in applying optimisation procedures in order to select the best stimulation sites of the electrode array, is the limitation put on the number of tests (iterations) that can be performed. The optimal stimulation profile must be identified in a relatively short time, with as few tests performed on patients as possible. The more trials involving stimulation of subject's muscles, the greater the risk of fatigue and the less comfortable the procedure is for the patient. The previously described general approach is based on very well defined underlying theory, however it involves multiple trials, which necessitates lengthy identification experiments. This is not ideal, hence to overcome the practical difficulties and reduce number of experiments a single trial was first tested.

The single-step methods of finding optimal stimulation pattern for the electrode array have been firstly analysed and compared in numerical studies. The data were collected from unimpaired participants to obtain the steady-state matrices and selected reference postures, used in analysis of three optimisation procedures. These preliminary results are presented next.

Penalty function method

This method limits the number of stimulation levels, but the number of elements that can be made active is unlimited. The effectiveness of the method depends strongly on the appropriate selection of stimulation level, which is shown in Table 5.4

1	Error Norm	Normalized Error	Non-zero elements of vector of inputs \mathbf{u}
5	32.252	0.369	$[u_3 = 0.2, u_4 = 0.2, u_5 = 0.2, u_8 = 0.2]$
8	24.815	0.284	$[u_3 = 0.25, u_4 = 0.25, u_5 = 0.25, u_8 = 0.125, u_{39} = 0.125]$
10	24.745	0.283	$[u_3 = 0.2, u_4 = 0.3, u_5 = 0.2, u_8 = 0.2, u_{39} = 0.1]$

Table 5.4: Numerical Results for 5, 8 and 10 stimulation levels

Accelerated Proximal Gradient

The effectiveness of the APG algorithm is strongly related to the experimental data and appropriate selection of parameter L . Generally, APG converges to the sparsest optimal solution. Thus for some experimental data the number of non-zero elements in the optimal solution, may exceeds the number of available stimulation channels. To overcome these difficulties, a brute-force searching algorithm was developed.

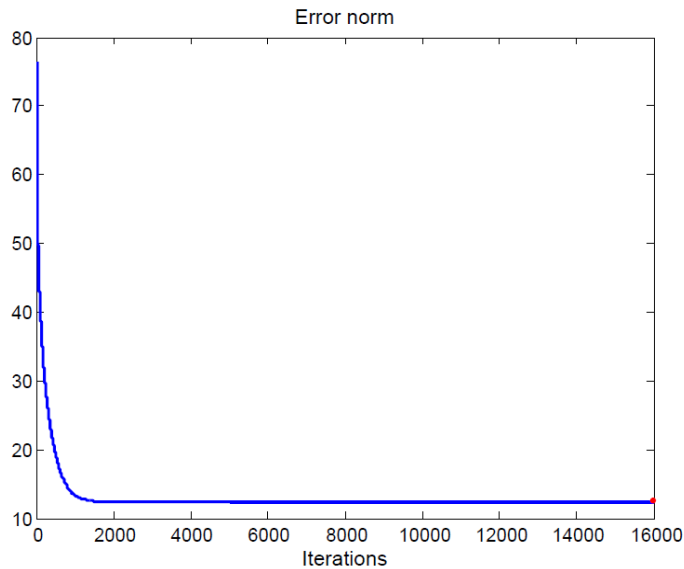


Figure 5.6: Accelerated Proximal Gradient error norm for 16 joints.

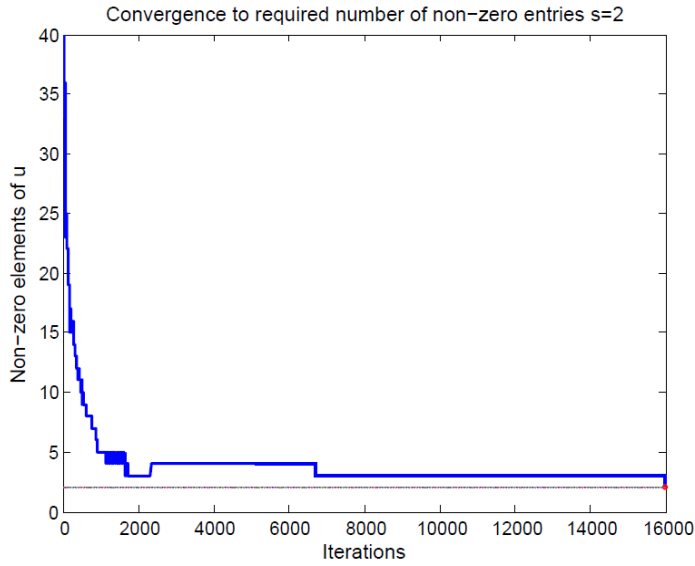


Figure 5.7: Accelerated Proximal Gradient convergence results for $s = 2$.

Name	s	Error Norm	Normalized Error	Non-zero elements of vector of inputs \mathbf{u}_k	k -last iteration
APG	2	12.505	0.143	$[u_{k,1} = 0.99, u_{k,23} = 0.01]$	15991
APG	3	14.04	0.183	$[u_{k,1} = 0.897, u_{k,23} = 0.04, u_{k,25} = 0.051]$	1539
APG	4	20.948	0.241	$[u_{k,2} = 0.551, u_{k,6} = 0.0109, u_{k,7} = 0.121, u_{k,30} = 0.159]$	5663

Table 5.5: Numerical results for APG for 2, 3, 4 elements

Brute-force Searching Method

This approach combines the two previously described methods, due to the fact that it limits both, the number of stimulation levels and non-zero elements in the optimal vector input \mathbf{u} , respectively.

u_{rate}	Error Norm	Non-zero elements of vector of inputs \mathbf{u}
0.025	14.48	$[u_{11} = 0.225, u_{12} = 0.225, u_{39} = 0.675, u_{40} = 0.675]$
0.025	21.368	$[u_2 = 0.375, u_{23} = 0.45]$
0.15	14.829	$[u_{11} = 0.3, u_{12} = 0.3, u_{40} = 0.6]$
0.15	13.277	$[u_2 = 0.45, u_3 = 0.45, u_{24} = 0.45, u_{25} = 0.45, u_{29} = 0.45, u_{30} = 0.45]$

Table 5.6: Numerical Results for different parameters

The parameters of the method dictate the speed and accuracy of the searching procedure. Small u_{rate} , can improve the performance of the algorithm, but increases the search space for the algorithm.

Qualitative comparison of methods

Method	Penalty Method	Proximal Gradient	Searching Algorithm
Method	Heuristic	Gradient-based	Greedy
Iterations	Predefined	Data-dependent	Predefined
Elements Number (N)	Unconstrained	$N \geq$ Sparsest Optimum	Predefined
Stimulation Levels	Predefined	Unconstrained	Predefined
Convergence	Parameter-Dependent	Monotonic	Parameter-Dependent
Optimum	Parameter-Dependent	Sparsest Optimal Solution	Parameter-Dependent
Parameter Selection	Ad-hoc	Analytically	Ad-hoc

Table 5.7: Qualitative comparison of methods

Although any of the methods introduced in this chapter results in obtaining a sparse vector of inputs \mathbf{u} . The Brute-Force searching method was selected for further testing, due to its simplicity and flexibility in setting the different types of initial constraints as shown in Table 5.7. It was found in practice that appropriate selection of number of elements n_{active} was most important. The number of elements was predefined based on the average sparsest solution of APG algorithm for different set of data and was set to be $n_{active} \leq 8$. Experimental investigations indicated that satisfactory results can be obtained using $u_{rate} = 0.15$ as shown in Table 5.6.

5.4.3 Selection of Virtual Elements

During practical tests with electrode arrays it was observed that single element stimulation can induce movement of single fingers, i.e. index and little fingers. However, single element stimulation requires a higher level of pulse-width to cause visible movement of the hand and wrist. This higher level of stimulation can result in discomfort or even pain sensation. To overcome this problem and increase the practical level of selectivity and accuracy of the optimized stimulation sites, four types of single elements were selected. These are: single element of electrode array (1-element), 2-elements oriented horizontally, 2-elements oriented vertically and 4 - elements respectively, as shown in Figure 5.8.

	Virtual Element	Observed Movement
1	single element	single fingers movement: index finger, little finger
2	2 elements (horizontally)	group of fingers: index and middle, weak wrist movement
3	2 elements (vertically)	group of fingers: index and thumb,
4	4 elements	four fingers movement, strong wrist response

Figure 5.8: Types of virtual elements

5.5 Experimental Results

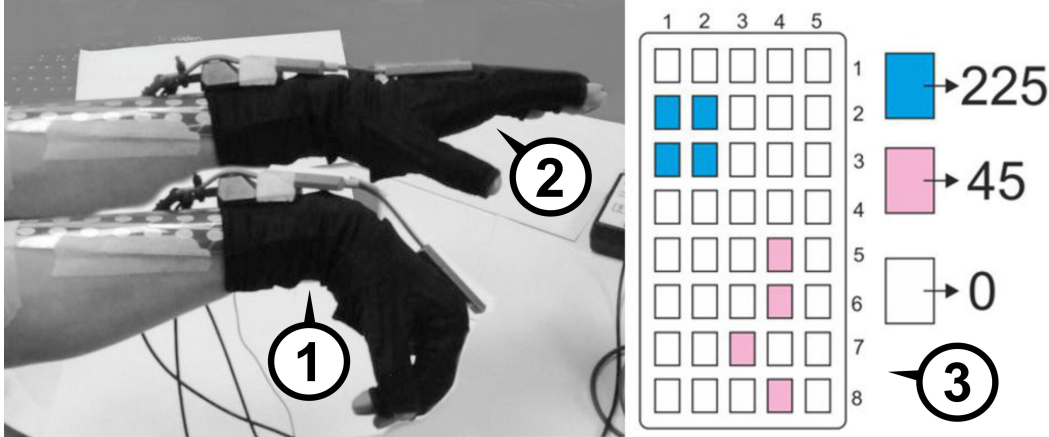


Figure 5.9: FES schematic for hand and wrist control with hardware components: (1) initial posture, (2) reference posture, (3) optimal stimulation pattern, defined by following vector of normalized non-zero elements of vector $\mathbf{u} = [u_6 = 0.75, u_7 = 0.75, u_{11} = 0.75, u_{12} = 0.75, u_{24} = 0.15, u_{29} = 0.15, u_{33} = 0.15, u_{39} = 0.15]$ where $u_{max} = 1$ represents the normalized maximal value of pulse-width = $300\mu s$.

The clinically relevant task considered during experimental testing was to move the hand from an initial flexed position \mathbf{y}_0 to a final extended position \mathbf{y}_d . This represents hand opening, with a starting posture which emulates a typical posture of a spastic hand.

A single trial of the procedure was undertaken on three unimpaired participants who each provided no voluntary effort. The optimized solution was tested 5 times and Table 5.8 shows mean error norm results. Normalized error is given by $\|e\| / \|y_d - y_0\|$. The results show that error was reduced to between 0.3 and 0.38 of its starting value using only two levels of stimulation.

No.	Normalized Error (for 16 joints)	Standard deviation
1.	0.3875	0.0335
2.	0.3538	0.0222
3.	0.3080	0.0530

Table 5.8: Normalized errors for 3 subjects.

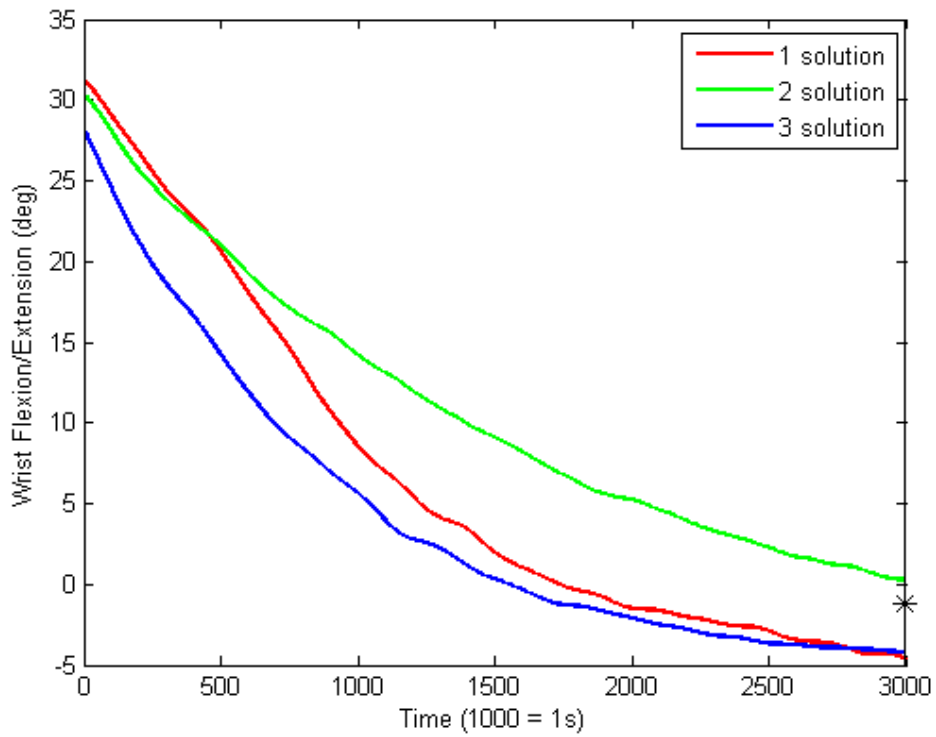


Figure 5.10: Wrist Flexion/Extension.

The results show that the optimal stimulation pattern differs from subject to subject. Additionally, the test results indicate that there is significant variability in the results for the same participant on different trials, which is shown in Table 5.10.

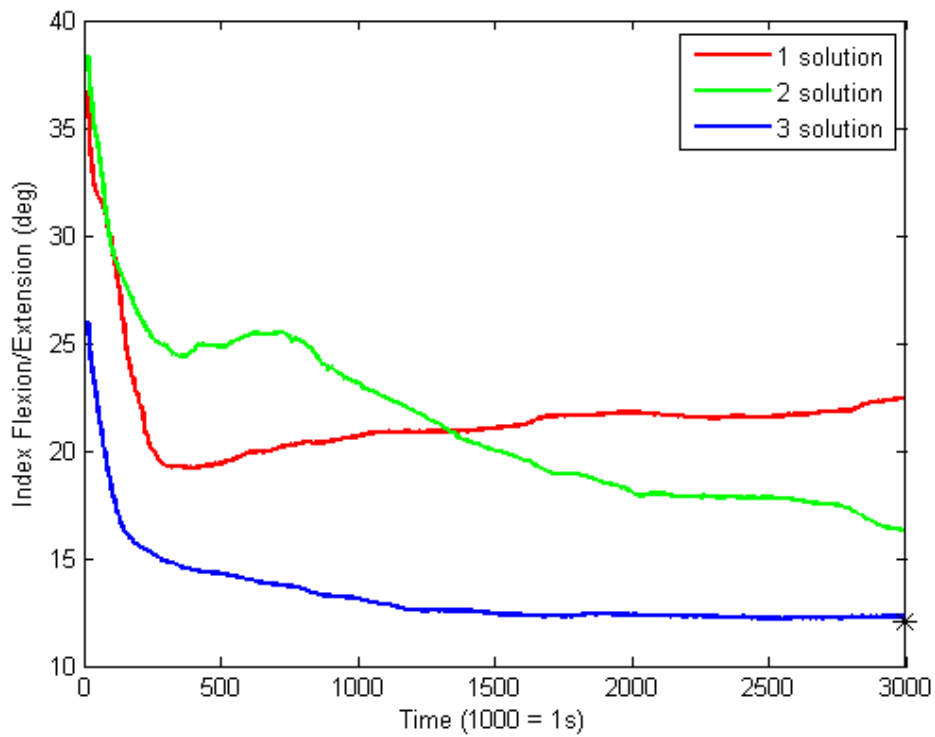


Figure 5.11: Index Finger Flexion/Extension.

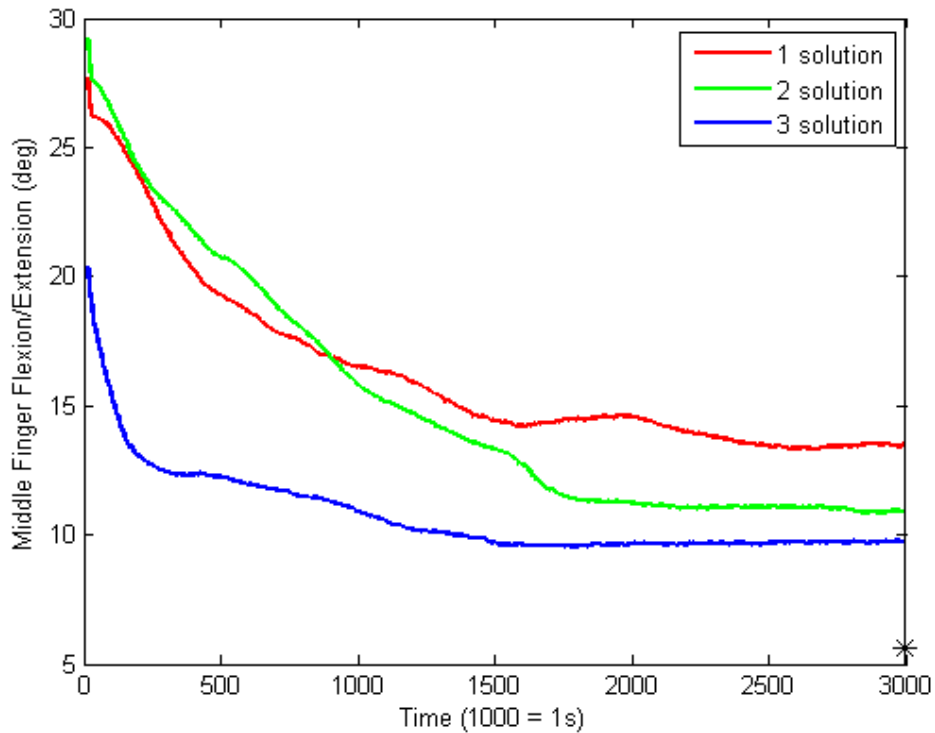


Figure 5.12: Middle Finger Flexion/Extension.

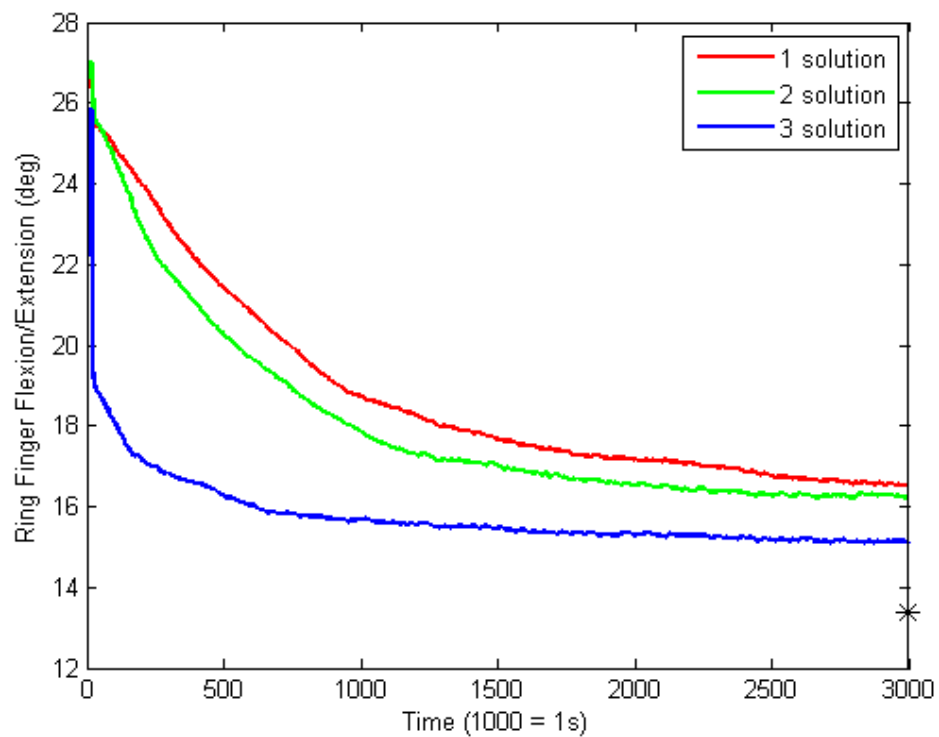


Figure 5.13: Ring Finger Flexion/Extension.

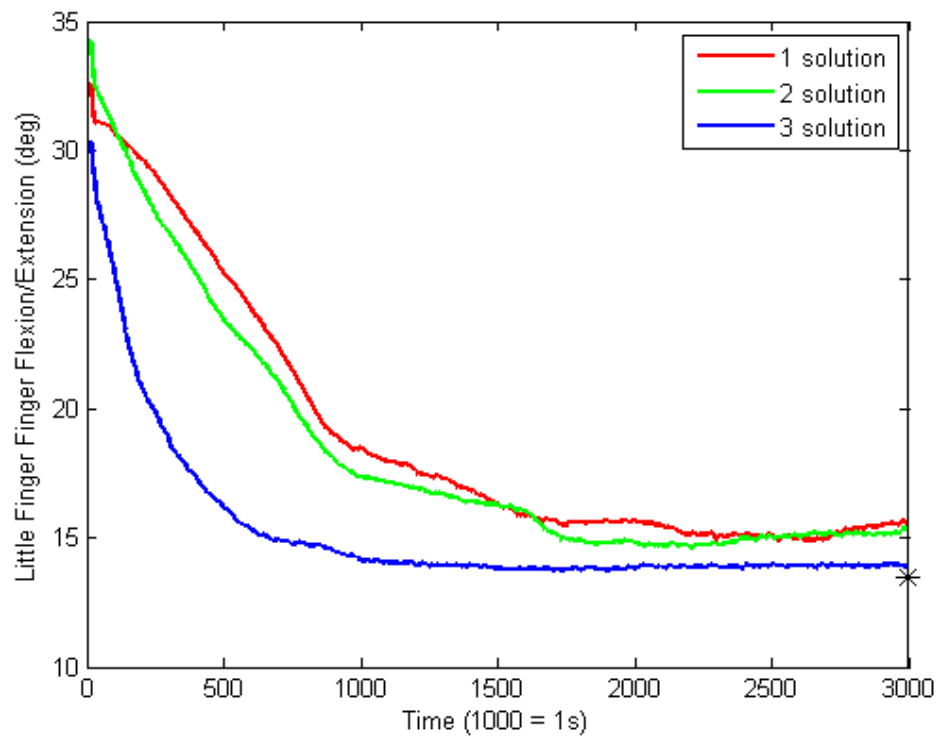


Figure 5.14: Little Finger Flexion/Extension.

No.	Active elements
1.	$[u_3 = 0.3, u_{26} = 0.6]$
2.	$[u_1 = 0.15, u_2 = 0.15, u_6 = 0.75, u_7 = 0.75, u_{11} = 0.75, u_{12} = 0.75]$
3.	$[u_6 = 0.75, u_7 = 0.75, u_{11} = 0.75, u_{12} = 0.75, u_{24} = 0.15, u_{29} = 0.15, u_{33} = 0.15, u_{39} = 0.15]$

Table 5.9: Optimal Stimulation Patterns for Opened Hand

Trial	Active elements of the array	Predicted Error	Test Error
1.	$[u_3 = 0.45, u_4 = 0.45, u_{32} = 0.45, u_{37} = 0.45]$	20.5454	22.2878
2.	$[u_1 = 0.45, u_2 = 0.45, u_{21} = 0.45]$	15.2696	25.2973
3.	$[u_2 = 0.3, u_{21} = 0.6]$	15.3477	25.7593

Table 5.10: Optimal Stimulation Patterns for Open Hand for the same participant on different trials

Preliminary trials have shown that the method gives acceptable results, considered assumptions that were made. This partially confirms the findings of Popović and Popović (2009), that the electrical field in human body is quasi-static. However, the identification of nonlinear model of the musculo-tendon structure of the hand and wrist is significant in the case of dynamic trajectory tracking. Therefore, to increase the efficacy of the simple approach presented in this chapter, other methods need to be investigated and tested, in order to obtain algorithm that would include as rich model information as possible and could be still applicable in practice.

Chapter 6

Conclusions and Future work

The main objective of this thesis was to investigate an application of Surface Electrode Array Stimulation (SEAS)-based control of hand and wrist for hand restoration after stroke. A few different approaches were developed based on theoretical and experimental findings. These include: optimal ILC methods for control of the hand and wrist and sparse optimisation algorithms to automatic configuration of electrode array, such as i.e. Proximal Gradient Method. A comparison of the methods was presented, taking into account both: theoretical and practical constraints.

Additionally, to overcome difficulties associated with system identification and standard model-based ILC a novel 'Virtual-Element' based methodology for control of hand and wrist has been introduced. Preliminary results confirmed practical usability of proposed methods, however further research and experimental tests are needed to obtain more accurate patient-specific models and parameters for different stimulation sites of electrodes.

Generally, the control of human hand using model-based ILC is a complex research problem. To enable control of more complex movements of hand and wrist, a parallel activation of both types of muscles flexor and extensor must be supported by the hardware. Additionally, a use of electrode array instead of using single return electrode should be considered in the future to increase selectivity of the muscles. All the modifications, requires development more advanced stimulation devices, that would support complex signal routing and advance multi-channel stimulation.

Based on literature and research findings, a new Hand Rehabilitation System (HaReS) has been designed and is being developed. The key element of the system is a game-based task oriented training environment designed for a wide group of stroke patients, including patients with spasticity and hemiplegia. The platform is being developed especially to increase the motivation in the patients and encourage them to perform high

number of repetitive movements.

Developing an effective rehabilitation system for hand and wrist, that would be beneficial for a wide group of stroke survivors is a challenging and multidisciplinary task. It involves analysis, design, application and comprising many different aspects and methods from different fields of science: such as control, computer science, health science, anatomy, psychology and engineering. The efficacy of the system is strongly related to the accuracy of each of these aspects.

The methods of SEAS-based control of the wrist and hand are of significant importance for the general effectiveness and usability of the system. The assumptions and simplifications, such as setting a compromise between the high accuracy of the model and the problem of its practical application, make the problem of the SEAS-based control of the hand and wrist an interesting and open research subject. Thus the main focus of the future work will be on improvement of the methods of array optimisation and the control algorithms described in this dissertation. The presented iterative approach for finding optimal stimulation levels, must be extended to more general dynamic tracking control cases, in order to precisely control complex hand movements. This includes development and application of more advanced identification methods.

The complete system will be tested in practical trials with unimpaired subjects, however the long-term objective of the work is to test the effectiveness of HaReS in clinical trials with stroke patients. The system has been specially designed to collect a large amount of data. Hence it can be a research tool, that can be used for further comparison studies of different rehabilitation interventions such as: UMT with game-based therapy, FES-based therapy of hand and wrist mediated by ILC, etc. The data collected in long term perspective can be used to develop more advanced methods and algorithms described in this thesis.

List of Figures

2.1	Hand bones and joints (Kowalczewski (2009))	8
2.2	Hand muscles Kowalczewski (2009)	9
2.3	Movements of the thumb and fingers (for Surgery of The Hand, 1990) . .	10
2.4	Schematic illustration of a muscle acting on a single joint, where q_1, q_2 are the joint angles, f is the pulling force applied by the muscle, L_1, L_2 are muscle lengths and r is the moment arm of the joint-muscle system.	14
2.5	Example of FES schematic for hand and wrist rehabilitation.	17
2.6	Planar arm movements rehabilitation system	24
2.7	3D Arm rehabilitation system for stroke patients. The system includes a mechanical robotic unweighting system used to support patient's arm - ARMEO (1), FES hardware (2,3), control system and user software including custom-made virtual reality module (4,5,6).	25
3.1	Planar hand model	28
3.2	The network of the finger tendons (Vigouroux et al., 2006)	35
3.3	The III Landsmeer model of the finger (Armstrong and Chaffin, 1978) . .	36
3.4	Stimulation of extrinsic and intrinsic muscles using Newton method-based point-to-point ILC with inequality constraint.	43
3.5	Stimulation of extrinsic muscles using Newton method-based point-to-point ILC with inequality constraint.	44
3.6	Stimulation of extrinsic and intrinsic muscles using Newton method-based point-to-point ILC: error norm.	45
3.7	Stimulation of extrinsic muscles using Newton method-based point-to-point ILC with inequality constraint: error norm.	45
4.1	Surface Electrode Array Stimulation - schematic of technique	48
4.2	Linearization points for u_i with $u_p = 0$, $p \neq 0$	51
4.3	Linearization points about u_a	52
4.4	Optimal Stimulation Pattern - schematic of mapping array elements → input vector \mathbf{u}	63
4.5	General Iterative Approach for SEAS-based control of the hand and wrist	64
5.2	Graphical User Interface	70
5.3	Hares game	71
5.4	Interactive cycle in the playing game experience	72
5.5	Selection of a task	73
5.6	Accelerated Proximal Gradient error norm for 16 joints.	75
5.7	Accelerated Proximal Gradient convergence results for $s = 2$	76
5.8	Types of virtual elements	78

5.9 FES schematic for hand and wrist control with hardware components: (1) initial posture, (2) reference posture, (3) optimal stimulation pattern, defined by following vector of normalized non-zero elements of vector $\mathbf{u} =$ [$u_6 = 0.75, u_7 = 0.75, u_{11} = 0.75, u_{12} = 0.75, u_{24} = 0.15, u_{29} = 0.15, u_{33} =$ $0.15, u_{39} = 0.15$] where $u_{max} = 1$ represents the normalized maximal value of pulse-width = $300\mu s$	78
5.10 Wrist Flexion/Extension.	79
5.11 Index Finger Flexion/Extension.	80
5.12 Middle Finger Flexion/Extension.	80
5.13 Ring Finger Flexion/Extension.	81
5.14 Little Finger Flexion/Extension.	81

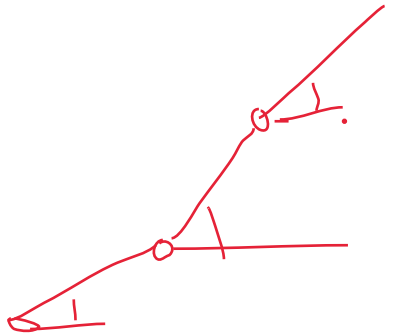
List of Tables

2.1	Intrinsic Muscles of the hand	9
2.2	Extrinsic Muscles of the hand	10
2.3	Games in Stroke Rehabilitation	13
4.1	Exemplar methods for selected configuration of different parameters of the general procedure	65
5.1	Range of movements for the joints MCP and PIP of the fingers used in calibration	69
5.2	Range of movements for the joints MCP and PIP of the fingers used in calibration	70
5.3	Reference postures	74
5.4	Numerical Results for 5, 8 and 10 stimulation levels	75
5.5	Numerical results for APG for 2, 3, 4 elements	76
5.6	Numerical Results for different parameters	76
5.7	Qualitative comparison of methods	77
5.8	Normalized errors for 3 subjects.	79
5.9	Optimal Stimulation Patterns for Opened Hand	82
5.10	Optimal Stimulation Patterns for Open Hand for the same participant on different trials	82

Appendix A

Model and parameters

A.1 Model of the hand and wrist



The dynamic model of the finger/wrist is formulated using the Lagrange method and can be rewritten in the form

$$\mathbf{M}(\mathbf{q})\ddot{\mathbf{q}} + \mathbf{C}(\mathbf{q}, \dot{\mathbf{q}}) + \mathbf{G}(\mathbf{q}) + \mathbf{F}(\mathbf{q}, \dot{\mathbf{q}}) = \boldsymbol{\tau} \quad (\text{A.1})$$

where $\mathbf{M}(\mathbf{q})$ is the inertia matrix, $\mathbf{C}(\mathbf{q}, \dot{\mathbf{q}})$ denotes the centrifugal and Coriolis forces, $\mathbf{G}(\mathbf{q})$ is the vector of gravitational force, and the generalized coordinates of the system are $\mathbf{q} = [\theta_1 \ \theta_2 \ \theta_3]$. During purely horizontal movement of the finger gravity can be neglected.

The elements of the symmetric inertia matrix are

$$\begin{aligned} m_{11} &= m_1 c_1^2 + m_2 l_1^2 + m_2 c_2^2 + 2m_2 l_1 c_2 \cos \theta_2 + m_3 l_1^2 \\ &\quad + m_3 l_2^2 + 2m_3 l_1 l_2 \cos \theta_2 + 2m_3 l_1 c_3 \cos(\theta_2 + \theta_3) \\ &\quad + 2m_3 l_2 c_3 \cos \theta_3 + m_3 c_3^2 + J_1 + J_2 + J_3 \\ m_{12} &= m_2(c_2^2 + l_1 c_2 \cos \theta_2) + m_3 l_2^2 + m_3 c_3^2 + m_3 l_1 l_2 \cos \theta_2 \\ &\quad + m_3 l_1 c_3 \cos(\theta_2 + \theta_3) + 2m_3 l_2 c_3 \cos \theta_3 + J_2 + J_3 \\ m_{13} &= m_3 c_3^2 + m_3 l_1 c_3 \cos(\theta_2 + \theta_3) + m_3 l_2 c_3 \cos \theta_3 + J_3, \\ m_{22} &= m_2 c_2^2 + m_3 l_2^2 + m_3 c_3^2 + m_3 l_2 c_3 \cos \theta_3 + J_3, \\ m_{23} &= m_3 c_3^2 + m_3 l_2 c_3 \cos \theta_3 + J_3 \\ m_{33} &= m_3 c_3^2 + J_3 \end{aligned} \quad (\text{A.2})$$

where $m_1 = 0.3$, $m_2 = 0.015$, $m_3 = 0.009$ are masses, $J_1 = 5e - 4$, $J_2 = 5e - 6$, $J_3 = 3e - 6$, are inertias, and the assumed lengths are $l_1 = 0.08$, $l_2 = 0.05$, $l_3 = 0.048$

and $c_i = 0.5l_i$, $i = 1, 2, 3$. The elements of $\mathbf{C}(\mathbf{q}, \dot{\mathbf{q}})$ are

$$\begin{aligned}
 c_{11} &= -[m_3 c_3 l_1 s_{23} + m_3 c_3 l_2 \sin \theta_3](2\dot{\theta}_1 \dot{\theta}_3 + 2\dot{\theta}_2 \dot{\theta}_3 + \dot{\theta}_3^2) \\
 &\quad - [(m_2 l_1 c_2 + m_3 l_1 l_2) \sin \theta_2 + m_3 l_1 c_3 s_{12}](2\dot{\theta}_1 \dot{\theta}_2 + \dot{\theta}_2^2) \\
 c_{21} &= [(m_2 c_2 l_1 + m_3 l_1 l_2) \sin \theta_2 + m_3 c_3 l_2 s_{23}] \dot{\theta}_1^2 \\
 &\quad - m_3 c_3 l_2 \sin \theta_3 (2\dot{\theta}_1 \dot{\theta}_3 + 2\dot{\theta}_2 \dot{\theta}_3 + \dot{\theta}_3^2) \\
 c_{31} &= [m_3 c_3 l_2 \sin \theta_3 + m_3 c_3 l_1 s_{23}] \dot{\theta}_1^2 \\
 &\quad + m_3 c_3 l_2 \sin (2\dot{\theta}_1 \dot{\theta}_2 + \dot{\theta}_2^2)
 \end{aligned} \tag{A.3}$$

where $s_{ij} = \sin(\theta_i + \theta_j)$. The vector of moments produced through application of FES is $\boldsymbol{\tau}$, and $\mathbf{F}(\mathbf{q}, \dot{\mathbf{q}})$ is the vector of frictional components acting about each joint, with the form

$$\mathbf{F}(\mathbf{q}, \dot{\mathbf{q}}) = \begin{bmatrix} k_1(\theta_{0,1} - \theta_1) - b_1 \dot{\theta}_1 \\ k_2(\theta_{0,2} - \theta_2) - b_2 \dot{\theta}_2 \\ k_3(\theta_{0,3} - \theta_3) - b_3 \dot{\theta}_3 \end{bmatrix} \tag{A.4}$$

where $b_1 = 0.05$, $b_2 = 0.014$, $b_3 = 0.01$ are the viscous friction coefficients and $\boldsymbol{\tau}$ represents the vector of applied torque. It has been assumed that the muscle groups which actuate each joint produce a stiffness that may be represented by a spring with zero elongation at the initial position $\theta_{0,1} = \frac{2}{3}\pi$, $\theta_{0,2} = \frac{\pi}{2}$, $\theta_{0,3} = \frac{\pi}{3}$ and with stiffness coefficients $k_1 = 6.5$, $k_2 = 0.9$, $k_3 = 0.8$. All previously given parameters are in SI units.

A.2 Simulation parameters

Tendon - type (joint)	d	y	r	h	b
EC - extrinsic (wrist)	-	-	14.12	-	-
ECR - extrinsic (wrist)	-	-	-	-11.72	1.14
ECU - extrinsic (wrist)	-	-	-	-8.51	1.55
FDP - extrinsic (MCP)	8.32	8.32	-	-	-
RI - intrinsic (MCP)	-	-	-	-1.29	5.62
UI - intrinsic (MCP)	-	-	-	-8.16	18.76
LU - intrinsic (MCP)	-	-	-	-2.17	12.53
EC (MCP)	-	-	8.3	-	-
FDP (PIP)	5.76	7.5	-	-	-
ES - intrinsic (PIP)	-	-	2.92	-	-
RB - intrinsic (PIP)	-	-	-	-0.47	2.54
UB - intrinsic (PIP)	-	-	-	0.57	1.7

% Parameters of the finger model described in chapter ??.

```

m1 = 0.05; % mass of the proximal phalangeal [kg]
m2 = 0.04; % mass of the middle phalangeal [kg]
m3 = 0.03; % mass of the distal phalangeal [kg]
l1 = 0.05; % length of the proximal phalangeal [m]

```

```
l2 = 0.02; % length of the middle phalangeal in [m]
l3 = 0.02; % length of the distal phalangeal in [m]
c1 = 0.025; % distance from MPC joint to the mass centre
              % of the proximal phalangeal in [m]
c2 = 0.01; % distance from PIP joint to the mass centre
              % of the middle phalangeal [m]
c3 = 0.01; % distance from DIP joint to the mass centre
              % of the distal phalangeal [m]
b1 = 0.4; % viscous friction parameter in kg m s^-2
b2 = 0.4; % viscous friction parameter in kg m s^-2
b3 = 0.4; % viscous friction parameter in kg m s^-2
k1 = 0.8; % torsional spring constant in Nm/rad
k2 = 0.8; % torsional spring constant in Nm/rad
k3 = 0.8; % torsional spring constant in Nm/rad
theta0_1 = (2/3)*pi;
theta0_2 = pi/2;
theta0_3 = pi/3;
J2 = 1e-4;
J4 = 1e-4;
J6 = 1e-4;
```

The parameters were taken from [Brook et al. \(1995\)](#), [Theodorou et al. \(2011\)](#).

References

- H.S. Ahn, Y.Q. Chen, and K.L. Moore. Iterative learning control: brief survey and categorization. *IEEE Transactions on Systems, Man and Cybernetics, Part C*, (37):1109–1121, 2007.
- I. Albrecht, J. Haber, and H. Seidel. Construction and animation of anatomically based human hand models. In *SIGGRAPH Symposium for Computer Animation*, volume 22, pages 98–109. ACM Press / ACM SIGGRAPH, 2003.
- S. Arimoto, S. Kawamura, and F. Miyazaki. Bettering operations of robots by learning. *Journal of Robotic Systems*, 1:123–140, 1984a.
- S. Arimoto, F. Miyazaki, and S. Kawamura. Bettering operation of dynamical systems by learning: a new control theory for servomechanism or mechatronics systems. In *Proceedings of the 23rd Conference on Decision and Control*, pages 1064–1069, Las Vegas, Nevada, 1984b.
- T. J. Armstrong and D. B. Chaffin. An investigation of the relationship between displacements of the finger and wrist joints and the extrinsic finger flexor tendons. *Journal of Biomechanics*, 11(3):119–128, 1978.
- J. Biggs, K. Horch, and F. J. Clark. Extrinsic muscles of the hand signal fingertip location more precisely than they signal the angles of individual finger joints. *Experimental brain research*, 125(3):221–230, 1999.
- B. Brewer, S. McDowell, and L. Worthen-Chaudhari. Poststroke upper extremity rehabilitation: A review of robotic systems and clinical results. *Topics in Stroke Rehabilitation*, 14(16):22–44, 2007.
- D. Bristow, M. Tharayil, and A. Alleyne. A survey of iterative learning control. *Control Syst Mag, IEEE*, 26(3):96–114, 2006.
- J. Broeren, A. Bjorkdahl, and L. Claesson. Virtual rehabilitation after stroke. *Studies in Health Technology and Informatics*, (136):77–182, 2008.
- N. Brook, J. Mizrahi, M. Shoham, and J. Dayan. A biomechanical model of index finger dynamics. *Medical engineering & physics*, 17(1):54–63, 1995.
- G. Burdea. Virtual rehabilitation: Benefits and challenges. *Schattauer J Methods Information in Medicine*, pages 519–523, 2003.
- J. Burke, M. McNeill, D. Charles, P. Morrow, J. Crosbie, and S. McDonough. Serious games for upper-limb rehabilitation following stroke. pages 103–110, 2009.
- Z. Cai, D. Tong, C. Freeman, and E. Rogers. Application of newton-method based ilc to 3d stroke rehabilitation. In *18th IFAC World Congress*, Milano, Italy, August 28 - September 2 2011. In Press.
- E. Y. Chao, J. D. Opgrande, and F. E. Axmear. Three dimensional force analysis of finger joints in selected isometric hand functions. *Journal of Biomechanics*, 9:387–396, 1976.

- S. Cobos, R. Aracil, and M. Ferre. Low dimensionality space for controlling human hand models. Tokyo, Japan, 2010a.
- S. Cobos, M. Ferre, and R. Aracil. Simplified human hand models based on grasping analysis. In *International Conference on Intelligent Robots and Systems (IROS)*, pages 610–615, 2010b.
- S. Cobos, M. Ferre, M. A. Sànchez-Urà, and J. Ortego. Constraints for realistic hand manipulation. 2007.
- S. Cobos, M. Ferre, S. Uran, J. Ortego, and C. Pena. Efficient human hand kinematics for manipulation tasks. 2008.
- R. Colombo, F. Pisano, and A. Mazzone. Design strategies to improve patient motivation during robot-aided rehabilitation. *Journal of Neuroengineering and Rehabilitation*, 3(4):1196–1207, 2007.
- A. D. Deshpande, J. Ko, D. Fox, and Y. Matsuoka. Anatomically correct testbed hand control: muscle and joint control strategies. In *Robotics and Automation, 2009. ICRA'09. IEEE International*, pages 4416–4422, 2009.
- J. E. Deutsch, M. Borbely, J. Filler, K. Huhn, and P. Guarnera-Bowlby. Use of a low-cost, commercially available gaming console (wii) for rehabilitation of an adolescent with cerebral palsy. *Physical Therapy*, 10(88):1196–1207, 2008.
- P. Le Dinh. Fes-based stroke rehabilitation of the hand and wrist using a multi-electrode array. *Individual research*, 2012.
- K. K. Dou, K. Tan, T. H. Lee, and Z. Zhou. Iterative learning feedback control of human limbs via functional electrical stimulation. *Control Engineering Practice*, 7(3):315–325, 1999.
- E. Ernst. A review of stroke rehabilitation and physiotherapy. *Stroke*, 21:1081–1085, 1990.
- A. Esteki and J. M Mansour. A dynamic model of the hand with application in functional neuromuscular stimulation. *Annals of biomedical engineering*, 25(3):440–451, 1997.
- B. Europa. Surface arrays for functional electrical stimulation. *Individual research*, 2009.
- S. Flynn, P. P. Palma, and A. Bender. Feasibility of using the sony playstation 2 gaming platform for an individual poststroke: a case report. *IEEE Control Systems Magazine*, 4(31):180–189, 2007.
- American Society for Surgery of The Hand. *The Hand: Examination and Diagnosis*. Churchill Livingstone, 3 edition, 1990.
- C. Freeman, Z. Cai, E. Rogers, and P. Lewin. Iterative learning control for multiple point-to-point tracking application. *IEEE Transactions on Control Systems Technology*, 19(3):590–600, 2011.
- C. T. Freeman. Constrained point-to-point iterative learning control with experimental verification. *Control Engineering Practice*, page In Press, 2012.
- C. T. Freeman, I. Davies, P. Lewin, and E. Rogers. Iterative learning control of upper limb reaching using functional electrical stimulation. In *the 17th IFAC World Congress*, pages 13444–13449, Seoul, Korea, 2008.
- C. T. Freeman, A. M. Hughes, J. Burridge, P. Chappell, P. Lewin, and E. Rogers. Design and control of an upper arm FES workstation for rehabilitation. pages 66–72, 2009a.
- C. T. Freeman, A. M. Hughes, J. Burridge, P. Chappell, P. Lewin, and E. Rogers. Iterative learning control of FES applied to the upper extremity for rehabilitation. *Control Engineering Practice*, 26(3):368–381, 2009b.

- C. T. Freeman, E. Rogers, A.-M. Hughes, J. H. Burridge, and K. L. Meadmore. Iterative learning control in healthcare electrical stimulation and robotic-assisted upper limb stroke rehabilitation. *IEEE Control Systems Magazine*, 1(32):18–43, 2012.
- C. T. Freeman and Y. Tan. Point-to-point iterative learning control with mixed constraints. In *American Control Conference*, pages 3657–3662, San Francisco, CA, 2011.
- K. Fujita, K. Shiga, and H. Takahashi. In *20th annual international conference of IEEE Engineering in Medicine and Biology Society*, volume 20, pages 2588–2589, 1998.
- R. Hart, K. Kilgore, and P. Hunter. A comparison between control methods for implanted FES hand-grasp systems. *IEEE Transactions on Rehabilitation Engineering*, 6(2):208–218, 1998.
- H. Hendricks, M. Ljzerman, J. Kroon, and G. Zilvold. Functional electrical stimulation by means of the ness handmaster orthosis in chronic stroke patients: an exploratory study. *Clinical Rehabilitation*, 15, 2001.
- T. Hill. The heat of shortening and the dynamic constants of muscle. *Proceedings of the Royal Society of London. Series B, Biological Sciences*, 126:135–195, 1938.
- M. Huber, B. Rabin, and C. Docan. Playstation 3- based tele-rehabilitation for children with hemiplegia. *Virtual Rehabilitation*, pages 105–112, 2008.
- A.-M. Hughes, C. T. Freeman, J. H. Burridge, P. H. Chappel, P. L. Lewin, and E. Rogers. Feasibility of iterative learning control mediated by functional electrical stimulation for reaching after stroke. *Journal of Neurorehabilitation and Neural Repair*, 6(23):559–568, 2009a.
- A. M. Hughes, C. T. Freeman, J. H. Burridge, P. H. Chappell, P. Lewin, and E. Rogers. Feasibility of iterative learning control mediated by functional electrical stimulation for reaching after stroke. *Journal of Neurorehabilitation and Neural Repair*, 23(6):559–568, 2009b.
- J. N. Ingram, K. P. Körding, I. S. Howard, and D. M. Wolpert. The statistics of natural hand movements. *Experimental Brain Research*, 188(2):223–236, March 2008. ISSN 0014-4819.
- D. G. Kamper, R. L. Harvey, S. Suresh, and W. Z. Rymer. Relative contributions of neural mechanisms versus muscle mechanics in promoting finger extension deficits following stroke. *Muscle Nerve*, (28):309–318, 2003.
- D. G. Kamper and W. Z. Rymer. Impairment of voluntary control of finger motion following stroke: role of inappropriate muscle coactivation. *Muscle Nerve*, (24):673–681, 2001.
- J. Kowalczewski. Upper extremity neurorehabilitation. thesis. 2009.
- J. Landsmeer. Anatomical and functional investigations on the articulation of the human fingers. *Acta Anatomica* 24, 2(25):1–69, 1955.
- C. E. Lang, J. R. MacDonald, and C. Gnip. Counting repetitions: an observational study of outpatient therapy for people with hemiparesis post-stroke. *Journal Neuro. Phys. Therapy*, 1(31):3–10, 2007.
- P. Langhorne, F. Coupar, and A. Pollock. A motor recovery after stroke: a systematic review. *The Lancet Neurology*, 8(8):741–754, 2009.
- F. Le, I. Markovsky, C. T. Freeman, and E. Rogers. Identification of electrically stimulated muscle models of stroke patients. *Control Engineering Practice*, 18:396–407, 2010.
- T. Lin, D. H. Owens, and J. Htnen. Newton method based iterative learning control for discrete non-linear systems. *International Journal of Control*, 79(10):1263–1276, 2006a.

- T. Lin, D. H. Owens, and J. J. Hätkönen. Newton method based iterative learning control for discrete non-linear systems. *International Journal of Control*, 79(10):1263–1276, 2006b.
- C. L. Lynch and M. R. Popovic. Functional electrical stimulation. *IEEE Control Systems Magazine*, 28(2):40–50, 2008.
- G. M. Lyons, G. E. Leane, M. Clarke-Moloney, J. V. O’Brien, and P. A. Grace. An investigation of the effect of electrode size and electrode location on comfort during stimulation of the gastrocnemius muscle. *Med Eng Phys*, 10(26), 2004.
- N. Malešević and L. Popović. Muscle twitch responses for shaping the multi-pad electrode for functional electrical stimulation. *Journal Of Automatic Control*, 20:53–57, 2010.
- K. L. Meadmore, A. M. Hughes, C. T. Freeman, J. H. Burridge, D. Tong, Z. Cai, and E. Rogers. Iterative learning mediated FES and 3D robotics reduces motor impairment in chronic stroke. *Journal of NeuroEngineering and Rehabilitation*, 23:Submitted, 2011.
- K. L. Meadmore, A.-M. Hughes, C. T. Freeman, C. Z. Tong, D. Tong, J. H. Burridge, and E. Rogers. Function electrical stimulation mediated by iterative learning control and 3d robotics reduces motor impairment in chronic stroke. *Journal of Neuroengineering and Rehabilitation*, 9(32), 2012.
- A. Miller, P. Allen, V. Santos, and F. Valero-Cuevas. From robotic hands to human hands: a visualization and simulation engine for grasping research. *Industrial Robot: An International Journal*, 32(1):55–63, 2005. ISSN 0143–991X.
- L. J Miltner, W. H. Bauder, M. Sommer, C. Dettmers, E. Taub, and C. Weiller. Motor cortex plasticity during constraint induced movement therapy in stroke patients. *Neurosci Lett*, 250(1):58, 1998.
- Y. Nesterov. *Introductory Lectures on Convex Optimization*. Kluwer Academic Publisher, Dordrecht, The Netherlands, 2004.
- Y. Nesterov. Gradient methods for minimizing composite functions. *Mathematical Programming*, 140(1):125–161, 2013.
- R. J. Nudo. Adaptive plasticity in motor cortex: Implications for rehabilitation after brain injury. *Journal of Rehabil. Med.*, (41):710, 2003.
- S. B. O’Dwyer, D. T. O’Keeffe, S. Coote, and G. M. Lyons. An electrode configuration technique using an electrode matrix arrangement for fes-based upper arm rehabilitation systems. *Medical Engineering and Physics*, 28:166–176, 2006.
- S. B. O’Dwyer, D. T. O’Keeffe, S. Coote, and G. M. Lyons. An electrode configuration technique using an electrode matrix arrangement for FES-based upper arm rehabilitation systems. *Medical Engineering & Physics*, 28:166–176, 2006.
- J. M. Ortega and W. C. Rheinboldt. *Iterative Solution Of Nonlinear EquationsIn Several Variables*. Academic Press, New York, 1 edition, 1970.
- V. M. Pomeroy, L. M. King, A. Pollock, A. Baily-Hallam, and P. Langhorne. Electrostimulation for promoting recovery of movement or functional ability after stroke: a review. *Cochrane Database of Systematic Reviews*, 2006.
- D. Popovic. Clinical evaluation of the bionic glove. *Archives of Physical Medicine & Rehabilitation*, 80:299–304, 1999.
- D. B. Popović and M. B. Popović. Automatic determination of the optimal shape of a surface electrode: Selective stimulation. *Journal of Neuroscience Methods*, (178):174–181, 2009.

- A. Popović-Bijelić, G. Bijelić, N. Jorgovanović, D. Bojanić, M. B. Popović, and D. B. Popović. Multi-field surface electrode for selective electrical stimulation. *Artificial Organs*, 29(6):448–452, 2005.
- A. Prochazka. The bionic glove: an electrical stimulator garment that provides controlled grasp and hand opening in quadriplegia. *Archives of Physical Medicine & Rehabilitation*, pages 608–614, 1997.
- P. Raghavan. The nature of hand motor impairments after stroke and its treatment. *Curr. Treat. Options Cardiovasc. Med.*, (9):221–228, 2007.
- I. Roloff, V. R. Schoffl, L. Vigouroux, and F. Quaine. Biomechanical model for the determination of the forces acting on the finger pulley system. *Journal of Biomechanics*, 39:915–923, 2006.
- D. N. Rushton. Functional electrical stimulation and rehabilitation: an hypothesis. *Medical Engineering and Physics*, 25, 2003.
- J. L. Sancho-Bru, A. Perez-Gonzalez, M. Vergara-Monedero, and D. Giurintano. A 3-D dynamic model of human finger for studying free movements. *Journal of Biomechanics*, 34(11):1491–1500, 2001.
- O. Schill, Rupp R., and C. Pylatiuk. Automatic adaptation of a self-adhesive multielectrode array for active wrist joint stabilization in tetraplegic sci individuals. In *N2009 IEEE Toronto International Conference Science and Technology for Humanity*, 2009a.
- O. Schill, R. Rupp, C. Pylatiuk, S. Schulz, and M. Reischl. Automatic adaptation of a self-adhesive multi-electrode array for active wrist joint stabilization in tetraplegic sci individuals. In *Science and Technology for Humanity (TIC-STH), 2009 IEEE Toronto International Conference*, pages 708–713, 2009b.
- M. Selzer, S. Clarke, P. Duncan, and F. Gage. *Textbook of Neural Repair and Rehabilitation*. Cambridge University Press, Cambridge, UK, 2006.
- A. B. Sghaier, L. Romdhane, F. B. Ouezdou, and F. Vélizy. Biomechanical analysis of the normal and reconstructed human hand: Prediction of muscle forces in pinch and grasp. In *12th IFTOMM World Congress*, 2007.
- M. Shaughnessy, B. M. Resnick, and R. F. Macko. Testing a model of post-stroke exercise behavior. *Journal of the Assoc. of Rehabil. Nurses*, 31(1):15–21, 2006.
- D. K. Shin, Z. Gurdal, and O. H. Griffin Jr. A penalty approach for nonlinear optimization with discrete design variables. *Engineering Optimization*, 16:29–42, 1990.
- M. W. Spong and M. Vidyasagar. *Robot Dynamics and Control*. John Wiley and Sons, New York, 1989. 1st edition.
- S. Sueda, A. Kaufman, and D. K. Pai. Musculotendon simulation for hand animation. In *ACM SIGGRAPH 2008 papers*, pages 1–8, 2008.
- P. Taylor, J. Esnouf, and J. Hobby. The functional impact of the freehand system on tetraplegic hand function, clinical results. *International Spinal Cord Society*, 40:560–566, 2002.
- R. W. Teasell and L. Kalra. What's new in stroke rehabilitation, stroke. (35):383–385, 2004.
- E. Theodorou, E. Todorov, and F. J. Valero-Cuevas. Neuromuscular stochastic optimal control of a tendon driven index finger model. In *American Control Conference*, 2011.
- W. Tsang, K. Singh, and E. Fiume. Helping hand: an anatomically accurate inverse dynamics solution for unconstrained hand motion. In *Proceedings of the 2005 ACM SIGGRAPH/Eurographics symposium on Computer animation*, pages 319–328, 2005.

- R. Tubiana, J.-M. Thomine, and E. Mackin. *Examination of the hand and wrist*. Martin Dunitz Ltd. The Livery House, 2 edition, 1996.
- F. J. Valero-Cuevas. A mathematical approach to the mechanical capabilities of limbs and fingers. *Prog Mot Cont*, pages 619–633, 2009.
- F. J. Valero-Cuevas, V. V. Anand, A. Saxena, and H. Lipson. **Beyond parameter estimation: Extending biomechanical modeling by the explicit exploration of model topology**. *IEEE Transactions on Biomedical Engineering*, 54(11):1951–1964, nov 2007. ISSN 0018-9294.
- F. J. Valero-Cuevas, M. E. Johanson, and J. D. Towles and towards a realistic biomechanical model of the thumb: The choice of kinematic description is more critical than the solution method or the variability/uncertainty of musculoskeletal parameters. *Journal of Biomechanics*, 36(7):1019–1030, 2003.
- L. Vandenberghe. Convex optimization techniques in system identification., 2012.
- L. Vigouroux, F. Quaine, A. Labarre-Vila, and F. Moutet. Estimation of finger muscle tendon tensions and pulley forces during specific sport-climbing grip techniques. *Journal of biomechanics*, 39(14):2583–2592, 2006.
- Y. Wang, F. Gao, and F.J. Doyle. Survey on iterative learning control, repetitive control, and run-to-run control. *Journal of Process Control*, (19):1589–1600, 2009.
- T. Watanabe. A method of multichannel pid control of two-degree-of-freedom wrist joint movements by functional electrical stimulation. *Systems and Computers in Japan*, 34(5):25–36, 2003.
- A. J. Westerveld, A. C. Schouten, P. H. Veltink, and H. van der Kooij. Selectivity and resolution of surface electrical stimulation for grasp and release. *IEEE Trans Neural Syst Rehabil Eng*, 20(1), 2012.
- D. L. Wilson, Q. Zhu, J. L. Duerk, J. M Mansour, K. Kilgore, and P. E. Crago. Estimation of tendon moment arms from three-dimensional magnetic resonance images. *Annals of biomedical engineering*, 27(2):247–256, 1999.